Dynamic Judgments of Spatial Extent: Behavioural, Neural, and Computational Studies

by

Marc Hurwitz

A thesis
presented to the University of Waterloo
in fulfillment of the
thesis requirement for the degree of
Doctor of Philosophy
in
Psychology

Waterloo, Ontario, Canada, 2010

Author's Declaration

I hereby declare that I am the sole author of this thesis. This is a true copy of the thesis, including any required final revisions, as accepted by my examiners.

I understand that my thesis may be made electronically available to the public.

Abstract

Judgments of spatial relationships are often made when the object or observer are moving. Behaviourally, there is evidence that these 'dynamic' judgments of spatial extent differ from static judgments. For example, in one of the simplest probes of spatial extent – the line bisection task – the typically observed leftward bisection bias of about 1% of line length is increased considerably after left-to-right scanning (Jewell & McCourt, 2000). Here I used three separate techniques for exploring dynamic judgments: first, a line bisection paradigm

was employed to study ocular and pointing judgments of spatial extent while manipulating line length, position, speed, acceleration, and direction of scanning (Experiments 1-4); second, functional MRI (fMRI) was used to examine whether distinct brain regions were involved in dynamic versus static judgments of spatial extent (Exp 5); and finally, a mathematical and computational model of dynamic judgments was developed to provide a framework for interpreting the experimental results.

In the behavioural experiments, substantial differences were seen between static and dynamic bisection, suggesting the two invoke different neural processes for computing spatial extent. Surprisingly, ocular and pointing judgments produced distinct bisection patterns that were uncorrelated, with pointing somewhat more impervious to manipulations such as scan direction and position than ocular bisections. However, a new experimental task for probing dynamic judgments (the 'no line' Experiment 4) found that scan direction can influence both hand behaviour.

Functional MRI demonstrated that dynamic relative to static judgments produced activations in the cuneus and precuneus bilaterally, left cerebellum, and medial frontal gyrus, with reduced activation relative to static judgments observed in the supramarginal gyrus bilaterally. Dynamic bisections relative to a control condition produced activations in the right precuneus and left cerebellum, as well as in left superior parietal lobule, left middle temporal gyrus, and right precentral gyrus. It may be the case that velocity processing and temporal estimates are integrated primarily in the cuneus and precuneus bilaterally to produce estimates of spatial extent under dynamic scanning conditions. These results highlight the fact that dynamic judgments of spatial extent engage brain regions distinct from those employed to make static judgments, supporting the behavioural results that these are separate and distinct.

Finally, a mathematical model was proposed for dynamic judgments of spatial extent, i.e., the Cumulative Representational Strength (CRS) model. The CRS model is based on the idea that, rather than using an 'all-or-none' approach, spatial working memory actually takes about 100 ms to reach full representational strength for any given point in space. The model successfully explains many of the effects seen in the behavioural experiments including the effects of scan direction, velocity, line length, and position. In conjunction with the neuroimaging data, it also suggests why neglect patients may fail to show rightward bisection biases when making dynamic judgments of spatial extent. As a proof-of-concept, the mathematical model was implemented using the Neural Engineering Framework – a methodology for simulating behaviour from interconnected populations of neurons. The simulation provides a good fit with data and it suggests how a CRS model of dynamic bisection could be implemented in the brain.

Overall, this work provides novel insights into how the brain executes dynamic judgments of spatial extent. Generally speaking, dynamic judgments differ from static judgments in the magnitude of biases and in the factors affecting such biases. However, it is also likely that most dynamic judgments are a mixture of static and dynamic judgments.

Acknowledgements

I would like to thank my co-supervisor, Dr. James Danckert, for his gracious and unstinting support not only as I came up to speed in a new discipline, but also as I groped my way towards understanding a complex, messy, and unexpected set of results.

I would like to thank my other co-supervisor, Dr. Chris Eliasmith, for assisting me in this long endeavour and for showing patience with various challenges as I developed the skills needed.

There are two other key contributors to this thesis. First and foremost is my main research assistant, friend, and associate, Derick Valadao. I am convinced you will become a much better researcher than me and I'll be extremely happy one day to say that I had a small part in it! Next, a heartfelt thanks to Jeff Bruce, my first research assistant, for his support as I began the research program leading up to this thesis.

A number of others have had a special hand in this work including my lab mates in Cognitive Neuroscience: Chris Striemer, Lana Goldberg, Jason Locklin, Carol Broderick, Colleen Merrifield, Linda Carson, Cecilia Meza, Yael Goldberg, and Brandon Vasquez; the lab coordinators Danielle Striemer, Andrea Schneider, and Nadine Quehl; my lab mates in Theoretical Neuroscience of which there are many but a special mention goes out to Terry Stewart, Xuan Choo, and Bryan Tripp for helping me muddle through the intricacies of the NEF; and, finally, the other members of the Cognitive Neuroscience department who have, as a group (both professors and graduate students) been welcoming, helpful, and considerate.

Finally, a huge thanks to my large and fantastic family: the 'boys', Sean and Ben, for having me around the university with them for four years and only being slightly mortified at the prospect; the 'new' girls (Natalia, Jazmin, Naomi, and little Naiymah); my mother, Charlotte, who would have enjoyed this day immensely; my older brothers Chris and Sebastian for being such great brothers; my younger sibs (Dianne, Ian, Robin) for bringing new life into my family; my great friend Chris Tchorzewski; and, importantly, to an incredible step-mom, Hilde, who supported me for many years under all sorts of circumstances.

Dedication

This thesis is dedicated to two people:

Dr. Harry M. B. Hurwitz, professor emeritus, University of Guelph, the intellectual hub of my life and a great father besides. There are not enough words or sufficient time in a dedication to say what needs to be said.

Samantha Kerr Hurwitz, for the emotional and personal support to pursue my dream of obtaining a PhD. A bright spirit and a fabulous life partner. I couldn’t wish for better.

Table of Contents

List of Figures

List of Tables

Chapter 1: Static and Dynamic Judgments of Spatial Extent

Judgments of spatial extent are central to our interactions with the physical world. Consider the daily task of crossing the street: first, you move up to the curb; then you look to see what is coming and make judgments about the speed, distance, and acceleration of the cars or bicycles; finally, you judge what walking speed will allow you to cross safely. While the task is ordinary, the computational requirements to do this safely under many different circumstances are extraordinary. It is unsurprising, then, that after over a century of research there are still many questions to be answered about how spatial extent is processed in the human brain.

1.1 Behavioural Studies

One simple probe of the capacity to judge spatial extent is the line bisection task, in which individuals are presented with a line and are asked to mark the subjective midpoint (Wolfe, 1923). This task was chosen by Wolfe to explore whether Weber's Law (i.e., that the bisection error would be proportional to the length of the line) was as applicable to judgments of spatial extent as it was to other psychophysical variables such as luminance discrimination.

Since Wolfe's early experiments, line bisection has been used repeatedly with healthy individuals to probe spatial perception because of the ease with which it can be administered and because the results represent a quantifiable probe of how the brain interprets spatial extent. The task has also been used extensively as a diagnostic tool for disorders of spatial cognition including hemispatial neglect, a condition in which patients typically fail to attend to the left half of space (Danckert & Ferber, 2006). Neglect patients bisect lines (far) to the right of true center whereas healthy participants show an opposite bias (i.e., small leftward errors), a phenomenon known as 'pseudoneglect' (Bowers & Heilman, 1980). The pseudoneglect shown by healthy individuals depends on many factors (Table 1).

Table 1. A partial list of factors affecting line bisection biases in healthy individuals

Factor	Experimental papers
Line orientation and location	Bradshaw, Nathan, Nettleton, Wilson, & Pierson, 1987; Butter, Mark, & Heilman, 1988; Halligan & Marshall, 1993; Ishiai, Furukawa, & Tsukagoshi, 1989; Luh, 1995; McCourt & Jewell, 1999; McCourt & Garlinghouse, 2000a; Mennemeier, Rapcsak, Pierce, & Vezey, 2001; Mennemeier, Vezey, Chatterjee, Rapcsak, & Heilman, 1997; Nicholls, Mattingley, Berberovic, Smith, & Bradshaw, 2004; Nielsen, Intriligator, & Barton, 1999; Reuter-Lorenz, Kinsbourne, & Moscovitch, 1990; Wolfe, 1923
Line length	Manning, Halligan, & Marshall, 1990; Mennemeier et al., 2001; Mennemeier, Pierce, Chatterjee, Anderson, Jewell, et al., 2005; Rueckert, Deravanesian, Baboorian, Lacalamita, & Repplinger, 2002
Line geometry	McCourt & Garlinghouse, 2000b; McCourt, Garlinghouse, & Reuter-Lorenz, 2005
Scanning direction	Brodie & Pettigrew, 1996; Brodie & Dunn, 2005; Nicholls & Roberts, 2002
Cueing	Harvey, Pool, Roberson, & Olk, 2000; Mennemeier et al., 2005; Milner, Brechmann, & Pagliarini, 1992; Nichelli, Rinaldi, & Cubelli, 1989
Other stimulus properties	Bradshaw, Bradshaw, & Nathan, 1986; Gallace, Auvray, & Spence, 2007
Task instruction	Fink, Marshall, Weiss, Toni, & Zilles, 2002; Nicholls, Mattingley, & Bradshaw, 2005; Riestra, Womack, Crucian, & Heilman, 2002
Sense modality	Baek et al., 2002; Bradshaw, Nettleton, Nathan, & Wilson, 1983; Bradshaw, Bradshaw, & Nettleton, 1989
Body position	Bradshaw, Nettleton, Nathan, & Wilson, 1985; Chokron & Imbert, 1993a
Participant age	Bradshaw, Nettleton, Wilson, & Bradshaw, 1987; Failla, Sheppard, & Bradshaw, 2003; Fujii, Fukatsu, Yamadori, & Kimura, 1995; Varnava & Halligan, 2007
Handedness and hand used to perform bisection	Bradshaw et al., 1983; Fukatsu, Fujii, Kimura, Saso, & Kogure, 1990; Hatta & Yamamoyto, 1986; Lavanchy, Mayer, & Hauert, 2004; Levander, Tegnér, & Caneman, 1993; Sampaio & Chokron, 1992
Learned reading direction	Chokron & Imbert, 1993b; Chokron & Agostini, 1995; Chokron, Bartolomeo, Perenin, Helft, & Imbert, 1998; Speedie et al., 2002
Non-neglect clinical conditions	ADHD: Sheppard, Bradshaw, Mattingly, & Lee, 1999 Tourette's: Sheppard, Bradshaw, & Mattingley, 2002 Schizophrenia: Cavézian, Danckert, Lerond, Daléry, d'Amatao, & Saoud, 2007; McCourt, Shpaner, Javitt, & Foxe, 2008

In a meta-analysis of line bisection in healthy individuals, Jewell & McCourt (2000) concluded that scanning direction was one of the strongest factors influencing biases. Scanning is particularly interesting because many (if not most) judgments of distance, midpoints, or other spatial information are actually made when objects are moving across the visual field such as when catching a ball, making use of optic flow during walking, looking at very large objects, performing visual searches, or crossing the road. Results of their meta-analysis indicated that left-to-right (L-R) scans resulted in bisection behaviour biased to the left of centre whereas no bias was found for R-L scans. The experiments included in the meta-analysis, as well as those conducted since (Appendix A) suggest scanning results have actually been quite variable, with one paper even finding that R-L scans produce bisections to the left of L-R scans (Nicholls & Roberts, 2002). Furthermore, none of these experiments investigated whether scanning produced overall differences (i.e., collapsed across direction) from the viewing of objects that were not scanned, or whether judgments of spatial extent were affected by the speed of the scan. Prior to addressing these questions, it is useful to consider how the specific tasks used might explain the disparate results seen between dynamic bisection experiments.

1.1.1 Scanning Protocols

Two scanning protocols (i.e., eye movement in a specific direction prior to direction) have been used to investigate dynamic bisection[1]: in the first, participants were instructed to scan a horizontally presented line either L-R or R-L (Brodie & Pettigrew, 1996; Brodie & Dunn, 2005) and to manually bisect the line with a pencil. Bisections preceded by a L-R scan were uniformly leftwards of those preceded by a R-L scan (mean bisection biases for both scan directions were left of center; Appendix A). In the second protocol a vertical mark began at one end of the line and traversed it either L-R or R-L (Chiba, Yamaguchi, & Eto, 2006; Chokron et al., 1998; Nicholls & Roberts, 2002; Reuter-Lorenz & Posner, 1990). Participants tracked the mark with their eyes and stopped it at the perceived midpoint. With this protocol, some (Chiba et al., 2006; 1990) have found no effect of scan direction, including no significant bias away from true center. Chokron and colleagues (1998) found that L-R

[1] In this thesis, studies which use reading direction as a proxy for scanning behaviour have been left out as it is unclear to what extent scanning influenced the results (Chokron & Imbert, 1993b; Chokron & Agostini, 1995; Nicholls & Roberts, 2002 - multiple paradigms were investigated in this paper including reading direction; Speedie et al., 2002).

scanning led to a leftward bias and R-L scanning to a rightward bias. Finally, Nicholls & Roberts (2002) found that all bisections were left of center with this protocol, however R-L scanning produced a greater leftwards bias than L-R scanning. In other words, bisection biases in scanning experiments using the second protocol were far from consistent, unlike those using the first protocol.

One reason for the lack of agreement could be that scanning in each case refers to different tasks. For the first protocol, because there was no moving object, scanning involved saccadic eye movements made to the lines' end points with the assumption that such eye movements required participants to attend to the full length of the line in a specific order (e.g., L-R vs. R-L). While the second protocol involved following a slowly moving mark (smooth pursuit eye movements), only half the line was ever explored directly. In addition, all instances of this protocol used very slowly moving objects which, in turn, meant the task took a substantial amount of time to complete (i.e., the moving mark traveled at about 2 cm/sec thus taking 2.5 seconds to reach the midpoint of a 10 cm line). The slow speed of the mark was in fact deliberate, "so as not to restrict the visual exploration," (Chokron et al., 1998, p. 176) presumably for the benefit of the neglect patients involved in the experiment. However, for the healthy participants, it leaves open the question as to what else they were doing during the long scan time. There is also the question as to how differences in speed might influence bisection results, especially as scanning in a natural setting is rarely done so slowly. For instance, it is possible that the length of time spent scanning the object is a factor in bisections. In addition, the second protocol did not allow for post-scan saccades which may be crucial in verifying one's judgment of spatial extent. Finally, responses in the first protocol were made via paper-and-pencil line bisection (i.e., the hand), whereas the second protocol relied on the participant stopping a mark either by verbal command or button press, which is likely to have been directed by the eyes and hence utilized a gaze-centered reference frame. This last difference, which essentially invokes either a hand or gaze-centered reference frame, is non-trivial as each reference frame may compute spatial extent in an effector-specific manner. Surprisingly, the dissociation between hand and eye coordinate systems has not been quantified in line bisection, nor has it been incorporated as a potential confound (Jewell & McCourt, 2000) even though a number of authors have remarked upon it.

1.2 Neural Correlates

Hemispatial neglect is a common consequence of damage to the right inferior parietal and superior temporal cortex in which the patient behaves as if the left half of the world has ceased to exist

(Karnath et al., 2001; Mesulam, 1981; Mort et al., 2003). As noted previously, when left neglect patients perform the line bisection task they typically bisect to the right of veridical center. The greater prevalence of neglect following right hemisphere damage has led some to posit the critical importance of right parieto-occipital regions in spatial judgments. In particular, regions of right inferior parietal cortex and the temporo-parietal junction have been primary candidates for judgments of spatial extent (Danckert & Ferber, 2006).

In support of this patient evidence, the regions found to be activated in studies of static line bisection using a variety of neuroimaging techniques such as functional magnetic resonance imaging (fMRI), event related potentials (ERP), and magnetic source imaging (MSI) include the cerebellum (with the vermis and an area near the left lateral fissure), striate and extrastriate cortex bilaterally, right superior parietal cortex, and regions of (generally right) inferior parietal and superior temporal cortex (Billingsley, Simos, Sarkari, Fletcher, & Papanicolaou, 2004; Fink, Marshall, Weiss, Shah, Toni, Halligan, & Zilles, 2000a; Fink, Marshall, Shah et al., 2000; Fink, Marshall, Weiss, & Zilles, 2001; Fink et al., 2002; Foxe, McCourt, & Javitt, 2003; R. S. Marshall et al., 1997; Waberski et al., 2008; Weiss, Marshall, Wunderlich, Tellmann et al., 2000). Evidence from ERPs suggests that, in response to a line stimulus, neural activation starts in striate cortex and spreads throughout lateral and medial occipital cortex within the first 100 ms (Foxe et al., 2003; Waberski et al., 2008). Shortly after, right superior parietal cortex is engaged, followed by an iterative activation between occipital cortex and right superior parietal cortex, along with additional activations of right inferior parietal cortex (Billingsley et al., 2004; Foxe et al., 2003; Waberski et al., 2008).

These activations may depend on the task and even on the task instructions. Fink and colleagues conducted a series of fMRI experiments exploring a host of factors including different line orientations (vertical vs. horizontal), different shapes (bisecting a line compared to finding the centroid of a rectangle), different task instructions (Fink, Marshall, Weiss, Shah, Toni, Halligan, & Zilles, 2000b; Fink et al., 2001; Fink et al., 2002), and regions of space (i.e., peripersonal vs. extrapersonal space; Weiss, Marshall, Wunderlich, Halligan et al., 2000). Each of these factors changed the activation patterns observed. As just one example, the lingual gyrus was activated bilaterally when participants were asked to determine whether a transection mark was at the centre of a line but not when they were asked to compare the lengths of the line on either side of the same transection mark (Fink et al., 2002).

Importantly, none of these neuroimaging studies used a dynamic line bisection task. When neglect patients were given a dynamic bisection task (i.e., requiring some form of scanning of the line), instead of bisecting to the right of centre they showed a leftward bias after a L-R scan and a rightward bias after a R-L scan (Chokron et al., 1998; Reuter-Lorenz & Posner, 1990). Indeed, scanning a line from right-to-left *reduced* the rightward bisection biases evident in neglect patients under static bisection conditions. In other words, neglect patients did not show leftward neglect during dynamic bisection but, rather, behaved like healthy individuals with greater biases and variability of response. Similar experimental paradigms involving smooth pursuit eye movements have shown a reduction or reversal of biases in line bisection for neglect patients including object motion (Dunai, Bennett, Fotiades, Kritikos, & Castiello, 1999; Plummer, Dunai, & Morris, 2006), coherent background motion (Kerkhoff, Schindler, Keller, & Marquardt, 1999; Kerkhoff, Keller, Ritter, & Marquardt, 2006), optokinetic stimulation (Choi et al., 2007; Mattingley, Bradshaw, & Bradshaw, 1994), and other techniques that temporarily induce optokinetic nystagmus such as vestibular stimulation or neck muscle vibrations (Adair, Na, Schwartz, & Heilman, 2003; Karnath, Fetter, & Dichgans, 1996; Rubens, 1985). These results have been interpreted to suggest that smooth pursuit eye motion remediates neglect, although no mechanism has been proposed for such an effect[2]. A more parsimonious theory is that symptoms of neglect are largely absent in these circumstances because dynamic bisections recruit brain regions distinct from those engaged in static bisection and that these regions may not be typically damaged in neglect.

Thus, based on both the behavioural and functional evidence, there is good reason to investigate the possibility that separate neural networks exist for dynamic vs. static judgments of spatial extent. Having reviewed the experimental results on dynamic bisection, it is important to complete the picture by considering the various models used to explain bisection data.

1.3 Models of Static Bisection Judgments

There are many theories and models for static judgments of spatial extent. The key phenomena these models attempt to explain include pseudoneglect, i.e., the tendency for bisection errors in short lines to be opposite those observed with long lines (i.e., crossover, first noted by Wolfe, 1923, in healthy

[2] There are known differences between the neural correlates of smooth pursuit eye movements and the networks invoked when making saccades during static judgments (Petit & Haxby, 1999).

individuals and later by Halligan & Marshall, 1988, in neglect patients), a constant Weber fraction (the original Wolfe hypothesis, which also suggests that error grows proportionately with line length), and some task-based effects. Broadly speaking, the models divide along a number of dimensions: the distinction between perceptual explanations and those attributing causes to attentional factors (Chiba et al., 2006); the primary effector or coordinate system used (motor vs. sensory or, put another way, hand-centred vs. gaze-centred coordinate systems); the way the task is carried out (e.g., symmetry judgment vs. line length computation); and the type of modeling used including qualitative, mathematical, or computational approaches. Of course, hybrids and combinations of these exist. The following is a brief review of some of the models and theories, focusing on those which can explain bisection in healthy individuals and exploring their viability as models for dynamic bisection.

The earliest model (Wolfe, 1923) suggested that bisection errors were comparable to other psychophysical results in that they should exhibit a constant Weber fraction. After conducting 80,000 trials on college and school age students, he concluded that there was some evidence for the Weber's Law hypothesis as well as some context effects (i.e., the Weber's Law property failed primarily for the shortest and longest lines). He also noted effects of age and line orientation, and large individual differences in bisection accuracy and bias location (left vs. right for horizontal bisection and up vs. down for vertical bisection).

Another early explanation of line bisection biases was Kinsbourne's theory of hemispheric activation (Kinsbourne, 1970). It proposes that asymmetries of activation in one hemisphere of the brain bias attention to the contralateral side. The causal chain resulting in a line bisection bias starts with hemispheric activation due to a contralateral stimulus. This activation, in turn, over-represents length on the hyper-attended side of the object, thus biasing bisection to one side (Bowers & Heilman, 1980; Bradshaw et al., 1987). If right parietal regions are mostly responsible for static spatial judgments (i.e., line bisection preferentially activates the right hemisphere), then hemispheric activation theory predicts that the left side of the line would appear longer than the right. In other words, there would be a leftward bias in all spatial judgments. In general, Kinsbourne's model has been useful for explaining pseudoneglect in healthy individuals and also has some ability to explain the biases produced by asymmetric task characteristics such as the influence of the hand being used to bisect the line (Bradshaw et al., 1983; Fukatsu et al., 1990; Levander et al., 1993; Rolfe, Hamm, & Waldie, 2008). For example, in a standard paper-and-pencil line bisection task, the hand used to make

the bisection would initially activate the contralateral hemisphere, creating a generalized overrepresentation of the side coincident with the hand being used (i.e., bisecting using the right hand would increase the perceptual length of the right side of the line), thus biasing bisection towards the same side as the hand. In a meta-analysis of data, Jewell & McCourt (2000) did find this pattern, however there were a number of papers which failed to show an effect of hand (Dellatolas, Vanluchene, & Coutin, 1996; Harvey, Milner, & Roberts, 1995a; Mefferd Jr., Wieland, & Dufilho, 1969) and one even demonstrated the reverse pattern (Chokron & Agostini, 1995). By itself, however, this theory is unable to explain crossover due to line length and does not discriminate between hemispheric activations that do or do not produce an effect (although it does make specific predictions about the direction of the effect).

Attentional explanations have focused on task-based asymmetries of attention (Bradshaw et al., 1989; Nichelli et al., 1989). For example, some evidence has been found that cueing attention to one side increases bisection biases towards that side (Harvey, Milner, & Roberts, 1995b; Harvey et al., 2000; Mennemeier et al., 1997; Milner et al., 1992; Reuter-Lorenz & Posner, 1990, however see Mattingley, 1993, who suggested that earlier studies were confounded by the geometry of the placement of the cues). Nicholls & Roberts (2002) investigated which of three factors – scanning direction, pre-motor hemispheric activation, or an attentional bias to the left – was the most likely cause of pseudoneglect in healthy individuals. In their study of native L-R readers and R-L readers, both were biased to the left in two tasks. In the first task, participants made a forced choice between which of two bars with graded luminance (one increasing in luminance from left-to-right and the other from right-to-left, i.e., the 'grayscales task') was darker. If scanning direction was the primary factor, then R-L readers should be biased to the right and L-R readers to the left. Both groups showed a similar leftward bias, however, suggesting that neither hemispheric activation due to pre-motor response nor scanning direction was a valid explanation of the effect. A second task required participants to stop a moving mark when the mark reached the centre of a line it was traversing, having started at one or the other endpoint. The positive correlation between the two tasks lent credence to the possibility of a central mechanism, such as a general leftward attentional bias. In Nicholls' and Roberts' next experiment, attention was cued by the presentation of a brief non-informative cue before (but not during) the grayscales task. Once again, participants showed an overall leftward bias, however this bias was reduced significantly when participants were cued to attend to the right of the line. This was taken as direct evidence for the attentional hypothesis.

Quantitative models of line bisection also exist. Chatterjee and colleagues proposed a psychophysical power law (Chatterjee, Mennemeier, & Heilman, 1994) of the form:

$$\psi = K\varphi^{\beta} \tag{1.1}$$

where φ is the physical length of the line, ψ is the psychological length, and K is a scaling constant which converts physical into psychological dimensions. In an experiment manipulating line length and position, this equation explained 99% of the variance over a range of lengths from 2-32 cm, with both parameters close to unity for healthy participants, and β slightly less than 1 (i.e., a sub-linear relationship between the bisection error as a proportion of the line and the line length). However, different parameter values were needed depending on the presentation position of the line, with the largest variance from unity for lines in right space. The model was updated (Chatterjee, 2002) to quantify the line length effect more precisely. Casting some doubt on the value of this model for individual differences, the exponents and coefficients have been shown to have only moderate test-retest reliability (Pierce, Jewell, & Mennemeier, 2003).

One challenge to attentional models (at least in the case of neglect) is that they fail to explain the hyper-extension of the left side when neglect patients are asked to reproduce a previously viewed line, given only the midpoint to start from (Bisiach, Rusconi, Peretti, & Vallar, 1994; Bisiach, Pizzamiglio, Nico, & Antonucci, 1996). An attentional theory would suggest that leftward production would produce smaller rather than larger leftward extensions. A different view is that representational space is linearly or logarithmically distorted with compression in the ipsilesional side for neglect patients (Bisiach et al., 1996; Bisiach, Ricci, & Mòdona, 1998; Halligan & Marshall, 1991; Milner, 1987, although see Doricchi et al., 2008, and Ferber & Karnath, 2001, for a different interpretation). A subsequent experiment by Geminiani and colleagues (2004) manipulated the velocity profile of a moving object across the screen. An object moving at a constant speed from left to right would look to be accelerating if perceptual or representational space were compressed on the right relative to actual space. This effect was found for the two neglect patients tested relative to healthy individuals. It has also been suggested that the same result could be explained by timing differences between left and right sides of space (Bisiach et al., 1996; Geminiani et al., 2004). By extension, pseudoneglect for healthy individuals could be interpreted either as a slight imbalance between the perceptual

representations of space with the right side of space expanded relative to the left, or as a slight difference in the representation of time between left and right space.

Anderson (1996) suggests that lines are bisected at the point at which the 'salience' is equal on the left and right of the point (i.e., a weighted symmetry judgment where salience represents the weighting factor). Salience is operationally defined by Anderson in two formulae representing the relative contributions of left and right parietal regions, where the coordinate system, represented by the variable *x*, is object-centric (the interpretation of the parameters in Anderson's formulation are illustrated in Figure 1):

$$SD_{L,R}(x) = \frac{SF_{L,R}}{1 + \left(x - M_{L,R}\right)^2 / SD_{L,R}^2} \tag{1.2}$$

Finding the point of symmetry could be done by the brain in one of two ways. The first, as suggested by Anderson (1996), involves guessing the midpoint, computing the total salience to the left and right of the point, and then using the difference between the left and right total salience to choose a new candidate for midpoint (e.g., employing a Newton-Raphson method). The second method involves computing the mean of the distance with a probability density function given by SD_L+SD_R. Given that the brain already encodes spatial position, it would be straightforward and possibly even more computationally efficient to use a weighting method. It is also possible that the technique used depends on the task and the task instructions (Fink et al., 2002). Another possibility is that angles, rather than lengths, are the physical dimension bisected (Nielsen et al., 1999).

Usefully, the Anderson model simulates normal line bisection biases to the left of centre, as well as quite a few of the features of bisection for neglect patients such as crossover, line extension (Bisiach et al., 1994), cueing (including the geometry of the cue-line combination), and the landmark task. In addition, this model produces a power-like scaling law over a range of parameters compatible with the experiments of Chatterjee and colleagues (1994).

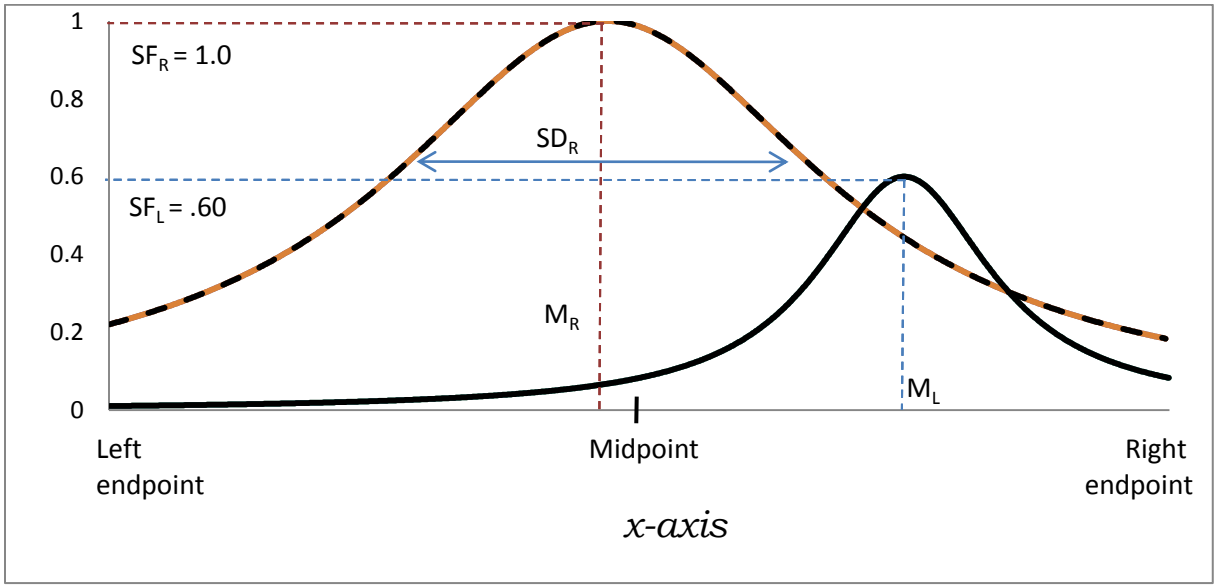

Figure 1. Salience maps for left and right parietal regions.

The dashed line is the salience map for the right parietal region. It over-represents the left side of the line because it is displaced slightly to the left of the midpoint. Similarly, the blue line is the salience map for the left parietal region, and it is highly skewed to the right. The sum of these two salience maps produces a very small leftward bisection bias. SD is the standard deviation; SF is the maximum value of the salience curve; and M is the x-value at which the maximum occurs.

Computational models have also been developed for line bisection. One such, MORSEL, was originally proposed to simulate letter and word perception, but subsequently adapted to explain some of the phenomena associated with line bisection in both healthy and neglect populations (Mozer, 1991, 1997). The model consists of an input array which, for each point in the space being represented, feeds five different types of detectors with a variety of functions (e.g., a line orientation detector for each input point). Both bottom-up and top-down attentional mechanisms guide the processing of information from the detectors but this information transfer is less than perfect, with the result that the standard deviation of bisection errors are proportional to line length. The general leftward bisection error is dues to an in-built attentional bias. MORSEL successfully predicts the effects of line length, line orientation, and some neglect bisection behaviours (see Monaghan & Shillcock, 1998, for a related connectionist model).

In a series of papers, Pouget and colleagues (Pouget & Sejnowski, 1995; Pouget & Sejnowski, 1997; Pouget, Deneve, & Sejnowski, 1999; Pouget & Snyder, 2000; Pouget & Sejnowski, 2001) developed a computational neural model of line bisection that suggests parietal neurons recode combinations of input coordinate system representations for performing sensory-motor transformations. The choice of coding is critical here as some coding schemes are more useful than others. To understand this, consider the navigational problem posed by traveling in a ship across an ocean. In this circumstance, the best way to code position would be using the ship's latitude and longitude. Compare this to the problem of navigating across New York by foot while trying to find the Museum of Modern Art; in this case, it is far more useful to code location and destination by street numbers (i.e., you want to get to the corner of 53rd St. and 6th Ave.). Similarly, Pouget and Sejnowski found that a useful coding scheme for parietal neurons combines Gaussian basis functions for the retinal location of the object with sigmoidal basis functions for the gaze-based location (i.e., each parietal neuron has a tuning curve which is the product of one retinal and one gaze basis function). Motor commands are then produced by linear combinations of this new basis space (the sum of neural outputs). Using this approach, the centre of the line is the sum of activations normalized by the line length. This model does not explain pseudoneglect or the cross-over effect in healthy individuals (although it could easily be modified for pseudoneglect), but it does predict line orientation and length effects, as well as some of the bisection biases found in neglect.

Each of the models discussed above deals only with the static bisection case. Only one theory explicitly incorporates scanning: the 'zone-of-indifference theory' (Manning et al., 1990; Marshall & Halligan, 1989; Marshall & Halligan, 1990) proposes that bisection biases are the by-product of scanning behaviour which, given that most experiments have been conducted on left-to-right readers, is biased toward L-R scanning. The theory proposes that when participants scan into an 'indifference zone' – a point on the line where the line appears to extend the same distance to the left and right – they stop and mark that point as the centre. Since the indifference zone is symmetric about the actual centre of the line, L-R scanning always enters the zone-of-indifference from the left of centre, thus generating a leftward bias. In addition, because the size of the zone-of-indifference region is related to the just noticeable difference measure, errors increase with line size. To explain contrary results that have been found, Marshall and Halligan suggest that some participants adopt a strategy where the zone-of-indifference is traversed and the bisection point is placed where symmetry is broken rather than where it is first observed, i.e., the point of exit from the zone-of-indifference. In this case, the bias would be opposite to the scan direction. There are two problems with this explanation. First, the zone-of-indifference theory can explain within-subject variability (Olk, Wee, & Kingstone, 2004), but it should still yield consistent results for a sufficiently large random sample. However, experiments explicitly controlling the direction of scan have not been consistent, showing biases towards or away from the starting point of the scan. More importantly, the second problem with the zone-of-indifference theory is that normal ocular behaviour is saccadic as opposed to smooth pursuit; experiments measuring ocular behaviour during line bisection have found that healthy participants primarily look towards the centre of the line starting from the *initial* saccade (Barton, Behrmann, & Black, 1998; Ishiai, Furukawa, & Tsukagoshi, 1987; Schuett, Kentridge, Zihl, & Heywood, 2009).

1.4 A Framework for Dynamic Judgments

Most theories assume that distance is 'directly' measured. Imagine, for a moment, computing the midpoint of a line based on an incoming signal from two cameras set nose-width apart. If the cameras were stationary and the full extent of the line easily discernable, software could compute the degree of visual angle subtended, bisect the angle (Nielsen et al., 1999), and choose the radial extension of the bisection angle as the middle – this is an example of a direct computation of spatial extent because it

does not rely on scanning to obtain a measure of the length of the line[3]. There is no reason in this instance for scanning to influence the measurement of spatial extent.

A second direct solution would be to compare the left/right signal strength ratio for points on the line (i.e., a symmetry judgment). This could be done algorithmically as follows:

Step 1. Select a point on the line;

Step 2. If the signal strength is greater to the left of that point than the right, for example, then uses a procedure such as Newton-Raphson to choose a new point to the left of the current position;

Step 3. Repeat steps 1 & 2 until the point chosen is in a zone-of-indifference where signal strength is effectively the same in both directions.

Scanning could influence the choice of an initial bisection point which, in turn, determines the first entry into the zone-of-indifference, the exit point as the eyes leave the zone-of-indifference, or an intermediate value. Thus, while this second model ('pure symmetry judgment') makes no explicit predictions about the relative biases to the left or right of center, it accommodates scanning results which differ from that of free viewing. It is possible to test the pure symmetry judgment theory by considering its correspondence to the results of the experiments where participants only scanned one side of a line, and were asked to stop the mark at the perceptual midpoint (Chokron et al., 1998; Nicholls & Roberts, 2002; Reuter-Lorenz & Posner, 1990). In these experiments, the zone-of-indifference was entered from the same side as the endpoint where the marker started. There would be no need for additional saccades (i.e., steps 1 or 2, above) and the participant should not have exited the zone-of-indifference. In this circumstance, the pure symmetry theory would predict that L-R (R-L) scanning produces bisections to the left (right) of center, a result neither Chokron et al. (1998) nor

[3] This logic can be extended to longer lines which span ocular angles larger than that of peripheral vision. Segments of space can be parsed together as the eye/camera samples it. Doing so requires holding remapped coordinates in working memory (i.e., remembering the angle with which the eye/camera turns between each sample). In other words, saccadic distance is tracked and used as part of the computation. I consider this to be a direct computation of spatial extent although more steps are involved.

Nicholls & Roberts (2002) found. Thus, both of the above direct theories, angle bisection and pure symmetry judgments, are unsupported by dynamic judgment experiments.

Other theories for static judgments discussed in Section 1.3 are also unable to explain dynamic results. There are, however, 'indirect' solutions to the spatial extent problem (by indirect it is meant that distance or position is calculated from variables that are non-spatial rather than a primary measured quantity). The simplest such theory calculates distance using the relationship: distance = velocity x time. For example, if a person runs at a speed of 7 m/s for 10 sec they cover a total distance of 70 m. This theory, called velocity-to-displacement integration (VDI), was proposed by Diekmann and colleagues (2009) based on their experiment investigating the neural correlates for the computation of angular displacement. Participants in a virtual reality environment viewed either the clockwise or counterclockwise movement of a natural scene in which the speed of angular displacement (rotation) was changed at various intervals. During the spatial judgment condition, participants were required to estimate total angular displacement. When the spatial judgment task was contrasted with a suitable control (counting the number of times the angular velocity changed), significant activations were found in the precuneus and cuneus. From this, Diekmann and colleagues proposed that the precuneus acts as a velocity-time integrator. That is, small changes in distance are first calculated by multiplying velocity with time such that angular distance = angular velocity x time. These small computed distances are then summed or integrated to create a total distance estimate. Most generally, VDI suggests that distance estimates can be derived from velocity and time estimates using the integral $d = \int v(t)dt$. This formulation allows distance to be veridically computed even for non-constant velocity profiles such as might be expected for a naturally moving object, or during normal scanning of a scene or object. Of course once the total distance is computed using VDI, it must then be bisected. A method by which bisection can be done using a framework similar to VDI is described in Chapter 4.

Indirect mechanisms imply the existence of a separate neural mechanism for computing distance under dynamic conditions. Interestingly, this possibility has not been investigated in the broader case of dynamic judgments of spatial extent. If such a mechanism does exist then it suggests some interesting consequences. First, a separate dynamic mechanism might produce different biases for dynamic judgments of spatial extent than for static judgments *independent* of factors such as the direction of motion or the speed of scanning. This follows not from anything intrinsic to the

mathematical formulation of the model but, rather, because the neural system invoked may have its own computational biases. Finding overall differences between static and dynamic bisection biases would be strong evidence for separate underlying neural or computational systems. Next, the velocity profile (not simply direction but also speed) of scanning might affect bisection biases. As just one example, Choi and colleagues (2005) set up a moving background of vertical stripes behind a horizontally presented line to induce illusory motion of the line. They found a relationship between bisection biases and the perceived speed of the illusory motion such that the magnitude of the bias (which was in the direction of the illusory motion) increased with the perceived speed of the line (i.e., faster perceived motion induced larger biases). Finally, a separate neural basis for dynamic bisections has implications for the presentation of symptoms of spatial disorders such as neglect. Indeed, it might also be important in considering how various clinical procedures aimed at remediating such disorders work, and how they can be modified to work better.

The overall purpose of this thesis, therefore, is to investigate dynamic judgments of spatial extent from a number of complementary approaches:

1. **Behavioural** (Chapter 2)
    - ascertain differences between static and dynamic bisection biases relative to known factors such as the position of the line in space, and the length of the line
    - determine the influences of velocity (and time) on dynamic bisection
    - ascertain to what extent dynamic bisection behaviour depends on the effector or the scanning protocol
2. **Neuroimaging** (Chapter 3):
    - determine the neural correlates for dynamic bisection
    - investigate differences between static and dynamic bisection
    - investigate the differences (if any) due to scan direction as that is the most well-known of the factors in dynamic bisection
3. **Mathematical and Computational** (Chapter 4):
    - Develop a mathematical model of dynamic bisection

- Implement the mathematical model computationally and in a way that is biologically plausible

Baseline measures for static bisection are obtained in Experiment 1 (a 'free viewing' condition). These results are compared to dynamic bisection behaviour over the course of Experiments 2-4. As well, the latter three experiments investigate dynamic factors including scanning velocity and direction in Experiment 2, and scanning acceleration and timing in Experiments 3 & 4 to determine their influence. The second objective, investigating neural mechanisms, is probed in Experiment 5. The third objective, proposing a model for dynamic bisection, is explored through a mathematical and computational model – the Cumulative Representational Strength (CRM) model of dynamic judgments – which is then further examined using a spiking neural network based on the Neural Engineering Framework (NEF; Eliasmith & Anderson, 2003).

Chapter 2: **Behavioural Experiments**

Before considering dynamic line bisection, it is useful to obtain a baseline of results for static bisection with the same set-up as will be used in the dynamic experiments. The first experiment is a computerized version of the standard paper-and-pencil static task. Both the eyes and the hand used for bisection were measured in order to have comparisons that are relevant to either effector.

2.1 Experiment 1: Free viewing

Ocular and pointing behaviours were examined when bisecting a line under conditions of free viewing. Ocular data was recorded for fixation position, duration of fixation, and saccade amplitude. From this list, two key ocular variables were used throughout all the behavioural experiments: the first fixation (FF), a measure of initial biases in the gaze-centred frame of reference during free viewing or orienting; and the longest fixation (LF; the longest fixation for each trial). Longest fixations were often the final fixation and so might reasonably be assumed to represent the ocular fixation which 'guides' pointing or is most related to an ocular judgment of spatial extent. Also used throughout is pointing behaviour (PB) – the location on the screen touched by the participant – as a measure of biases in hand-centered judgments of centre.

2.1.1 Methods

Participants. Sixteen undergraduates (ages: mean = 18.3 yrs, S.D. = 1.1; 6 male) participated for course credit. Participants were all strongly right-handed as determined by the 22-item Waterloo Handedness Questionnaire. Participants had normal or corrected-to-normal visual acuity and gave consent to the experimental procedure but were naïve to its purpose.

Apparatus. Each participant was seated 57 cm from the monitor with head position fixed by a chin rest. Eye movements were monitored for the right eye only using an EyeLink II (SR Research Ltd.; Mississauga, Canada) with a sampling rate of 500 Hz. All pointing behaviour was performed with the right hand and pointing location was determined using an Elo Intellitouch touch screen (Tyco Electronics; Wilmington, Delaware) running an 17" NEC AccuSync 90 screen (NEC Display Solutions; Itasca, Illinois) with an NVIDIA GeForce 4 Mx440 graphics card (NVIDIA Corporation; Santa Clara, California).

Stimuli and procedure. Lines were 5, 10, or 20 cm long, subtending 5°, 10°, and 20° of horizontal visual angle respectively, and 5.3 mm high (~0.5° angle vertically) presented in black on a light grey background. Each line was positioned in left hemispace, midsagitally, or in right hemispace (L, C, R) such that L and R lines were 2.5 cm from the left and right edge of the screen respectively.

After calibration of the eye-tracker, a short practice session was provided to familiarize participants with the equipment and the instructions. Next, during the pre-trial phase, small circular dots appeared on the screen, one at a time, in one of nine locations forming a grid that covered the screen area used in the experiment for a total of three times at each location (3 x 9 = 27 total presentations). Participants were instructed to touch the dots as quickly and accurately as possible and averages of the top, middle and lower pointing results for each of the L, C, and R columns of the array were used to correct pointing data for the effects of parallax, arm movement, screen calibration biases, or other artifacts (Schuett et al., 2009). At the beginning of each trial a fixation cross, centered horizontally in a vertical plane 11 cm below the eventual position of the line to be bisected, was presented for 1000 ms (Figure 2).

The pre-trial period was followed by presentation of lines with each combination of position and line length pseudorandomly balanced across the nine conditions (10 trials per cell; 90 trials per participant) such that there were no more than two consecutive presentations of any position-length combination. Lines remained visible until the participant touched the screen (participants were instructed to touch the centre of the line as quickly and accurately as possible), followed by an inter-trial interval of between 500 and 1000 ms. During the inter-trial interval, a fixation cross was on-screen and the right hand rested on a pad located directly in front of the participant to ensure consistency of the starting eye and hand position for each trial. All results were collected in a single block of trials and, to prevent drift from contaminating the data, all ocular data was normalized on a trial-by-trial basis to the initial eye position relative to the fixation cross. Trials that included blink artifacts or first fixations that were more than 4 cm past either end of the line (evidence of 'gaze wandering') were excluded, which resulted in discarding about 2.8% of trials across the whole group. Output from the eye-tracker included separate graphs of vertical and horizontal displacements, with fixations represented by solid bars. The first vertical jump in eye-movement from fixation to the line (in the horizontal direction with no indication of gaze wandering) was considered FF, and the bar with the longest fixation time was the LF.

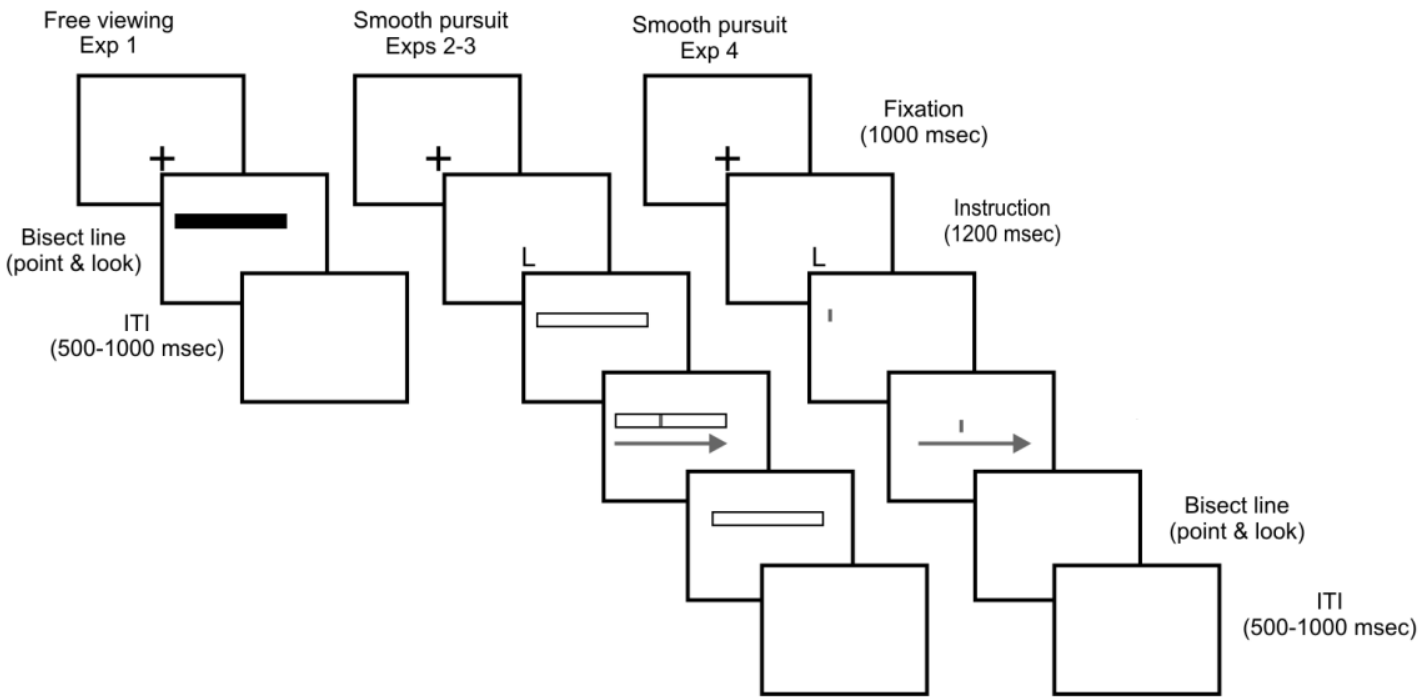

Figure 2. Schematic representation of a single trial for Experiments 1 through 4

In Experiments 1-3 a line (Experiment 1) or rectangular box (Experiments 2 & 3) was on-screen until touched. In Experiment 4, no line was present but, instead, a path was traced by the movement of a small vertical line. After the path was traced, a blank screen appeared until the participant touched it.

2.1.2 Results and Discussion

A repeated measures ANOVA was conducted on FF, LF, and PB separately with position (L, C, R) and length (5, 10, 20 cm) as within-subject variables. There were main effects of position and length for both FF (for position, F(1.05, 15.81) = 82.3, p < .001 [Greenhouse-Geisser corrected d.f. are used throughout wherever Mauchly's test indicates non-sphericity of the data; significance was set at an alpha level of .05 unless otherwise noted; Bonferroni corrections were made for multiple comparisons]; for length, $F(2, 30) = 4.16$, $p = .025$) and LF (for position, $F(2, 30) = 37.07$, $p < .001$; for length, $F(1.38, 20.72) = 4.78$, $p = .030$) but not for PB. Overall, FF was to the right of center when the line was in left hemispace and to the left of center when the line was in right hemispace (Table 4; Figure 3). Longest fixations were biased to the left in left space and to the right in right space whereas PB was biased to the left regardless of line position or length. Larger ocular deviations were seen for longer lines (FF, $M_{20cm\text{-}5cm} = 4.47$ mm, $p = .002$; LF, $M_{20cm\text{-}5cm} = 2.05$ mm, $p = .002$), an effect not seen for PB. There was a significant length-by-position interaction in FF ($F(4, 60) = 2.61$, $p = .044$), driven by a smaller leftward bias for the 5 cm lines presented in central and right, but not left, space, and a length-by-position interaction in LF ($F(4, 60) = 3.57$, $p = .011$), due to the bias increasing with increasing line length in left and central positions but not in right hemispace (Figure 3).

About 94% of trials had five fixations or less. A zero-order correlation analysis of ocular fixations and PB (Table 2) showed that all ocular fixations were highly correlated to each other: e.g., Fixation 1 and 2, $r = 0.74$, Fixation 2 and 3, $r = 0.95$, Fixation 3 and 4, $r = 0.96$. However, none of the correlations between ocular fixations and pointing were significant. Some additional measures of ocular behaviour are summarized in Table 3.

.

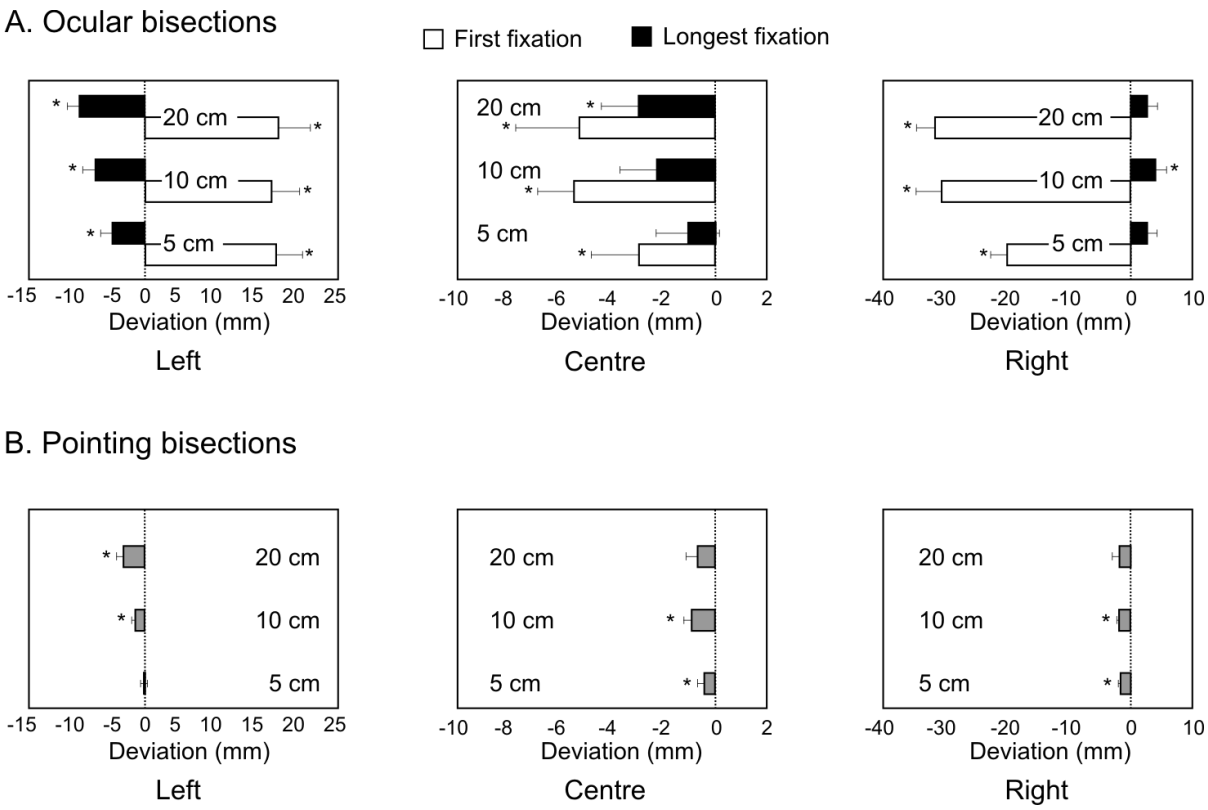

Figure 3. Bisection biases for Experiment 1

For the two sets of graphs: (a) ocular bisection biases are divided up into first fixations (the initial saccade from the fixation cross after the appearance of the line) and longest fixations which, in most cases, is also the fixation during or just before pointing; and (b) pointing, i.e., the place relative to the centre of the line where participants indicated their bisection point to be on the touch screen.

Leftward biases are represented as negative whereas rightward biases are represented as positive. Error bars represent the standard error, with asterisks indicating a value significantly different from zero (i.e., veridical bisection) at an alpha of .05. The two graphs in each column represent data for the spatial position (left, centre, right).

Table 2. Correlation matrix including ocular fixations and pointing

	Fix 1	Fix 2	Fix 3	Fix 4	Fix 5	Fix 6	Fix 7	Fix 8	Fix 9	Pointing
Fix 1	1	.740	.695	.660	.622	.577	.354	.548	.809	.014*
Fix 2	.740	1	.950	.913	.884	.773	.479	.589	.626	-.003*
Fix 3	.695	.950	1	.960	.921	.785	.398	.498	.382	-.004*
Fix 4	.660	.913	.960	1	.974	.854	.510	.593	.367	-.017*
Fix 5	.622	.884	.921	.974	1	.871	.509	.573	.397	-.061*
Fix 6	.577	.773	.785	.854	.871	1	.744	.773	.478	-.068*
Fix 7	.354	.479	.398	.510	.509	.744	1	.870	.417	.023*
Fix 8	.548	.589	.498	.593	.573	.773	.870	1	.897	.045*
Fix 9	.809	.626	.382	.367	.397	.478	.417	.897	1	-.093*
Pointing	.014*	-.003*	-.004*	-.017*	-.061*	-.068*	.023*	.045*	-.093*	1

Elements in the table represent correlations between the row-column. For example, there is a correlation of .740 between the location of fixation 1 and fixation 2. Virtually all fixations are strongly correlated. However, there is no correlation between pointing and any fixation.

*Not significantly different from 0. All other entries are significantly different from 0, and most at $p<.001$.

Table 3. Additional measures of ocular behaviour in Experiment 1

Measure	Line position		Length	
Proportion of line viewed	L	32.4%	5	41.0%
	C	12.4%	10	26.8%
	R	37.8%	20	14.7%
Leftmost Fixation*	L	-8.2%	5	-45.0%
	C	-20.5%	10	-26.3%
	R	-57.1%	20	-14.4%
Rightmost Fixation*	L	28.5%	5	5.5%
	C	-5.1%	10	3.8%
	R	-12.8%	20	1.3%

All measures were computed relative to the line length.

*Negative numbers refer to values left of line centre. Percents are proportion of the total line length.

Table 4. Experiment 1 bisection biases

Variable	Line characteristic	Bisection bias (mm)	SE (mm)
First fixation	Average over all conditions	-5.06*	1.51
	Left hemispace	16.87*	2.85
	Central hemispace	-4.66*	1.60
	Right hemispace	-27.40*	2.83
	5 cm long lines	-2.09	1.50
	10 cm long lines	-6.54*	1.70
	20 cm long lines	-6.56*	2.21
Longest fixation	Average over all conditions	-1.79	1.27
	Left hemispace	-6.37*	1.44
	Central hemispace	-2.12	1.28
	Right hemispace	3.12	1.54
	5 cm long lines	-0.88	1.26
	10 cm long lines	-1.56	1.38
	20 cm long lines	-2.93*	1.34
Pointing behaviour	Average over all conditions	-1.27*	0.25
	Left hemispace	-1.41*	0.52
	Central hemispace	-0.71*	0.24
	Right hemispace	-1.70*	0.46
	5 cm long lines	-0.70*	0.21
	10 cm long lines	-1.32*	0.23
	20 cm long lines	-1.80*	0.49

Biases are measured from the center of the line and negative values indicate a bisection bias left of center.

*Significantly different from 0.

2.2 Experiment 2: Constant velocity scanning

Next, the hypothesis that scanning, including both the direction and speed of scanning would influence bisection behaviour was explored.

2.2.1 Methods

Participants. Twenty-nine undergraduates (ages: mean = 18.6 yrs, S.D. = 1.7; 9 male) participated for course credit. Participants were all strongly right-handed as determined by the Waterloo Handedness Questionnaire and had normal or corrected-to-normal acuity. Participants gave consent to the experimental procedure but were naïve to its purpose.

Apparatus. The equipment and set-up were identical to that used in Experiment 1.

Stimuli and procedure. As before, there was a pre-trial phase during which calibration data was collected. Each experimental trial began with a centrally presented fixation cross (Figure 2) followed by either the letter L or R in the same location for a total time of 1200 ms. The letter indicated the direction from which participants were to start scanning the line. A narrow horizontal rectangle then appeared (5, 10, or 20 cm long; 5 mm high) positioned, as in Experiment 1, in left, central, or right space. After a brief delay a red vertical mark traversed the interior of the rectangle from one end to the other and participants were instructed to follow the moving mark across the entire line. Once the mark had traversed the line participants were instructed to touch the center of the line as quickly and accurately as possible. During the practice phase, ocular motion was informally monitored by the experimenter to ensure that participants understood the instructions and smooth pursued the mark. Position and line length were pseudorandomly balanced such that no more than two consecutive presentations of any combination of line, position, and scanning direction appeared (3 positions x 3 line lengths x 2 scanning directions = 18 cells, 5 trials per cell = 90 trials total). Two speeds, 11 cm/sec (N=11) and 22 cm/sec (N=18) were used as a between-subjects variable to ensure that the total completion time for the experiment was reasonable. Trials were discarded for the same reasons as in Experiment 1, but also if there was evidence that the participant had not smooth pursued the mark. This resulted in discarding approximately 1.1% of all trials.

2.2.1 Results and discussion

A 3 (position; L,C,R) x 3 (line length; 5, 10, 20 cm) x 2 (scan direction; L-R, R-L) x 2 (scan speed; 11 cm/s, 22cm/s) mixed model repeated measures ANOVA was computed with scan speed the only between-subjects variable (Figure 4, Table 5).

No main effects were found due to scanning speed but there was a significant length-by-speed interaction for FF. This was driven by the slower velocity mark producing an exaggeration of the leftward bias for the longest lines (Figure 5a). There was also a significant three-way interaction between position, scan direction and speed for FF (Figure 5b). For the faster speed, biases were to the left of centre following L-R scans and to the right of centre following R-L scans. Importantly, this was not modulated at all by the position of the line. In contrast, for the slower speed, bisection biases were modulated by the position of the line. For L-R scanning, bisection biases were to the left of center in left hemispace and to the right in right hemispace (centrally presented lines showed no bias). For R-L scans all bisection biases were to the left of centre and, although there appeared to be a trend for a larger leftward bias for lines in left versus right space, it was not statistically significant (Figure 5b).

There was a main effect of line length for FF, LF, and PB, with progressively larger leftward deviations for longer lines (Figure 6). In addition, there was a main effect of position for FF and LF but not for PB. In Experiment 1 the main effect of position on FF was a large rightward deviation for lines in left space and leftward deviations for lines in right space (Figure 3); in this experiment, however, when biases were collapsed across line length, both FF and LF were biased to the left in left hemispace and to the right in right hemispace (FF, M_{LH} = -2.94 mm, M_{RH} = 0.70 mm; LF: M_{LH} = -2.63 mm, M_{RH} = 1.56 mm), and such biases were smaller in magnitude than those observed in Experiment 1 (Table 4). Pointing behaviour, in contrast, was uniformly biased to the left (means of -1.85, -1.97, -1.52 mm for L, C, and R space lines respectively) as in Experiment 1 (Table 4).

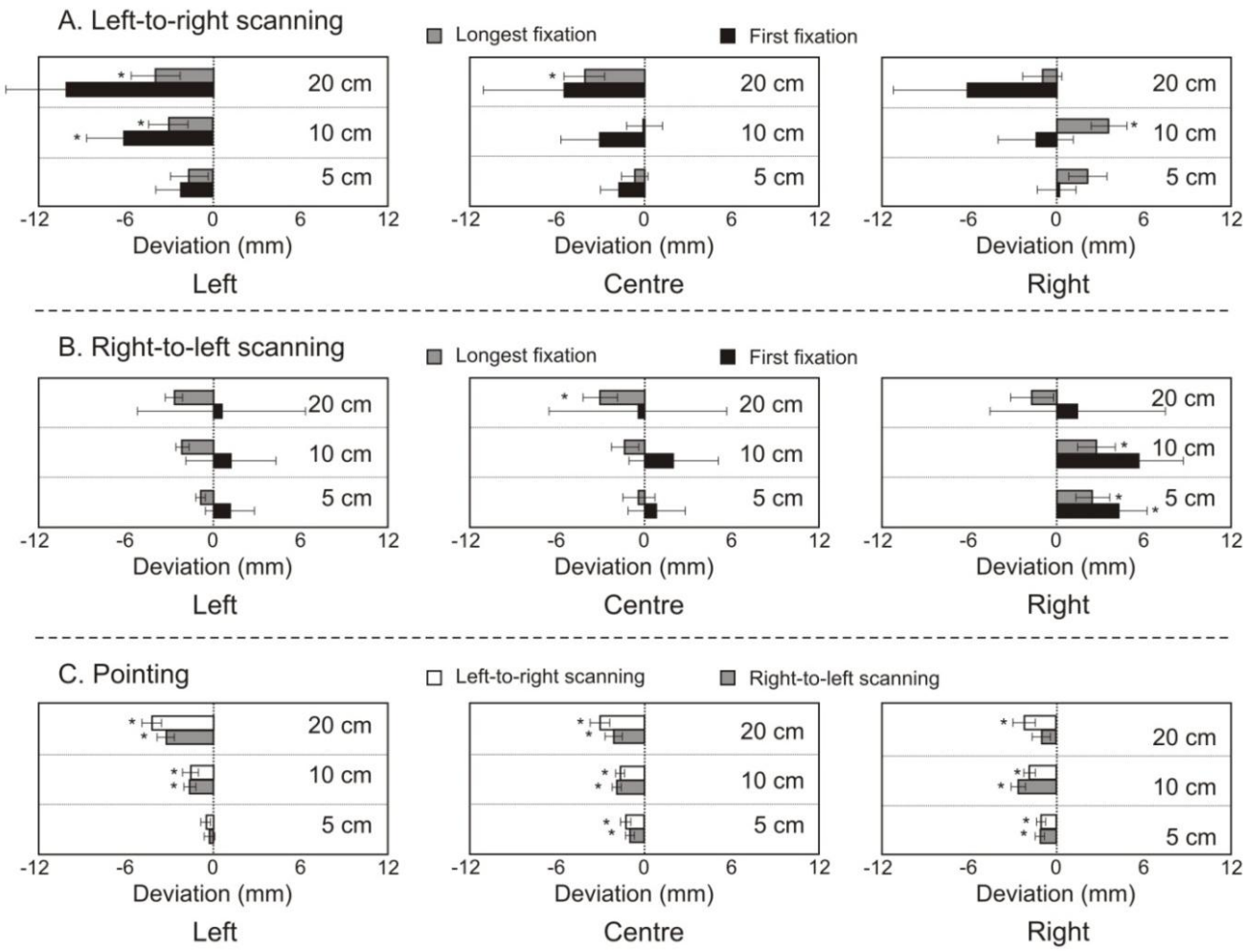

Figure 4. Bisection results, relative to the centre of the line, for Experiment 2

Results of Experiment 2 collapsed across speed: (a) left-to-right scanning presented for ocular measures (FF and LF); (b) right-to-left scanning presented for FF and LF; (c) pointing behavior presented with both L-R and R-L scanning on the same chart. Error bars represent standard error, and asterisks represent significance at an alpha of .05.

Table 5. Experiment 2 ANOVA results

Variable	Main Effect	*F*	*p*
First fixation	Position (P)	6.05*	.010
	Length (L)	16.15*	<.001
	Scan direction (Sc)	<1	n.s.
	Speed (V)	<1	n.s.
	P x Sc	3.73*	.035
	L x V	4.97*	.017
	P x Sc x V	4.06*	.027
Longest fixation	Position (P)	12.52*	<.001
	Length (L)	16.56*	<.001
	Scan direction (Sc)	<1	n.s.
	Speed (V)	<1	n.s.
	P x L	2.92*	.048
Pointing behaviour	Position (P)	<1	n.s.
	Length (L)	11.22*	.001
	Scan direction (Sc)	<1	n.s.
	Speed (V)	<1	n.s.
	P x L	18.19*	<.001
	L x Sc	3.52*	.050

*Significant at $p < .05$. Interactions were only included if significant.

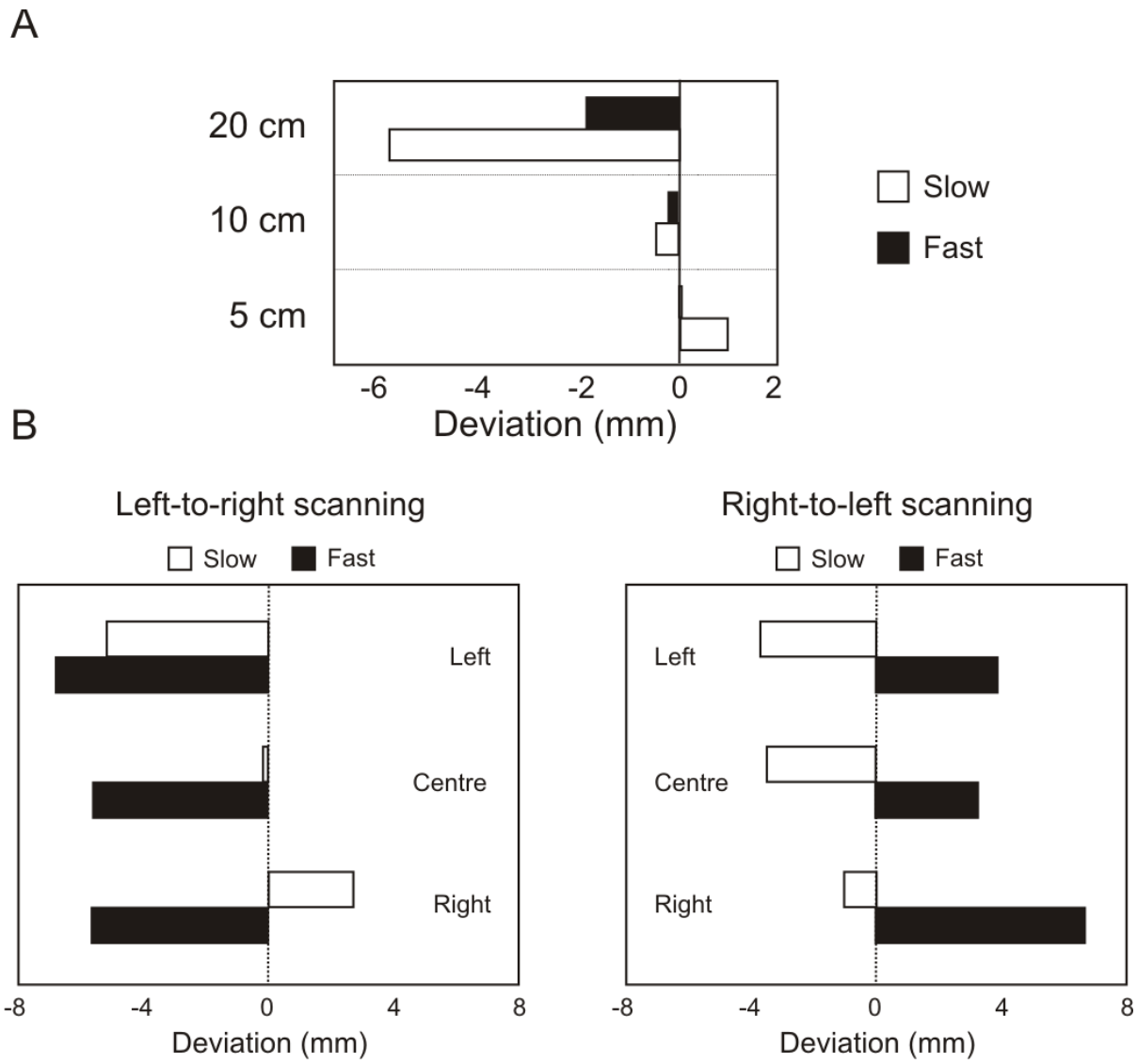

Figure 5. Bisection biases for first fixations (FF) in Experiment 2

Results for Experiment 2: (a) collapsed across scan direction and line position to illustrate the two-way line length-by-speed interaction; (b) collapsed across length to illustrate the three-way position-by-scan direction-by-speed interaction. The slow speed is 11 cm/s while the fast speed is 22 cm/s.

Four interactions not involving scanning speed were significant (Table 5). The position by length interaction for LF was due to the fact that, for 5 and 10 cm lines, bisections were biased leftward in left space but rightward in right space (Figure 6a). For the position by length interaction for PB, the shortest two lines showed a consistent leftward bias, with the same leftward biases being larger for the 20 cm line in left space (Figure 6a). The position by scan direction interaction for FF (Figure 6b) was driven by an exaggerated (leftward) bias in left space for L-R scanning, whereas there was a large (rightward) bias in right space for R-L scanning. Finally, there was a length by scan direction interaction for PB such that bisections of the longest lines made after scanning L-R were to the left of bisections made after scanning R-L (Table 5).

Next, to investigate whether there is a separate mechanism involved in dynamic judgments of spatial extent, Experiments 1 and 2 were compared using a mixed model ANOVA with position (L, C, R) and line length (5, 10, or 20 cm) as within-subject variables, and Experiment (1 vs. 2) as a between-subjects variable. The data from Experiment 2 was collapsed across scan direction and speed for the purposes of this comparison. There was a significant main effect of experiment for FF[4] (F(1, 49), p = .021) but not for LF or PB (F(1, 49) = 0.32, p = .576 and F(1, 49) = 3.19, p = .080, respectively). There were position by experiment interactions for FF (F(2, 98)= 163.50, p < .001), and LF (F(2, 98) = 7.74, p = .001).

The LF interaction was due to the fact that free viewing led to a larger leftward bias for lines viewed in left space with no difference across experiments for lines in central or right space (Figure 7). Next, there was a three-way interaction between position, length, and experiment for LF (F(2.6, 129.1), p = .032), due to a reversal of biases in right hemispace for the longest line only (Figure 7). Finally, as mentioned before for ocular behaviour (FF and LF), slower velocities produced larger biases in all locations (i.e., leftward biases in left space were larger following the slow velocities and vice versa for right space; Table 3). For PB, however, all biases were approximately the same regardless of the speed of the mark, or even whether the judgment was static or dynamic.

[4] First fixations in free viewing may be an orienting response to the appearance of the line. In the scanning experiments, however, the line is on-screen prior to FF and no orientation response was expected. Because of this it may not be appropriate to compare results for FF between Experiment 1 and any of the other behavioural experiments. The same is not true, however, for LF and PB – differences in either of these measures suggest differences in static versus dynamic judgments.

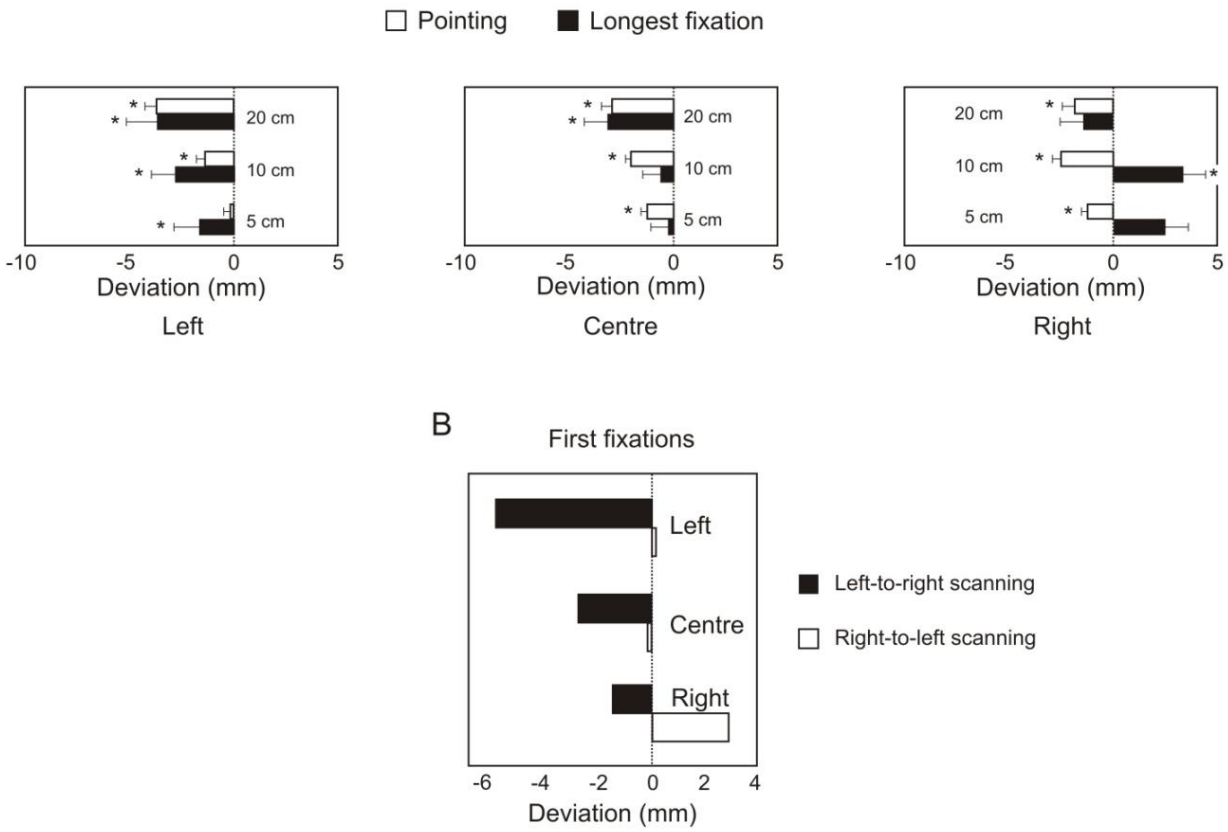

Figure 6. Experiment 2: Bisection results for interaction effects not involving scanning speed

Results for (a) the two-way length-by-position interactions for LF and PB, and (b) the two-way length-by-scan direction interaction for FF.

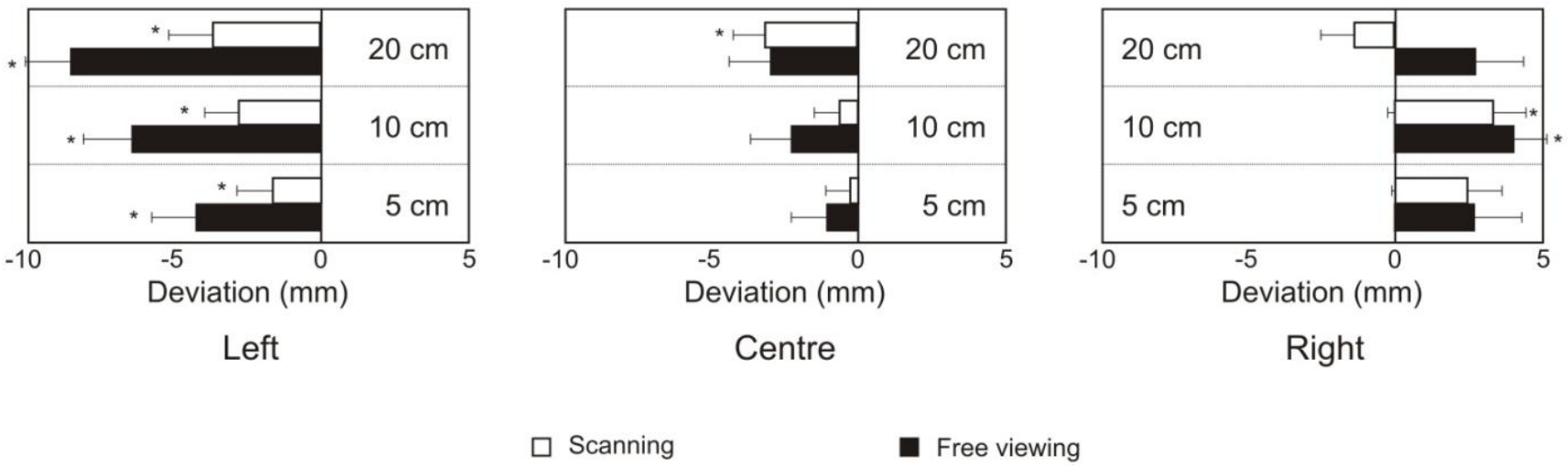

Figure 7. Comparison between Experiment 1 and Experiment 2 for longest fixations

The greater leftward biases for free viewing in left space illustrate the two-way position-by-experiment interaction. There is also a three-way position-by-length-by-experiment interaction seen in the leftward bias for the 20 cm line during scanning. Standard error bars are shown, with asterisks representing results significantly different from zero at an alpha of .05.

Table 6. Effects of velocity on bisection biases for Experiment 2

Measure	Condition	Slower velocity	Faster velocity	Static (Experiment 1)
First fixation	Average over all conditions	-1.38	-0.74	-5.06*
	Left hemispace	-3.93	-2.01	16.87*
	Center	-1.46	-1.04	-4.66*
	Right hemispace	1.26	0.82	-27.40*
Longest fixation	Average over all conditions	-0.89	-0.87	-1.79
	Left hemispace	-3.78	-2.08	-6.37
	Center	-1.47	-1.30	-2.12
	Right hemispace	1.26	0.76	3.12
Pointing behaviour	Average over all conditions	-1.87	-1.97	-1.27
	Left hemispace	-1.81	-1.75	-1.41
	Center	-2.35	-1.98	-0.71
	Right hemispace	-1.45	-2.18	-1.70

All results in mm. Negative values correspond to bisection biases to the left of line center.

*Given that first fixations in Experiment 1 were most likely an orientation response, it may not be useful to compare first fixation data from Experiment 1 with either the slower or faster velocity conditions of Experiment 2.

2.3 Experiment 3: Non-constant velocities

The effects of scanning direction and speed outlined in Experiment 2 support the notion that participants were influenced by both scanning speed and direction in their bisection behaviour. In addition, scanning produced biases between dynamic and static bisection. Experiment 2 did not, however, explore whether acceleration or timing influences bisection biases. Given that neglect, commonly induced by a lesion to right parietal cortex, leads to an anisotropy of perceived space (Bisiach et al., 1996; Geminiani et al., 2004; Halligan & Marshall, 1991; Milner, Harvey, Roberts, & Forster, 1993) and also involves the same brain area generally believed to be implicated in timing and time perception (Battelli, Pascual-Leone, & Cavanagh, 2007; Danckert et al., 2007; Harrington, Haaland, & Knight, 1998), it is conceivable that there is a coincident spatio-temporal mechanism important to the perception of space (Becchio & Bertone, 2006). In a single case study, Basso et al. (1996) demonstrated a spatio-temporal gradient in a neglect patient such that the further leftward an object was presented, the more temporal durations were overestimated. If similar, although potentially smaller, spatio-temporal distortions affect healthy individuals there would be interesting consequences. For instance, such distortions would not be affected by scan direction but could be affected by the position and/or length of the line. If so, the position-by-length interaction terms in Experiment 2 could have been due to spatio-temporal anisotropies.

Constant velocity probes cannot disambiguate between spatial anisotropies and spatio-temporal anisotropies. It is possible, however, to investigate spatio-temporal anisotropies by using non-constant velocity probes. This can be understood as follows: consider the case of a mark travelling L-R with two different accelerations: in the first condition, A, the mark starts at a slow speed, v_s and accelerates to a fast speed, v_f. In the second condition, D, the mark starts at v_f and decelerates to v_s. Now imagine we have chosen our conditions such that that the mark spends two seconds on the side with the slower velocity and one second on the faster side. In Condition A the mark spends two seconds on the left and one second on the right. In Condition D it spends one second on the left and two on the right. If bisection only depends on position (i.e., a spatial anisotropy only) we would predict the same bias for both A and D conditions. As well, because the velocity profile is the same (albeit reversed) in both conditions, speed should not introduce bisection biases between the conditions. However, if the participant has a spatio-temporal anisotropy such that time is overestimated on the left half of the line, for example, this overestimation magnifies the bias by a factor of two on the left in Condition A

relative to D. The reason for this is that, in the formula $d = v \times t$, d grows in direct proportion with t – any overestimation of t leads to an overestimation of d. Similarly, Condition D produces right side overestimation relative to A. The net effect would be a difference in biases between A and D. The failure to find such a difference would mean we should not accept the hypothesis that there are spatio-temporal anisotropies in healthy individuals.

2.3.1 Methods

Participants. Sixteen undergraduates participated for course credit in Experiment 3 (mean age= 18.6 yrs, S.D. = 1.2; 9 male). Participants were all strongly right-handed as determined by the Waterloo Handedness Questionnaire. Participants had normal or corrected-to-normal acuity and gave consent to the experimental procedure but were naïve to its purpose.

Apparatus. The equipment and set-up were identical to that used in Experiment 2.

Stimuli and procedure. To determine whether different acceleration/deceleration profiles would prove critical in demonstrating spatio-temporal distortions two distinct acceleration/deceleration profiles were used (Profile 1: velocity increased from 11 cm/s to 22 cm/s or decreased from 22 cm/s to 11 cm/s; Profile 2: velocity increased from15cm/s to 22.5 cm/s or decreased from 15 cm/s to 7.5 cm/s). In total, there were three acceleration/deceleration conditions in each profile: acceleration (A), constant velocity or no acceleration (N), and deceleration (D). For the N condition the mark traveled at a constant velocity which was the average of the velocity in the A condition (i.e., Profile 1 used 16.5 cm/s, Profile 2 used 15 cm/s). Each participant completed 2 trials for each cell of the 3 (position) x 3 (line length) x 2 (scan direction) x 3 (acceleration condition) design (108 trials total). Approximately 5.9% of all trials were discarded for artifacts including blinks, gaze-wandering, and failure to smooth pursue the mark.

2.3.2 Results and discussion

First, a mixed model ANOVA was run with acceleration profile as a between-subjects variable and with position, length, scan direction, and acceleration condition as within-subject variables. There were no significant main effects or interactions for the acceleration profile (all F's<1, n.s.) across all three measures – FF, LF, and PB. It appears, then, that using different acceleration profiles within the range considered is not a relevant factor. Given the lack of significant differences, all further analyses were collapsed across acceleration profile. Results of the ANOVA on the within-subject variables

(Table 7) showed a significant effect of position for FF and LF driven by a leftward bias for lines in left space ($M_{FF,left\ position}$= -1.5 mm, $M_{LF,left\ position}$= -3.4 mm) and a rightward bias for lines in right space ($M_{FF,right\ position}$= 6.0 mm, $M_{LF,right\ position}$= 2.4 mm). This effect was confirmed by post-hoc t-tests on the difference scores (FF left-right $t(15) = 3.70$, $p = .002$, LF left-right $t(15) = 4.38$, $p<.001$; Figure 8a). There was a significant main effect of line length for LF and PB which, in both cases, was driven by an increasing leftward bias for the longest lines (paired comparison t-tests for LF of 5 vs. 20 cm, $t(15) = 3.47$, $p = .003$; 10 vs. 20 cm, $t(15) = 3.07$, $p = .008$; and for PB with all comparisons significant at $p < .05$).

Only FF showed a main effect due to scan direction (Table 4). For this case, L-R scanning produced a rightward bias significantly different from the R-L scanning (M_{L-R} = 3.78 mm, M_{R-L} = -1.94 mm; t(29)=4.90, p<.001; Figure 8b). As in Experiment 2, there were two-way interaction terms for PB, i.e., position by line length and line length by scan direction (Table 7). There was an additional two-way interaction of line length and scan direction for FF such that, as line length increased, first fixations for L-R scans were increasingly rightwards whereas the opposite was true for R-L scans (i.e., first fixations were increasingly leftwards as length increased; Figure 8b).

Table 7. Experiment 3 ANOVA results

Variable	Main Effect	*F*	*p*
First fixation	Position (P)	9.73*	.001
	Length (L)	<1	n.s.
	Scan direction (Sc)	9.38*	.008
	Acceleration condition (A)	<1	n.s.
	L x Sc	11.08*	<.001
Longest fixation	Position (P)	17.90*	<.001
	Length (L)	9.43*	.001
	Scan direction (Sc)	2.98	.105
	Acceleration condition (A)	2.86	.099
	P x Sc	3.26	.052
Pointing behaviour	Position (P)	<1	n.s.
	Length (L)	10.88*	.002
	Scan direction (Sc)	1.31	.271
	Acceleration condition (A)	<1	n.s.
	P x L	7.14*	.002
	L x Sc	5.77*	.008

*Significant at $p < .05$. Interactions were only included if $p < .10$

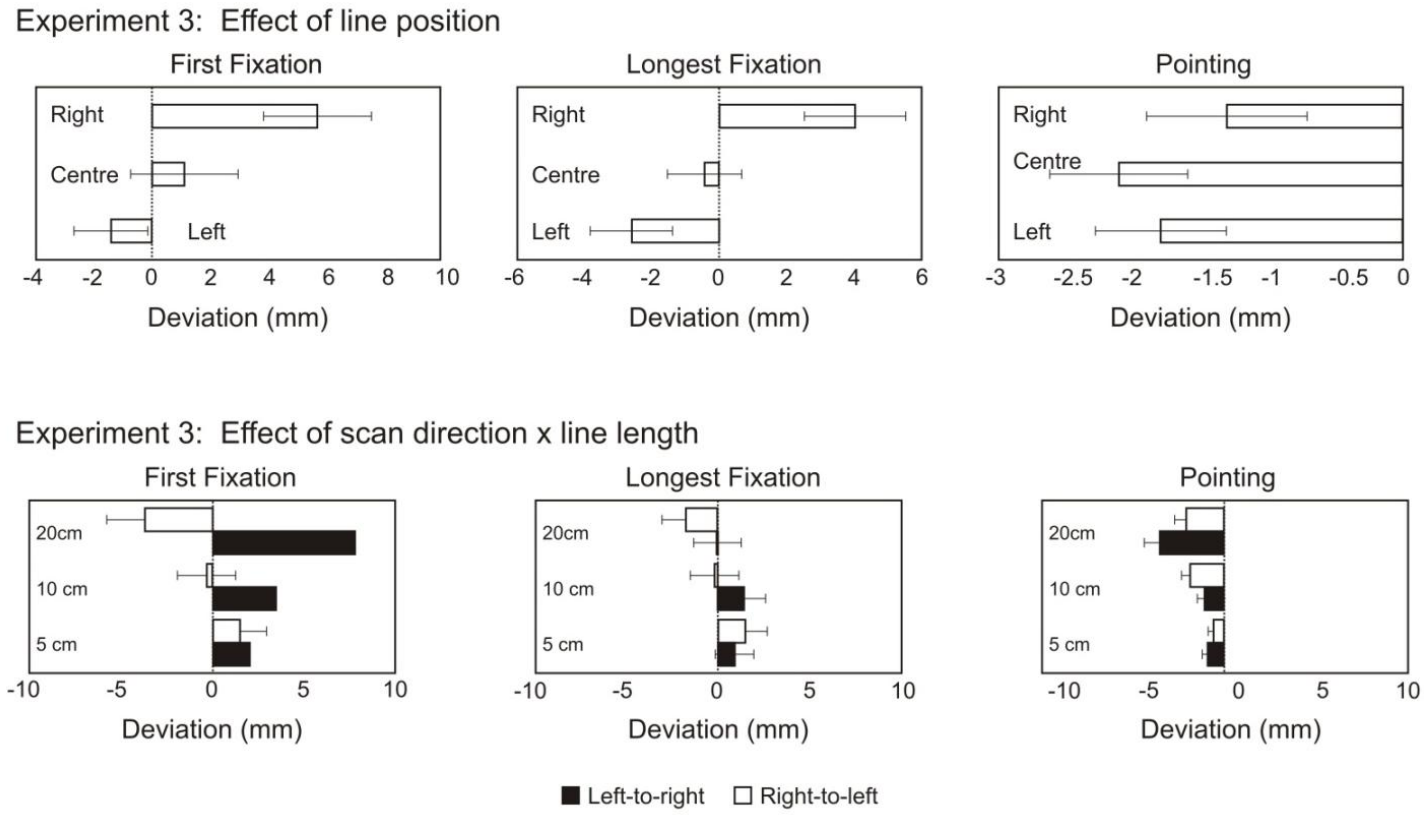

Figure 8. Bisection results of Experiment 3

In (a) both FF and LF show a main effect of position, but not PB. In (b), FF shows a main effect of scan direction while both FF and PB show a two-way length by scan direction interaction. For PB, this interaction is primarily due to the 20 cm (longest) line showing a greater leftward bias after a L-R scan than after a R-L scan

2.4 Experiment 4: Acceleration with invisible lines

Data from Experiment 3 confirmed many of the effects found in Experiment 2 but did not provide evidence for an influence of acceleration or timing on bisection behaviour. One reason for the lack of an effect could be the fact that the line to be bisected remained visible after participants had completed their scan. This would allow for additional processing of the line unrelated to the spatio-temporal probe. In other words, although participants clearly smooth pursued the mark over the full length of each line, it was possible to adopt a strategy akin to the one used under free viewing immediately subsequent to the mark disappearing. A novel task was developed to avoid this problem: the 'no-line experiment' in which the line was removed altogether.

2.4.1 Methods

Participants. Fifteen undergraduates participated for course credit in Experiment 4 (ages: mean = 19.1 yrs, S.D. = 0.8; 8 males). Participants were all strongly right-handed as determined by the Waterloo Handedness Questionnaire and had normal or corrected-to-normal acuity and gave consent to the experimental procedure but were naïve to its purpose.

Apparatus. The equipment and set-up were identical to that used in Experiment 3.

Stimuli and procedure. Experiment 4 was a variant of Experiment 3 in which no line was present (Figure 2). The moving mark traversed a blank screen and participants were to infer the midpoint of the distance traveled by the mark. Only 20 cm lines were used as most of the significant results in the previous experiments involved the longest lines and because longer lines are more likely to uncover spatio-temporal distortions. With only one line length it was necessary to add a spatial jitter to the starting position of the mark to prevent participants from using landmarks to judge the location of the line center. The jitter was chosen randomly from 0-10 mm in either direction on a trial-by-trial basis. Second, since the largest differences were consistently observed for bisections made for lines in left versus right space, centrally presented lines were eliminated. The number of cells in the design was 12 (2 positions x 2 scan directions x 3 acceleration conditions) allowing for 10 trials per cell (120 trials per participant). Only acceleration Profile 1 was used in this experiment, i.e., for the acceleration (deceleration) condition, the initial (final) velocity was 11 cm/s, the final (initial) velocity was 22 cm/s and, and for the constant velocity condition the speed was 16.5 cm/s. As before, trials were discarded for blink artifacts, gaze-wandering, and lack of smooth pursuit, resulting in a loss of approximately 6.9% of all trials.

2.4.2 Results and discussion

A 2 (position) x 2 (scan direction) x 3 (acceleration condition) repeated measures ANOVA conducted on the data (Table 8; Figure 9) showed a main effect of position for FF such that fixations were biased to the right in left space and to the left in right space. Longest fixation biases were more leftward in right space than in left space, which was opposite to the directional biases for LF in the previous three experiments (Table 9). Pointing behaviour, on the other hand, was similar to PB in the other three experiments (i.e., a small leftward bias) but, unlike previous experiments, showed a sensitivity to scan direction similar to that of LF (i.e., a leftward bias after L-R scans and a rightward bias after R-L scans; Table 9)

Left-to-right scans led to fixations that were significantly to the left of right-to-left scans both for LF ($F(1, 16) = 4.91$, $p = .044$, $M_{(L\text{-}R - R\text{-}L)} = -7.18$ mm) and PB ($F(1, 16) = 19.62$, $p<.001$, $M_{(L\text{-}R - R\text{-}L)} = -8.56$ mm). Longest fixations and pointing biases for L-R scans were also significantly different from zero (this was not true for the R-L condition). Acceleration effects approached significance for pointing behaviour ($p = .053$; Figure 10) but not for ocular behaviour. Interestingly, this effect was due to the combination of an exaggeration of leftward biases for decelerating objects in L-R scans with a considerably smaller rightward bias in R-L scans.

Table 8. Experiment 4: ANOVA results

Variable	Main Effect	*F*	*p*
First fixation	Position (P)	12.76*	.003
	Scan direction (Sc)	<1	n.s.
	Acceleration condition (A)	1.11	.345
Longest fixation	Position (P)	1.89	.190
	Scan direction (Sc)	4.91*	.044
	Acceleration condition (A)	<1	n.s.
Pointing behaviour	Position (P)	<1	n.s.
	Scan direction (Sc)	19.62*	<.001
	Acceleration condition (A)	3.28†	.053

*Significant at $p < .05$. Interactions were only included if $p < .10$.
†Approaching significance.

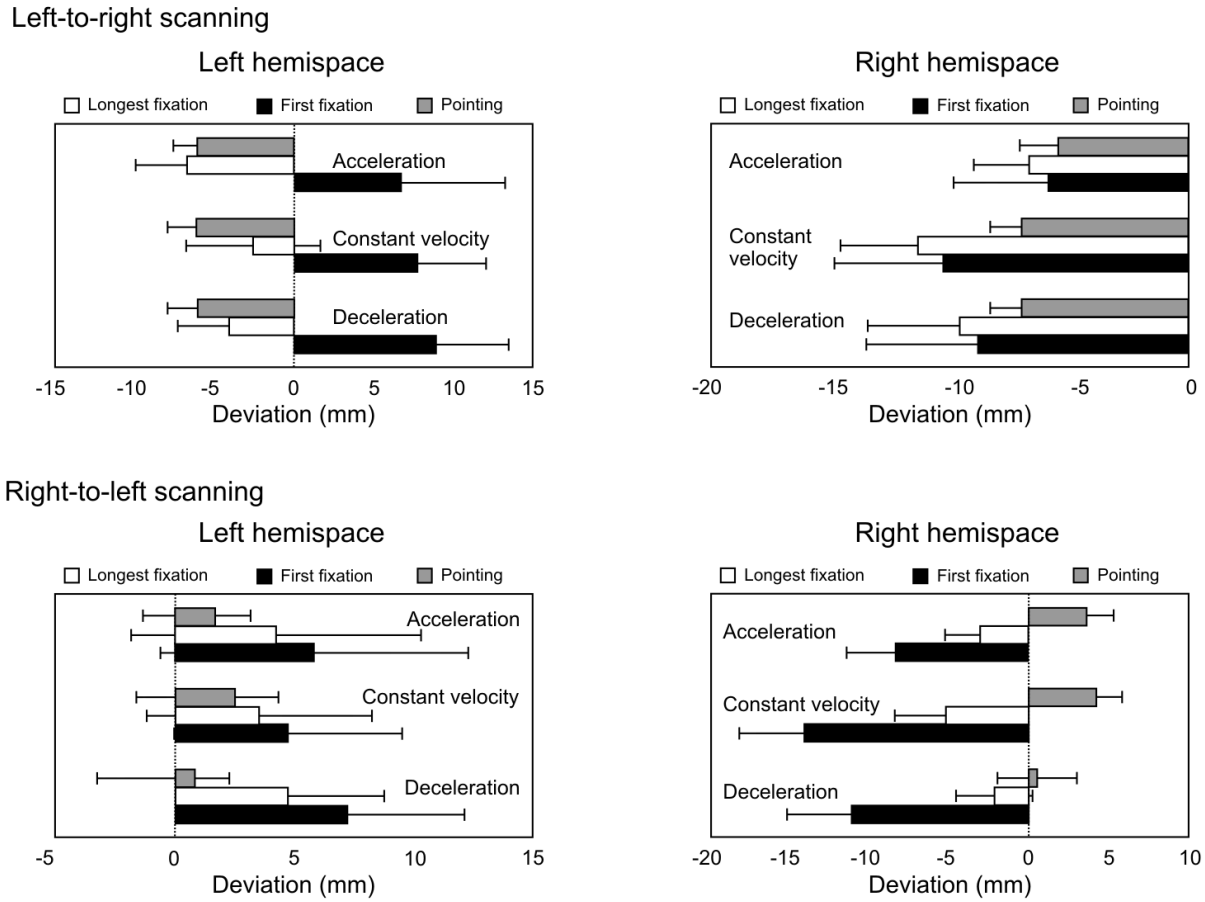

Figure 9. Bisection results of Experiment 4

Graphical representation of each cell in the no-line experiment.

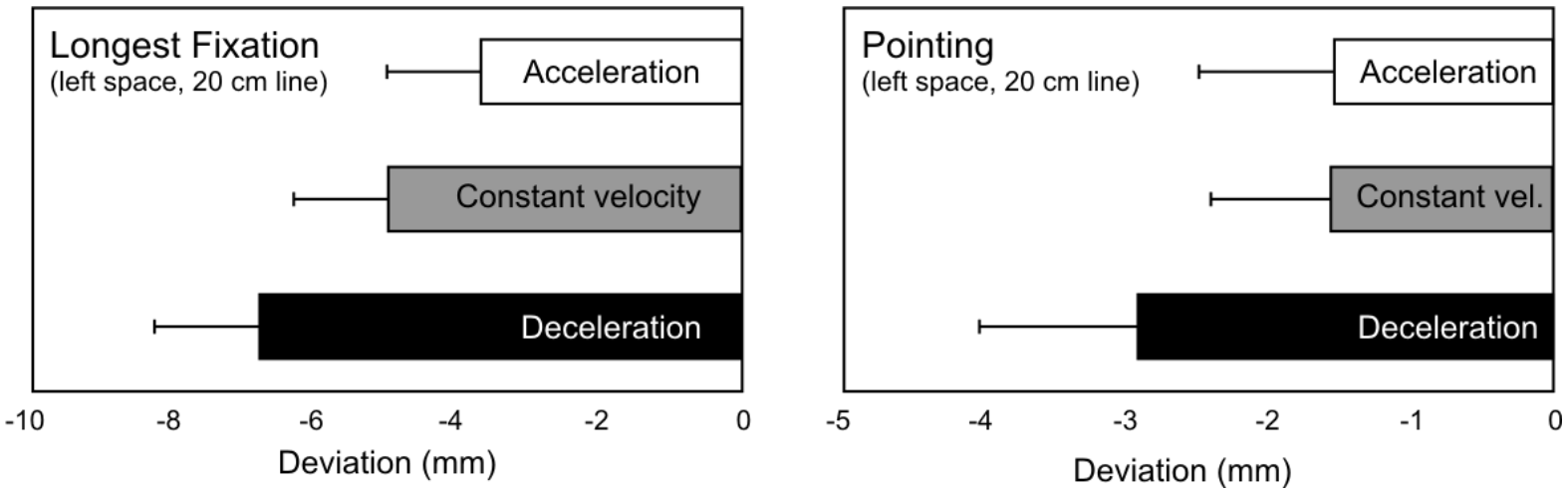

Figure 10. Acceleration main effects for LF and PB in Experiment 4

Data is collapsed across scan direction and position for this comparison. There is a trend towards a significant effect of acceleration for pointing (p = .053). Although there is no main effect of acceleration condition for LF, it has the same pattern as pointing.

2.5 General discussion

Although the objective of the first four experiments was to obtain measures of dynamic bisection in order to determine its similarities and differences with static bisection, the positional data produced a rather surprising result.

2.5.1 Position

In general, across all four experiments, the position of the line exerted greater influence on ocular than pointing behaviour. This suggests that, at the very least, the eyes and the hands perform these tasks somewhat differently, which in turn necessitates that previous research be reconsidered with respect to the effectors being measured (Appendix A). One possible reason for the difference is that eye movements are controlled bilaterally, whereas each hand is primarily controlled by the contralateral hemisphere. If each hemisphere computes spatial extent separately, and the computations are not combined for the hand, it would produce different responses even though the underlying computations are the same for both the hand and eyes. Alternatively, differences in hand and eye response could due to differences in the underlying computations for each effector.

Here pointing behaviour showed an overall leftward bias in all four experiments but no difference due to the position of the line (Table 9). Most previous research using the paper-and-pencil test has also found no positional biases (Brodie & Dunn, 2005; Butter et al., 1988; Fukatsu et al., 1990; Ishiai et al., 1989; Reuter-Lorenz et al., 1990; Rueckert et al., 2002) although in some cases greater leftward biases were seen in left space (Luh, 1995; Milner et al., 1992) and even mixed results have been observed (Mennemeier et al., 1997; Mennemeier et al., 2001; Nichelli et al., 1989). Thus the evidence suggests that the hand-centered reference frame is not as influenced by factors such as line position (Table 9), or static vs. dynamic judgments (Table 6). When no line is present (i.e., Exp. 4), although the average bisection point is the same as other conditions, it is now affected by scan direction suggesting that the continued presence of the line after the scan influences the hand perhaps by combining static with dynamic biases.

The other commonly used probe of spatial extent is the landmark task (Milner et al., 1992). In this task, pre-transected lines are presented to participants who are required to indicate which side of the line appears longer, or which end of the line is closest to the transection mark (Harvey, Milner, & Roberts, 1995b). Given that no pointing behaviour is involved in this task, one could suggest that the judgment involved preferentially recruits a gaze-centered frame of reference. The comparison of the

landmark task with ocular behaviour in the current set of experiments is not ideal – the landmark task requires participants to make a comparison of the two sides of lengths of a line (Ishiai, Koyama, Seki, & Nakayama, 1998) which has been shown to differ from the kind of symmetry judgments involved here (Fink et al., 2002). In addition, work in the Danckert lab has also shown distinct patterns of ocular behaviour between paper-and-pencil and landmark tasks (Cavezian & Danckert, unpublished data). Nevertheless, in all experiments (except LF in Experiment 4) both measures of ocular behaviour, FF and LF, demonstrated main effects due to line position similar to the effects commonly observed in research using the landmark task (Reuter-Lorenz et al., 1990; McCourt & Jewell, 1999; Rueckert et al., 2002; Milner et al., 1992; Luh, 1995; the one exception being Ishiai, 1989). Luh (1995) compared hand- and gaze-centered frames of reference directly. In these experiments participants were given two bisection tasks: the first was the standard paper-and-pencil test (i.e., a hand-centered task), and the second was to move a hash mark located above a line on a computer screen with a mouse (i.e., a gaze-centered task). The latter task showed more pronounced positional biases than the former. Taken together with the results of the current experiments, it appears that gaze-centered reference frames are more heavily influenced by experimental manipulations such as position than hand-centered reference frames. In other words, judgments of spatial extent are likely computed differently for the hands and eyes, although further research such as neuroimaging would be needed to discount the alternative hypothesis that each judgment relies on the same computations executed separately by each hemisphere (i.e., Chapters 3 and 4).

For Experiments 2 and 3, there were position by length interactions for hand-centred responses (PB) characterized by an exaggeration of biases in left hemispace for longer lines. For the longest lines, the line was on-screen much longer prior to pointing than it was for static judgments because pointing was not allowed until after the scan was completed (1-2 seconds after the initial presentation of the line). Perhaps, then, the eyes exert more influence over pointing behaviour when more time is first spent on ocular exploration prior to initiating the hand movement. This would be consistent with the idea that for some activities (e.g., skilled tool use) the eyes do in fact guide the hand; or that the more time spent planning a movement, the more influence gaze-position has on the calculations necessary for guiding the hand. When the time available to explore the line was limited, as in Experiment 3, there were no positional effects for PB. Overall, it appears that positional effects in line bisection are governed by gaze-centric coordinates and that it takes time for this coordinate system to influence hand-centric behaviours such as pointing or paper-and-pencil bisection tasks.

Table 9. Comparison of positional effects for each experiment

	First fixation		Longest fixation		Pointing behaviour	
	Left	Right	Left	Right	Left	Right
Exp 1	17.3	-31.7	-8.5	2.7	-2.8	-1.9
Exp 2	-4.8	-2.3	-3.3	-1.3	-3.8	-1.5
Exp 3	-1.5	6.0	-3.4	2.4	-4.1	-1.4
Exp 4	6.9	-9.8	-0.2	-6.3	-2.2	-1.8

Data is for 20 cm lines only so that a comparison could be made with Experiment 4. The table represents bisection biases collapsed across all variables except position. Negative numbers are biases left of centre, and all results are in mm.

2.5.2 The hand is not yoked to the eye for judgments of spatial extent.

Both reaching and ocular movements are governed by regions in the posterior parietal cortex (Buneo, Jarvis, Batista, & Andersen, 2002; Medendorp et al., 2003) and, clearly, *visual* input is used to guide both. There is no a priori reason for either the hand or the eyes to be the dominant effector (i.e., one guiding the actions of the other) in all instances. In fact, the hands and the eyes can be used to solve very different problems, making it ineffective to inflexibly yoke one to the other in all situations. Eye movements bring the fovea to bear on salient events throughout the visual field to acquire visual information for a variety of purposes. It is important that the eyes scan enough of the environment to allow for the collection of visual information to inform action. Once the information is collected, additional online control of action-specific effectors (e.g., the hand) would first require a gaze shift to the hand's target which would be computationally slow, and could interfere with subsequent ocular exploration. While it may make sense to yoke the hand-centered frame to the gaze-centered frame for more fine-grained manipulations, it does not make sense when making spatial judgments of the kind tested here possibly because in this series of experiments there is no specific physical target for the eyes to foveate on as might be the case when reaching for a physical object. Indeed, it is well known that *reaching* movements to a physical target involve dynamic online adjustments (Desmurget et al., 2005). Furthermore, this is clearly not the kind of motor behaviour invoked in line bisection as the target for the bisection movement is unspecified to the extent that the participant is free to choose any point along the line. In this instance it is unlikely that the eyes would induce changes to the movement of the hand unless some other factor led to a change in the initial motor plan.

In Experiment 1, correlational data (Table 2) indicated that all fixations were highly correlated and, because successive ocular movements were towards the centre of the line, it also suggests that the eyes were engaged in bisecting the line even in the absence of an explicit instruction to that effect. However, there was no correlation between fixations and pointing. The positional biases evident in pointing (i.e., left of center; Table 9) were constant across all experiments. Results were not consistent, however, for ocular behavior. As well, most participants reported that bisecting in Experiment 4, when no lines were present, was extremely hard and that they did not believe they had been accurate even though their responses were no different than for participants in all other experiments. These results add credence to the idea that the hand is not yoked to the eyes for this spatial judgment. In fact, the behaviour of the two effectors appears to be controlled by different systems both engaged in the same task (bisecting the line). Although the two effectors have often

been assumed to be indicative of the same underlying mechanism/system, these results suggest that they are engaged in the same task but under the control of different and unrelated systems.

2.5.3 Line length

Line length has been studied extensively in clinical populations primarily because the magnitude of bisection error observed in neglect depends on line length. Jewell & McCourt (2000) noted that the effect of line length in healthy populations is, at best, crudely measured. In a subsequent study (Rueckert et al., 2002), healthy participants bisected lines using both the paper-and-pencil and landmark tasks. There was no effect of line length on biases for paper-and-pencil bisection but there was an effect for the landmark task, which Rueckert and colleagues ascribed to differences in motor/intentional factors (paper-and-pencil task) versus perceptual/attentional factors (landmark task). In the current experiments, for *static* judgments, line length also only influenced ocular behaviour, again supporting the hypothesis that hand and eyes act independently.

For dynamic judgments, however, both ocular and hand behaviour depended on line length. Pointing showed a main effect of line length (Table 5 and Table 7) and, interestingly, there was a line length by scan direction interaction for pointing in Experiments 2 and 3, and a scan direction effect in Experiment 4 (Note: only the longest lines were presented as stimuli in this experiment). There are three possible explanations for this. First, dynamic judgments but not static judgments for the hand-centred frame are sensitive to line length. Second, it is the time spent scanning and not the line length per se that allows for effects of scanning to emerge. In other words, it is possible that scanning biases take time to develop and, since longer scan times were associated with longer lines, it is this time spent scanning that allows for a greater influence of dynamic mechanisms on bisection behaviour. Third, spatio-temporal effects only emerge when the spatial extent is sufficiently large. While there is insufficient evidence here to favor one explanation over another, all three require that the pointing response is not yoked to the gaze-centered coordinate system. A model is presented in Chapter 4 that suggests elements of these explanations.

2.6 Overall effect of dynamic judgments

The first hypothesis was that dynamic judgments of spatial extent would differ from static judgments if the neural mechanisms involved in the former were separate from those in the latter and if those neural mechanisms were subject to different computational biases. For LF, static judgments demonstrated a larger leftward bias in left space when compared with dynamic judgments. For the

longest line, this pattern was reversed in right space (Figure 7; in fact, dynamic judgments were to the left of center whereas static judgments were to the right). Explanations for these differences based on eye motion such as ocular or perceptual 'momentum' can be ruled out because this would necessarily depend on the direction of scanning and any such directionally specific effects would cancel out after collapsing across scanning direction. In other words, differences in bisection while making dynamic judgments of spatial extent cannot simply be due to the motoric effects of the eyes scanning the line. Rather, static relative to dynamic differences can only be due to separate processes or computations of spatial extent. By itself, this one result provides strong evidence for a separate mechanism involved in dynamic judgments of spatial extent.

2.7 Scanning direction

Experiments 2, 3, and 4 explored whether or not the scanning direction influenced bisection biases. All three experiments showed the same effect on pointing due to scan direction: a greater leftward bias after a L-R scan than after a R-L scan (Table 10; see also Brodie & Pettigrew, 1996, and Brodie & Dunn, 2005). The effects of scanning direction on ocular behavior, however, were inconsistent. For example, the main effect of scan direction on FF in Experiment 3 (L-R scanning was biased to the right and R-L scanning to the left) was reversed in Experiment 4 (i.e., L-R scanning was biased to the left of R-L scanning).

The inconsistencies found in ocular behaviour mirror those seen in previous studies using ocular behaviour: Reuter-Lorenz & Posner (1990) found no effect on bisection biases of scan direction; Chokron et al. (1998) found a leftward bias for L-R scanning but a rightward bias for R-L bisections; while Nicholls & Roberts (2002) found that R-L scanning led to greater leftward biases L-R scanning (Appendix A).

These results also defy a ready explanation from theories such as hemispheric activation (Kinsbourne, 1970) or zone-of-indifference (Marshall & Halligan, 1989). Hemispheric activation would predict the same biases in both ocular and hand behaviour. A zone-of-indifference theory would suggest that biases after a left-to-right scan would be in the opposite direction to those after a right-to-left scan. For example, if the greatest influence on bisection behaviour occurred when the eyes left the zone-of-indifference, a L-R scan would generate rightward biases and a R-L scan would produce leftward biases. However, contrary to predictions of the zone-of-indifference theory, results

from the current experiments showed that L-R and R-L scans generally were biased in the same direction (Table 10). Thus, no current theory explains these results.

Another possibility is that scanning actually is a form of cueing, and that differences in scan directions are a result of cueing effects. A number of results mitigate against this being a good explanation. First, unlike most previous experiments (Chokron et al., 1998; Chiba et al., 2006; Nicholls & Roberts, 2002; Reuter-Lorenz & Posner, 1990) where only half the line was scanned, participants scanned the entire line in these experiments. Therefore, there was no cueing of a specific part of the line to the exclusion of any other part. Indeed, the requirement to scan the entire line probably swamped any effects from the requirement to briefly fixate one end of the line prior to the scan. Additionally, it has been shown (Harvey et al., 2000) that the subsequent requirement to point eliminates the effects of cueing and that cueing effects are largely driven by the geometry of the cue (Mattingley, 1993). Finally, cueing does not explain the normalization of response due to scanning in neglect patients. While cueing effects might explain why L-R scanning creates an overall leftward bias in neglect patients, it cannot explain why it reduces the rightward bias in R-L scanning. Overall, then, cueing is not a particularly useful theoretical explanation for the results seen here.

Table 10. Comparison of scan direction effects on longest lines for each experiment

	First fixation		Longest fixation		Pointing behaviour	
	L-R	R-L	L-R	R-L	L-R	R-L
Exp 2	-6.18	-1.55	-3.10	-2.73	-3.05	-2.25
Exp 3	7.78	-3.67	0.01	-1.75	-3.62	-2.14
Exp 4	-0.27	-2.62	-6.83	0.35	-6.30	2.25

Data is for 20 cm lines (Exp. 4 used only 20 cm lines). Negative values represent bisection biases to the left of centre. All results in mm.

2.8 Scanning speed

Experiments 2 through 4 represent the first experiments to directly manipulate scanning speed during judgments of spatial extent. Scanning has generally been evaluated as a dichotomous variable – either 'on' or 'off', scanning or not-scanning. *A priori*, it was hypothesized that speed and scan direction would interact such that any influence of speed would be direction specific. In other words, if a faster stimulus moving from left-to-right shifted biases rightwards more so than a slower moving stimulus then a similar leftward pattern should occur for right-to-left scans. The two effects would cancel each other out when data was collapsed across scan direction. However, data from Experiment 2 showed an *overall* effect of scanning speed on FF such that slower scanning produced a significantly leftward bias in bisecting 20 cm lines (Figure 5a). This belies explanations that rely on inertial or other after-effects that depend on physical (rather than perceptual) influences, as any such explanation would also depend on the direction of scan. Rather, it further suggests that perception and gaze-centred references are tightly linked, and that they rely on a separate, speed dependent mechanism for dynamic judgments.

In addition, bisection biases at the slower speed were more sensitive to the location of the line (Figure 5b); L-R scans produced leftward biases in left space but rightward biases in right space. In contrast, the faster speed scans showed no sensitivity to line position. At least for ocular judgments of spatial extent then, velocity is taken into consideration and leads to distinct biases that interact with spatial location.

2.9 Acceleration and/or time

The basic indirect method for computing distance is the integral of velocity over time (i.e., $d = \int v(t)dt$). In this formulation, any spatial biases in measuring *t* would result in biases in *d*. There is some evidence that temporal asymmetries are indeed associated with spatial location (Basso et al., 1996; Frassinetti, Magnani, & Oliveri, 2009), thus it is possible that different spatio-temporal probes and conditions induce distinct bisection biases. As perceptual biases in judging stimulus intensities indicate that the left is preferentially responded to in healthy individuals (Mattingley et al., 2004), the same anisotropy may also exist for time.

The effect on pointing due to acceleration in Experiment 4 is an indicator that time is relevant to judgments of spatial extent. It was not, however, the time of exposure to the stimuli that was relevant because it was the same in all three conditions (acceleration, constant velocity, and deceleration) but,

rather, time as part of a spatio-temporal effect. Although dramatic or pervasive influences of acceleration on judgments of spatial extent were not found in Experiments 3 or 4, this lack of a significant result may be because such effects are small in the healthy brain. In addition, while it is relatively uncontroversial to suggest that the right parietal cortex plays a dominant role in both spatial and temporal processing, very little is known about how the two processes interact across a wide variety of circumstances. There are, however, two other possible explanations for the results we observed in Experiment 4. First, scanning speed was inversely related to a leftward bias such that, in Experiment 2, there was a greater influence of slower velocities on bisection behaviour (i.e., slower speeds induced greater leftward biases). If participants maintained a preferential reliance on the *final* velocity of the moving mark, then the current results could also be due to the fact that the deceleration condition has a slower final velocity than the acceleration condition. For Experiment 4, scanning speed only affected pointing behaviour in contradistinction to what this hypothesis would have predicted. As well, there should have been the reverse effect due to acceleration (i.e., a faster final velocity should demonstrate an equal but opposite effect on bisection behaviour). While Figure 10 is suggestive of both these effects, the statistical results were inconclusive. Finally, we cannot reject another alternative explanation for the results which would suggest that the effect on pointing was due to the two-way interaction of acceleration and position. Overall then, it is not possible from the current evidence to determine whether, or to what degree, time or acceleration are factors in the biases seen in dynamic bisection judgments.

2.10 Task instructions

In these experiments, participants were told to "touch the screen as quickly and accurately as you can at the centre of the line." However, they could have been asked to "look at the centre of the line, then touch the screen as quickly and accurately as you can at the centre of the line." In fact, this second instruction is similar to that first used by Ishiai and colleagues (1998), which they called 'line bisection by fixation' (except that they did not measure hand bisection). However, in most of their other experiments, Ishiai and colleagues give similar instructions to those used here (i.e., only instructing participants to point to centre; Ishiai et al., 1987, 1989, 1992). This was true even in their most recent article in which both pointing and eye fixations were measured (Ishiai, Koyama, Seki, Hayashi, & Izumi, 2006). This is true more generally in the line bisection literature. Task instructions do affect results (Fink et al., 2002; Nicholls et al., 2005; Riestra et al., 2002), however it is unclear which of the two should have been used or what, if any, the differences would be? Most experiments

and clinical procedures use the same directions we have given (e.g., Desmurget, et al., 2005, instructed participants to "point as accurately as possible with a single uncorrected movement" in an experiment explicitly exploring eye-hand yoking).

To what extent are the eyes involved in judging spatial extent without an explicit set of instructions? It could be argued that only the hand was involved in line bisection which would be a surprising conclusion because the eyes of participants consistently saccaded towards the centre of the line (Table 9 – consider that LF is always closer to the centre of the line than FF). Thus, it seems reasonable to propose that the hand and the eyes do in fact calculate spatial extent differently, although further research would be needed to determine whether or not task instructions would challenge this hypothesis.

2.11 General conclusions from the behavioural experiments

Results showed that velocity (speed + direction) exerts an influence on the perception of spatial extent. Clearly, slower speeds have an incremental effect on bisection biases. Direction of scan, on the other hand, had been investigated previously with widely varying results. The reason for this inconsistency is likely due to the different outputs being measured: gaze-centered vs. hand-centered reference frames. As well, it seems that, for static and dynamic judgments of spatial extent, the hands operate independently from, and somewhat more veridically than, the eyes. Finally, comparisons of static and dynamic judgments of spatial extent suggest that different computations and, by extension, different frames of reference underlie dynamic judgments.

Chapter 3: Neural Correlates of Judgments of Spatial Extent

Although static and dynamic bisections produce some different effects, it is possible that the computations are done by the same neural networks. The next experiment investigates the extent to which the neural networks subserving each process are in fact different.

3.1 Experiment 5: fMRI Study of Dynamic Bisection

3.1.1 Method

Participants: Sixteen (10 female; 14 right-handed; ages 28.1 years ± 8.7) neurologically normal participants with no history of psychiatric illness participated in this experiment. All had normal or corrected-to-normal visual acuity. Informed consent was obtained from each, and the study was approved by the Office for Research Ethics, University of Waterloo, as well as the Tri-Hospital Research Ethics Board of Waterloo, Ontario, Canada.

Experimental Design: The objects to be bisected were narrow rectangles subtending approximately 20° of visual arc horizontally and 0.5° vertically, in black on a light grey background. Each rectangle was pseudorandomly offset to the left or right of the midsagittal plane by an amount ranging from -2° to +2° of visual angle (a positive sign refers to right-of-centre offsets).

Five behavioural tasks were used within a block design (Figure 11). Each block consisted of nine trials lasting 2 s per trial and, prior to each block, an instruction was posted for 2 s indicating which block of trials was about to be presented. Trials all began with a central fixation cross (below the level of the rectangle, on-screen for 300 ms; Figure 11a). In the static bisection task (SB) the rectangle appeared on-screen (from now on, the rectangle will be called a 'line' because of its narrow vertical extent) after the fixation cross disappeared, at which time the participant was to look to where they thought the centre of the line was as quickly and accurately as possible (i.e., 'line bisection by fixation'; Ishiai et al., 1998). There were two dynamic bisection (DB) tasks depending on the direction of scan. In one, as soon as the line appeared, a vertical mark traversed the line starting from the left endpoint and moving to the right endpoint (L-R) at a speed of approximately 22°/s (task DB(LR)). Participants were to follow the mark and, once it had traversed the line completely, they were to look to where they thought the centre of the line was as quickly and accurately as possible. In the other dynamic condition the mark now travelled from right-to-left (task DB(RL)). The final two

conditions acted as controls for the dynamic bisection tasks. Both control conditions were identical to the dynamic bisection conditions with the exception that, once the mark had completely traversed the line, a new mark appeared somewhere in the line (at positions ranging from -2° to +2 ° around centre). Rather than bisect the line, participants were simply asked to saccade directly from the end of the line they had just scanned to the new mark and fixate there until the end of the trial. The L-R control condition was denoted Control (LR), while the R-L control condition was denoted Control (RL).

Each experimental run began with a 16 s fixation period followed by 15 blocks of trials – 3 blocks of each condition – in a pseudorandom sequence, ending with a 16 s fixation period (Figure 11b). Prior to the experiment each participant was given training on the different tasks. Four runs of the experiment were completed by each participant with nine trials per block (i.e., 3 x 4 x 9 = 108 trials of each of the five trial types per participant).

Data Acquisition: Functional data was collected using gradient echo-planar T2*-weighted images acquired on a Philips 1.5 Tesla machine (TR = 2000 ms, TE = 40 ms, slice thickness = 5 mm with no gap, 26 slices, FOV 220x220 mm^2, voxel size 2.75x2.75x5 mm^3, flip angle 90°). An experimental run consisted of 26 slices/volume, 166 volumes, eight per fixation baseline at the beginning and end of each run, and ten per block for the 15 experimental blocks. At the beginning of the session, a whole-brain T1-weighted anatomical image was collected for each participant (TR = 7.5 ms, TE = 3.4 ms, voxel size 1x1x1 mm^3, FOV 240x240 mm^2 , 150 slices, no gap, flip angle = 8°). Stimuli were presented on an Avotec Silent Vision^{TM} (Model SV-7021) fibre optic visual presentation system with binocular projection glasses controlled by a computer running E-Prime software (version 1.1 SP3, Psychology Software Tools, Pittsburgh, PA) synchronized to trigger-pulses from the magnet.

Data Analysis: Data were analyzed using Brain Voyager QX (version v2.1, Brain Innovation B.V., Maastricht, The Netherlands) with each participant's functional data aligned to their own three-dimensional anatomical images, and then transformed into a common stereotaxic space (Talairach, 1988). Each functional run was visually inspected for motion artifacts by playing a virtual movie of each functional volume in sequence (Culham et al., 2003).

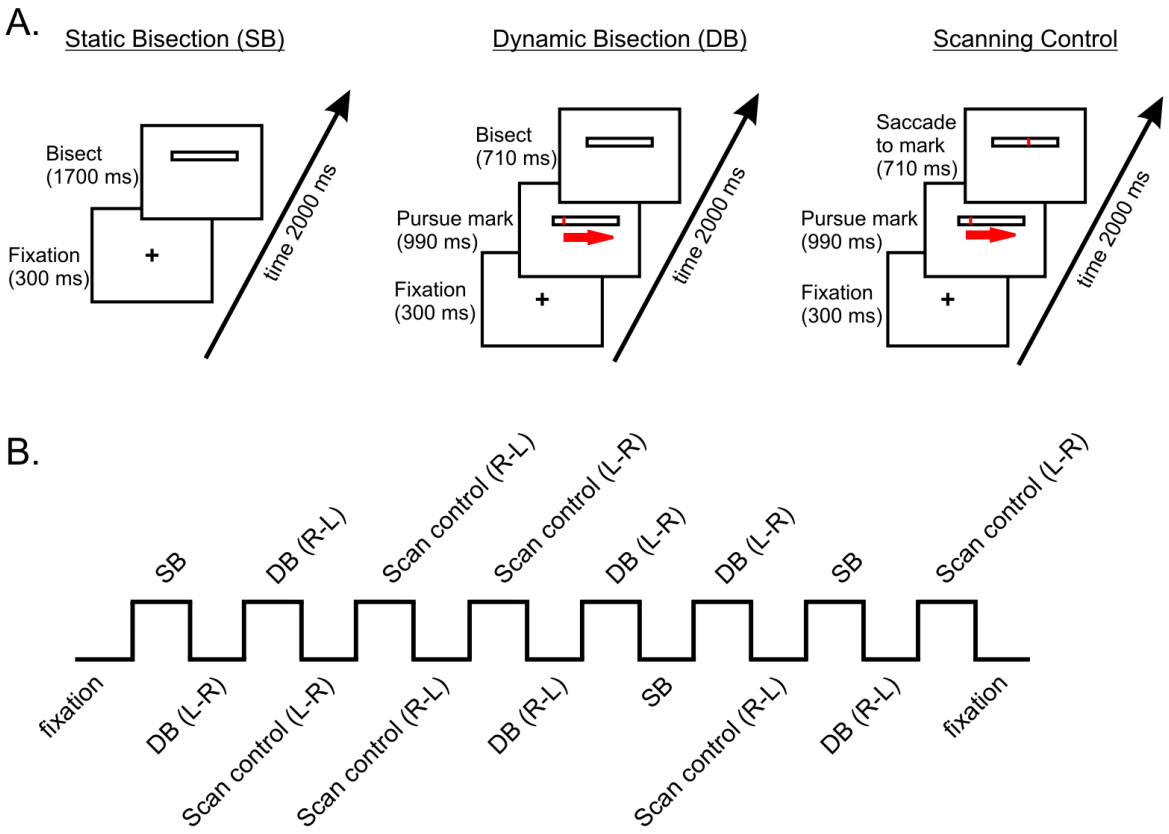

Figure 11. fMRI experimental procedure.

(A) Schematic representation of a single trial for each of the three experimental conditions (see *Experimental design* for full description). (B) Time course for a single run. Each run starts with a fixation cross for 16 seconds, followed by 15 blocks consisting of instructions (2 s) and 9 trials (see *Experimental design* for full description) and ending with another 16s fixation period.

Serious motion artifacts were detected in two participants (both female and right-handed) and these participants were subsequently removed from further analysis. For the remaining fourteen participants (8 female, 12 right-handed), trilinear interpolation was used to correct for motion artifacts in functional runs. All functional data were then pre-processed, which included linear trend removal. No spatial smoothing was applied to the data.

First, the blood oxygenated level-dependent (BOLD) response was convolved to the Boynton hemodynamic response function. Next, five linear predictors were created for each participant (i.e., one predictor for each of the tasks; Figure 11b) and these 70 linear predictors (14 participants x 5 predictors for each) were entered into a fixed effects general linear model. Activation of any voxel was only considered significant if it met two criteria: first, significance evaluated by a test statistic (Table 11) Bonferroni corrected to adjust for multiple comparisons; and, second, activations had to be part of a contiguous cluster of at least 50 other significant voxels. The Talairach coordinates of the centroid of each cluster was computed (Table 11) and the Brodmann Area (BA) corresponding to those coordinates provided by Talairach Daemon (Lancaster et al., 1997; Lancaster et al., 2000). The data were also tested using a random effects general linear model to reduce the effects of any one individual on the results.

Six contrasts were computed on the full set of predictors. First, to identify brain regions preferentially involved in dynamic judgments of spatial extent relative to static judgments, the BOLD signal of the two dynamic bisection conditions (collapsed across scan direction) was contrasted with the SB condition. Next, the BOLD signals for the DB condition were contrasted with the control condition collapsed across scan direction. This was done to explore which brain regions were involved in dynamic bisection judgments by explicitly controlling for the ocular motions required of the dynamic bisection task. Thus, differences in the BOLD signal for this contrast were due to the computation of the centre of the line under dynamic conditions. These first two contrasts made no distinction between the effects of L-R and R-L scanning. As there were behavioural differences due to scan direction evident in Experiments 2-4, two more contrasts were examined to explore the neural correlates of scan direction by comparing dynamic bisections with their associated control conditions for each direction of scanning separately. A further probe of directional differences in dynamic bisection judgments was made by directly comparing the L-R dynamic bisection with the R-L condition (i.e., L-R vs. R-L dynamic bisection and vice versa).

3.1.2 Results

Significant activations for the fixed effects model are presented in Table 11 along with the Talairach coordinates and associated Brodmann areas for the centroid of each cluster. Regions are marked that were also significant using a random effects analysis. The table notes whether or not the activation observed in a given region was scanning direction specific.

3.2 Effects independent of scan direction

Direct contrast of dynamic with static bisections (DB>SB; Table 11) revealed large bilateral regions of activation in the cuneus and precuneus on either side of the parieto-occipital sulcus (Figure 12). Event-related averages for all three activation regions (Figure 12a) indicated that both left-to-right and right-to-left scanning contributed equally to these activations as there was no difference in the peak activations or their time course. The reverse contrast (SB>DB; Table 11; Figure 12b) shows scan-direction independent bilateral activations in the supramarginal gyrus and right precuneus. The left cerebellum was activated more so for dynamic vs. static bisection (DB > SB) and the peak activations of both the left-to-right and right-to-left activations were not statistically different (Figure 12a).

When the BOLD signal related to dynamic bisection (collapsed across scanning directions) was contrasted with its control conditions (also collapsed across scan direction), activations were seen in the left cerebellum (an area in the same coronal plane but ventrolateral to the cerebellar region activated in the dynamic vs. static contrast) and superior parietal lobule (Figure 13). Furthermore, for this contrast, a smaller region of activation was seen in the right precuneus (Figure 13). Finally, the left middle temporal gyrus (MTG) was activated in both DB(LR) > Control(LR) and DB(RL) > Condition(RL) conditions (Figure 13) suggesting that activation in this region was also independent of the scan direction.

Table 11. Activation regions for bisection experiment with lines

Contrasts	Stereotaxic Coordinates (Talairach space)			Activation region	BA	Cluster Size	Direction Dependent
	X	Y	Z				
1a. DB > SB	13	-70	15	Right cuneus*†	18	821	N
	-11	-70	15	Left cuneus*†	18	969	N
	1	-70	24	Precuneus†	31	1246	N
	-7	-49	3	Left cerebellum		780	N
1b. SB > DB	-42	-41	52	Left inferior parietal lobule	40	667	N
	44	-43	53	Right inferior parietal lobule**	40	596	N
	19	-69	52	Right precuneus	7	1350	N
2. DB > Control	-55	-53	-9	Left middle temporal gyrus	37	210	N
	-34	-49	-29	Left cerebellum†		412	N
	-16	-62	53	Left superior parietal lobule	7	573	N
	20	-66	50	Right precuneus†	7	174	N
3. DB (LR) > Control (LR)	-17	-77	36	Left precuneus	7	52	Y
4. DB (RL) > Control (RL)	-8	-61	57	Left precuneus	7	57	Y
	-55	-54	-9	Left middle temporal gyrus	37	121	N
	-51	31	14	Left inferior frontal gyrus	46	75	Y
5. DB (LR) > DB (RL)	8	-76	43	Right precuneus	7	352	Y
	24	-74	-11	Right cerebellum (declive) †		352	Y
	53	-3	13	Right precentral gyrus	6	154	Y
6. DB (RL) > DB (LR)	-51	28	13	Left inferior frontal gyrus	46	197	Y

DB – dynamic scan with bisection; Control - scan then look at a mark presented within the line; SB – static line bisection. LR denotes left-to-right scanning, RL denotes right-to-left scanning; where scanning direction is not indicated data was collapsed across this factor. Clusters represent 50 contiguous voxels significant at $p<.001$ (Bonferroni corrected), except in one case where $p<.01$ (**).

*Note: medial cuneus showed large activation as well.

†Indicates regions that were also significant under a random effects analysis. In all cases except for the left cerebellum in the DB>Control condition, the cluster size was smaller for the random effects.

3.3 Direction specific effects

The L-R contrast between dynamic bisection and its control (DB(LR) > Control(LR)) showed activation of a small region of the left precuneus (Figure 14). A similar region of precuneus activity

was observed for dynamic bisections made after R-L scans when they were contrasted with the respective control condition. The two regions of left precuneus were spatially separated from each other, and from the areas of precuneus activated when contrasting dynamic with static bisections (Table 11).

Activity in the right precuneus was significant for both directions of scan, but was highest for L-R scanning (Figure 15). On the other hand, peak activations were the same for both L-R and R-L scanning in the right cerebellum (Figure 15), however activation during L-R scanning was more persistent.

3.4 Discussion

3.4.1 The role of the cuneus and precuneus in dynamic judgments

When participants performed dynamic bisections activation was seen bilaterally in the anterior portion of the cuneus and in adjacent regions of the precuneus close to the parieto-occipital junction (Figure 12). The medial region of the cuneus and precuneus have been shown to be activated when participants were required to integrate global field (background) motion and eye motion during smooth pursuit eye movements (Tikhonov, Haarmeier, Thier, Braun, & Lutzenberger, 2004). Given its proximity and connections with inferior/superior parietal regions including the intraparietal sulcus (IPS), dorsal motor regions, DLPFC, striatum, thalamus, and brainstem (Cavanna & Trimble, 2006), the precuneus is a natural region to integrate the lower levels of visual processing with object identity, motion, location, and time.

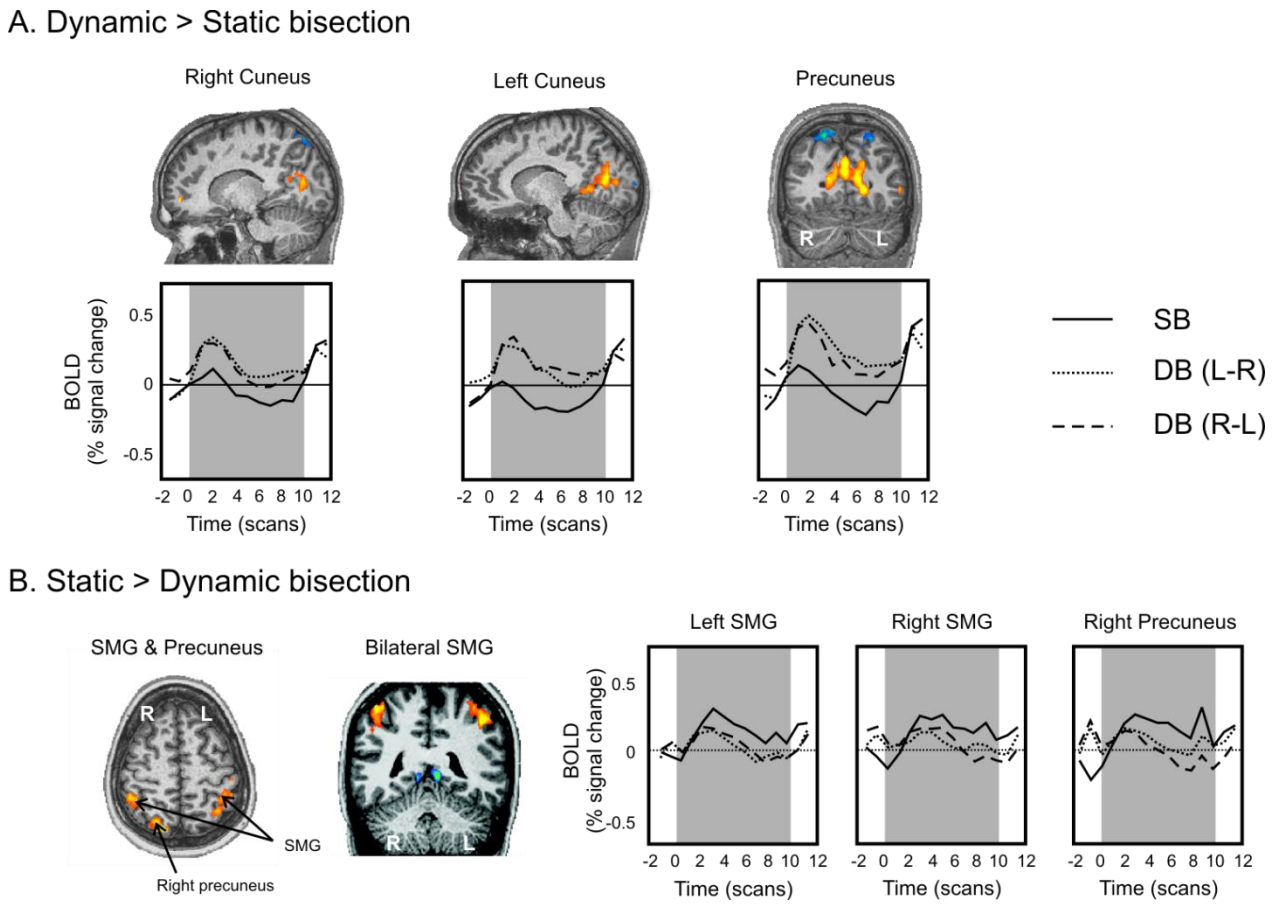

Figure 12. Contrasts of dynamic to static bisection, collapsed across scan direction

(A) The top pictures show some of the BOLD activations for dynamic line bisection. All *t*-value are indicated graphically by the progression from red (*t*=5.5, Bonferroni corrected) to yellow (*t*=8.0). Blue colours indicate regions with negative activations. Below each picture is a graph showing the event related averages for the region activated. Solid lines = static bisection (SB); dotted lines = dynamic bisection left-to-right scanning (DB(LR)) and the dashed lines = dynamic bisection right-to-left scanning (DB(RL)). (B) The reverse contrast (i.e., static bisection > dynamic bisection) is shown here. In this case the colour scheme for BOLD activations shows areas preferentially activated by static line bisection in shades of red to yellow. The first picture is an axial image showing the bilateral supramarginal gyrus (SMG) and precuneus activations for static bisection. The second image is a coronal image of the same SMG activations as the first image. Event related averages for these three activations are shown to the right of the pictures.

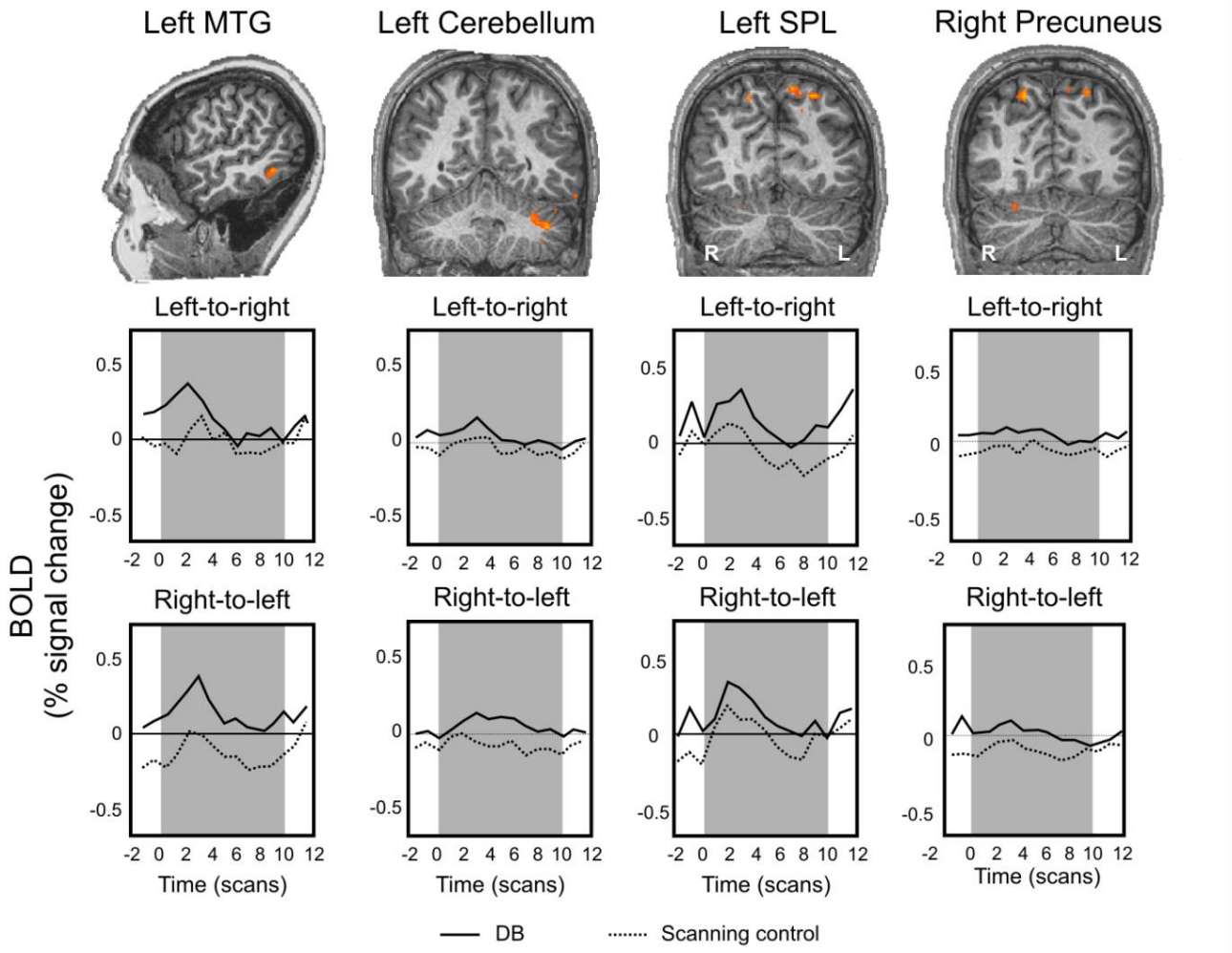

Figure 13. Contrasts of dynamic line bisection to the control condition

The images above show regions of BOLD activation for dynamic line bisection compared to its control, collapsed across direction. All *t*-value are indicated graphically by the progression from red (*t*=5.5, Bonferroni corrected) to yellow (*t*=8.0). Below each picture are two event-related averages for the activated region, separated by scan direction. The top graph shows the comparison between left-to-right dynamic bisection, and the left-to-right control condition (see *Experimental design* for complete details). The bottom graph is the same comparison for right-to-left scanning (bisection vs. control). Solid lines = dynamic bisection; dotted line = dynamic control task. SPL = superior parietal lobule; MTG = middle temporal gyrus.

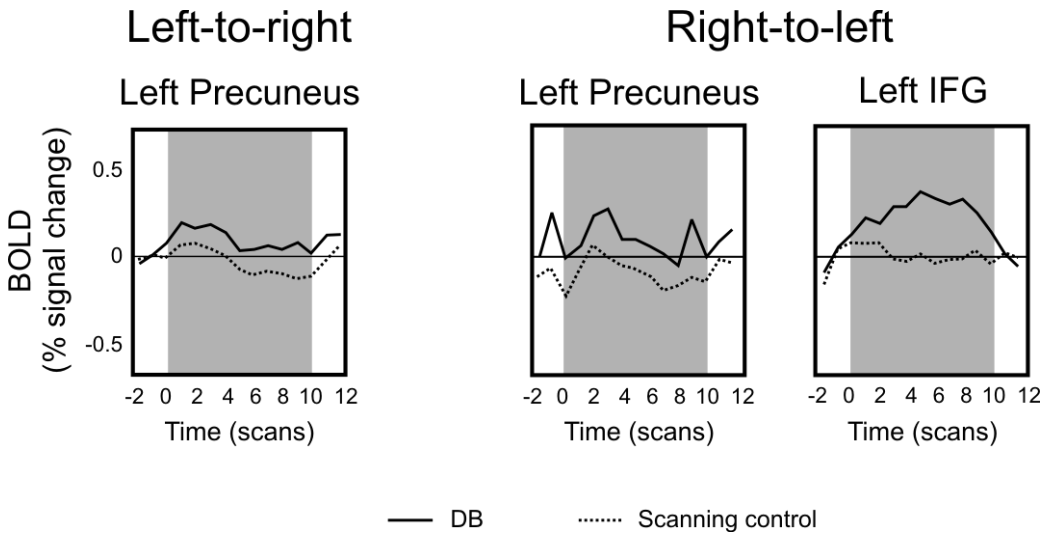

Figure 14. Contrasts of dynamic bisection to control, by direction of scan

Event -related averages for the regions activated. From left to right, the first event-related average is for DB(LR) > Control(LR), with the following three event-related averages showing results for DB(RL) > Control(RL). In each case, the number of voxels activated was relatively small (between 52-121 voxels; Table 1). IFG = inferior frontal gyrus. All other abbreviations and symbols as in Figure 13.

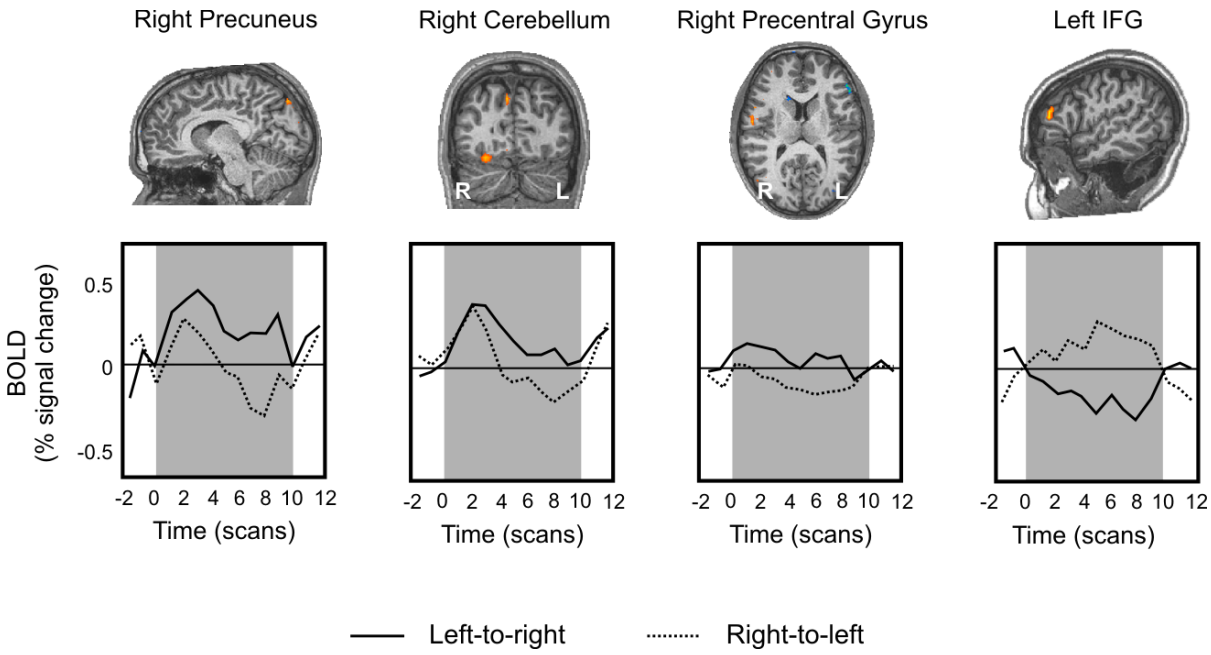

Figure 15. Contrasts between left-to-right and right-to-left dynamic line bisection

The last column shows the only region of BOLD activation for DB(RL) > DB(LR), while the first three columns all show regions activated by DB(LR) > DB(RL). As in earlier figures, *t*-value are indicated graphically by the progression from red (*t*=5.5, Bonferroni corrected) to yellow (*t*=8.0). Below each image are the event-related averages for left-to-right and right-to-left dynamic line bisection.

Malouin and colleagues (2003) noted a similar activation of the anterior cuneus when contrasting walking in a straight line with initiating gait. Comparable responses in the cuneus have also been seen for copying a figure compared with drawing it (Ferber, Mraz, Baker, & Graham, 2007) and, particularly, when copying non-real figures compared to real figures presumably because the former requires greater visual feedback of distance metrics. Diekmann and colleagues (2009) noted that this region appeared to be part of a system integrating timing with a hippocampal position map while Hahn and colleagues (2006) found that the cuneus (but not the precuneus) was involved in the bottom-up control of spatial attention. In general, then, the cuneus appears to subserve a network involved in dynamic tasks involving a broad range of judgments that could be characterized as involving the processing of spatial extent.

The precuneus has also been associated with higher order cognitive functions and, in particular, with complex visuo-spatial processing (Cavanna & Trimble, 2006). A variety of fMRI studies have demonstrated precuneus activation in dynamic judgments including attentional tracking of moving objects (Culham et al., 1998), obstacle avoidance (Malouin et al., 2003), the top-down control of spatial attention (Hahn et al., 2006), mental navigation and route walking (Ghaem et al., 1997), and the recent study by Diekmann and colleagues (2009) on the neural correlates for the computation of angular displacement which proposed that the precuneus acts as a velocity-time integrator. Velocity-time integration, by itself, is at most a single step in the process of dynamic line bisection. For example, one possible sequence of steps for dynamic bisection is as follows (omitting initial signal processing of the stimulus and execution of the final motor actions):

Step 1. Compute fine-grained time and velocity elements

Step 2. Combine time and velocity to compute line length and the bisection point

Step 3. Map the computed bisection point back onto the line

Step 4. Create a motor plan based on (3)

The first and second of these steps are specific to dynamic but not static bisections. Thus, activations specific to dynamic bisections should be most related to these steps (i.e., the computation of time and velocity, followed by computation of the bisection point). The cuneus and precuneus were strongly activated for dynamic relative to static bisections and both were activated regardless of scan direction. This suggests that the cuneus and precuneus perform the generalized function of integrating

velocity in dynamic judgments. Given that the precuneus has been shown to be involved in a wide variety of dynamic tasks not necessarily reliant on velocity processing (e.g., obstacle avoidance, Malouin et al., 2003), it suggests that the precuneus may take on the additional role of mapping the computed location of the midpoint onto the line. That is, the initial steps proposed above need only relate to an abstract distance metric (i.e., the distance travelled by the moving mark) that must then be remapped back onto the object of interest (i.e., the line itself). The precuneus may play a critical role in integrating the distance measured by the moving mark with the relevant object of interest (the line).

The precuneus is also implicated in both the default network and in smooth-pursuit scanning. However, it is unlikely that either of these were the reasons for the activations seen in this experiment. The default network results from activity not focused on external stimuli and, given the often 'strenuous' nature of the experiment (as reported by participants), not much time was available for mind-wandering. As well, there was little evidence for other regions associated with the default network showing additional activation such as the posterior cingulate, medial prefrontal regions, etc. A number of reasons suggest that the precuneus was not activated simply due to smooth pursuit. Importantly, the region of precuneus identified in this experiment (DB>SB) was significantly inferior and posterior to the location identified by Petit & Haxby (1999) for either saccades or smooth pursuit. Next, as Petit & Haxby (1999) noted, smooth pursuit activations were generally smaller than saccadic activations and co-located to a large degree. Because of this, we would not have expected the condition DB>SB to show activation of the precuneus. Finally, there was activation of the precuneus for the condition where specific effects of eye motion were carefully controlled (DB>Control).

Specifically, then, the cuneus may play a role in integrating the velocity-time information derived from eye position and timing signals and this computation is then forwarded to the precuneus for complex tasks such as bisection or processing of time-to-collision (i.e., mapping the information back to the external environment). Indeed, the specific region of precuneus activation for dynamic bisections versus the scanning control condition (Figure 13) overlaps that seen by others employing a broad range of dynamic visual tasks (Cavanna & Trimble, 2006; Diekmann et al., 2009; Malouin et al., 2003). Details of the form of the integration – the required terms and how they are combined – are outlined in Chapter 4.

This proposal of a separate pathway for dynamic bisection leads to an interesting reinterpretation of a puzzling result: neglect patients typically bisect lines to the right of centre when making a static judgment of the centre of a line (often used as a clinical marker of neglect) but, after engaging in

dynamic judgments of centre, bisect to the left of true centre following a left-to-right scan and to the right following a right-to-left scan (Chokron et al., 1998; Reuter-Lorenz & Posner, 1990). This is the same pattern we find in healthy individuals albeit with a greater magnitude of bias from centre. Importantly, scanning a line from right-to-left (i.e., dynamic bisection) *reduces* the typically large rightward bisection biases evident in neglect patients under static bisection conditions. In other words, neglect patients do not show leftward neglect during dynamic bisection but, rather, behave like healthy individuals albeit with more extreme and variable biases. Both studies showing this effect used experimental paradigms involving smooth pursuit eye movement (Appendix A). Other experimental paradigms involving smooth pursuit eye movements have also shown a reduction or reversal of biases in line bisection for neglect patients including object motion (Dunai et al., 1999; Plummer et al., 2006), coherent background motion (Kerkhoff et al., 1999; Kerkhoff et al., 2006), optokinetic stimulation (Choi et al., 2007; Mattingley et al., 1994), and other techniques that temporarily induce optokinetic nystagmus such as vestibular stimulation or neck muscle vibrations (Adair et al., 2003; Karnath et al., 1996; Rubens, 1985). These results have been interpreted to suggest that smooth pursuit eye motion remediates neglect, although no mechanism has been proposed for such an effect. Indeed, Bisiach and colleagues (Bisiach et al., 1996) tested whether the amelioration of neglect symptoms using these techniques was a restoration of normal functionality or mitigation of the symptoms (although the mechanism for mitigation was not specified). After optokinetic stimulation on neglect patients, the difference between leftward and rightward endpoints in a production paradigm (i.e., a midpoint is presented and the patient is asked to extend it to the left and right to reproduce a previously viewed line) increased, suggesting that the neural system was still impaired. A more parsimonious theory for these observed differences between static and dynamic performance in neglect would suggest that dynamic bisection recruits brain regions not typically lesioned in neglect. That is, the cuneus and precuneus are usually spared in neglect patients whose lesions generally encompass the right lateral inferior parietal cortex and the superior temporal gyrus (Karnath, Ferber, & Himmelbach, 2001; Mort et al., 2003) and it is these spared regions that perform dynamic judgments of spatial extent.

This reinterpretation can explain why there is a reduction or absence of neglect in dynamic bisection, as well as why interventions based on techniques such as vestibular stimulation produce only short-term effects. Such interventions may not alleviate neglect but, rather, temporarily induce

the patient to use a dynamic pathway for determining spatial extent. Once the patient reverts to engaging normal 'static' processing pathways, the visuospatial symptoms of neglect reappear.

The results of Experiment 5 provide one additional piece of evidence for this novel theory. Generally, neglect is due to a lesion of the right inferior parietal and superior temporal lobes (Karnath, 2001; Mort et al., 2003). For the contrast exploring which brain regions were more active for static versus dynamic bisection, results showed bilateral activation of the supramarginal gyrus which forms part of the inferior parietal cortex (Figure 12b). So while the medial parietal regions (precuneus) are important for dynamic bisection, the lateral inferior parietal cortices – a region typically damaged in the right hemisphere for neglect patients – are likely to be more important for static judgments of spatial extent.

3.4.2 The role of the left cerebellum in dynamic judgments

The first step in dynamic bisection requires the production of both a velocity and time signal. While timing mechanisms have recently been associated with inferior parietal function (Battelli et al., 2007; Danckert et al., 2007; Harrington et al., 1998; Lewis & Miall, 2003a), the cerebellum has more commonly been identified as integral to subsecond timing (Harrington, Lee, Boyd, Rapcsak, & Knight, 2004; Ivry, Keele, & Diener, 1988; Jueptner, Rijntjes, Weiller, & Faiss, 1995; Meck, 2005; Penhune, Zatorre, & Evans, 1998). Furthermore, the region activated when dynamic bisections were contrasted with the scanning control task (Figure 13) overlapped the cerebellar region found by others in timing studies (Diekmann et al., 2009; Ivry & Spencer, 2004; Tracy, Faro, Mohamed, Pinsk, & Pinus, 2000). In a meta-analysis of neuroimaging studies on timing, Lewis & Miall (2003b) noted that over 50% of the studies found activations in bilateral regions of the lateral cerebellum, and 29% in the medial cerebellum. In lieu of other plausible candidates (none of the non-cerebellar regions identified in earlier papers as critical to either cognitive or motor timing were activated in any of the contrasts), it is plausible that the left cerebellar activations observed here were indicative of the production of a timing signal integral to the dynamic bisection task.

Of course, the cerebellum could be involved in more than the production of a timing signal. For instance, the cerebellum is known to be involved in spatial processing for static line bisection judgments (Fink, Marshall, Weiss, Shah, Toni, Halligan, & Zilles, 2000a; Fink, Marshall, Weiss, Shah, Toni, Halligan, & Zilles, 2000b; Fink et al., 2001). Fink and colleagues (2000) found that the landmark task activated a part of left cerebellum overlapping with the region found in our contrast

between dynamic bisection and the scanning control condition. Thus, while it is difficult to identify a single role for the cerebellum in dynamic bisection, supplying the timing signal is a strong possibility.

3.4.3 Left superior parietal activation in dynamic judgments

An activation region was found in left superior parietal cortex (Table 11; Figure 13) that was independent of scan direction. Fink and colleagues (2002) found activations of left superior parietal cortex in line length relative to centre of mass judgments, as did Weiss and colleagues in a comparison between static line bisection and pointing toward a dot (Weiss, Marshall, Wunderlich, Tellmann et al., 2000). Hahn and colleagues (2006) associated this region with top-down attentional cueing, while Dieterich and colleagues (2009) noted that smooth pursuit activated the area relative to optokinetic nystagmus, and that both smooth pursuit and saccadic activity involved left superior parietal cortex. This region, then, appears to subserve a higher level attentional network required for the processing of dynamic stimuli. Because we saw activations in left superior parietal cortex for the contrast between dynamic bisections and the scanning control task (which, because it also involves moving stimuli, factors out any purely attentional or motoric components), this region must also have the more specific function of processing spatial extent for dynamic stimuli. Thus, along with the cuneus and precuneus, the left parietal region may form part of a network important for dynamic judgments of spatial extent. In left spatial neglect patients the left parietal cortex is undamaged, lending additional credence to the notion that dynamic judgments of spatial extent are largely preserved in neglect because they rely on a distinct neural network to that used for static judgments – a network not typically injured in neglect. It also raises an interesting possibility: could left parietal patients be impaired when making dynamic but not static judgments of spatial extent? As far as we know, although static bisection tasks have been done with left parietal patients, dynamic bisection tasks have not.

3.4.4 Direction specificity for dynamic judgments

Left-to-right relative to right-to-left scanning revealed small activations in the right hemisphere including the precuneus, cerebellum, and precentral gyrus. The opposite comparison showed a single left hemisphere area of activation in the inferior frontal gyrus (Figure 14 and Figure 15). While it is possible that line bisection is biased more to the left after left-to-right scanning because of left-to-right scanning producing relatively greater activation of the right hemisphere (i.e., Kinsbourne's hemispheric activation theory of line bisection), the activations were small and only the right

cerebellum in DB(LR) > DB(RL) contrast survived a random effects analysis. A specific region of activation in the left precuneus differed between left-to-right and right-to-left dynamic bisections (Table 11) which may also provide a mechanism for the differences due to scan direction. It is less clear what the contributions of the left inferior frontal gyrus were in bisection. Both were small activation regions, but further research is needed to determine their role in dynamic bisection tasks.

3.4.5 What part of the network is shared between static and dynamic judgments?

While there are differences between static and dynamic judgments, many of the areas identified in previous studies of static bisection did not appear in the reverse contrast (SB > DB). In fact, the contrast only identified inferior parietal cortex bilaterally and a somewhat lateral region of the right precuneus in the static bisection network (Table 11). Regions of the cerebellum, cuneus (particularly the right side) and other areas of the occipital gyrus bilaterally, superior parietal regions, and frontal gyri have all been identified with static bisection in one or more study (Appendix B).

There are three non-exclusive possibilities for why these regions did not appear in any of the contrasts here (including DB > Control): (1) the nodes in the network are used for both static and dynamic judgments; (2) the nodes are shared, but the functionality is different for each; or (3) the experiment was not sensitive enough to find differences between the two tasks and/or the statistical criteria applied excluded some positive results. Although it is not possible to distinguish among these possibilities, it seems likely that there are many more shared components to the bisection network than separate components. Resolving this would require further experimentation and case studies.

3.5 Conclusion

Dynamic judgments of spatial extent recruit a unique neural network including the precuneus and cuneus along with the cerebellum and left superior parietal lobe. Most likely, the cerebellum produces a timing signal which the cuneus integrates (along with velocity information). This integrated signal provides an estimate of distance which the precuneus and left superior parietal regions use in determining the centre of the line.

This sequence of steps (along with the functional and neurological evidence from other studies) further corroborates the notion that the cuneus and precuneus are specialized for building and interpreting dynamic spatial maps and making dynamic judgments of spatial extent. Such a model of dynamic bisection may also explain why neglect patients fail to show rightward biases on dynamic

bisection tasks, and why interventions that rely on temporarily shifting static judgments to dynamic judgments fail to have long-lasting effects.

Chapter 4: **Modeling Dynamic Bisection**

Having provided evidence in the previous two chapters for a different computational basis for dynamic bisection relative to static bisection, it is useful to consider how it could be modeled. Kinsbourne's hemispheric activation theory for line bisection biases is consistent with the observed difference in directional bias between L-R and R-L scanning, i.e., L-R relative to R-L scanning activates the right hemisphere and vice versa. In general, however, models such of this for static line bisection (Section 1.3) are not well-suited as explanations of the observed phenomena in dynamic bisection. First, they do not make *a priori* predictions about the effects of velocity (speed and direction). Second, it is unclear which neural mechanisms or populations are involved in translating concepts such as 'hemispheric activation' or 'attention' into biases, or under what conditions such explanations can be invoked. Finally, there is little precision to qualitative models of this sort. In contrast, mathematical models of static line bisection such as Anderson's salience functions or Chatterjee's power law, provide quantitative estimates but do not incorporate velocity or dynamic behaviour. The same is true of computational models (e.g., Monaghan & Shillcock, 1998; Mozer, 1997; Pouget & Sejnowski, 2001). In fact, only the zone-of-indifference model (Marshall & Halligan, 1989) incorporates scan direction, but it is unable to explain behavioural differences in L-R relative to R-L scanning without additional ad hoc assumptions. The zone-of-indifference theory also does not explain why velocity affects biases. The one model specific to indirect computations of spatial extent, VDI (Diekmann et al., 2009), involves processes of dynamic judgments but requires refinements to be made into a testable or refutable theory of line bisection biases. The objective of this section, then, is to build a testable, quantitative model for dynamic judgments of line centre. A number of principles guide the development of the model:

1) *Biologically plausible.* That is, the model should be constrained to what an actual brain can do given the resources and time available for making dynamic judgments. It should also use known properties of the brain to do so (e.g., not include back-propagation);

2) *Architecture*. Dynamic bisection enlists neural regions (Experiment 5) each of which is composed of specific types of neurons. The model should be built with due consideration to the types of neurons and the local/global structures of the brain regions known to be involved;

3) *Correspondence to data.* Dynamic bisection is sufficiently messy that it would be impossible to model all of the results from Experiments 2-4. Nevertheless, it is important to show that the main effects due to line length, position, scan direction, and scanning speed can be incorporated. The model should provide quantitative as well as qualitative predictions;

4) *Static bisection.* The model is not required to reproduce static results (i.e., this is not an attempt to model both static and dynamic bisection).

5) *Parsimony*. While not a strict requirement, per se, the fewer assumptions that need to be made, the better.

The main techniques that will be engaged are (1) creation of a mathematical model, and (2) an implementation of it based on a framework for constructing biologically plausible neural models, i.e., the Neural Engineering Framework (NEF; Eliasmith & Anderson, 2003; an overview of some core ideas and techniques from the NEF is presented in Appendix C).

4.1 The Cumulative Representational Strength (CRS) model

4.1.1 Model assumptions

The basic assumption underlying a system that would use velocity and time to compute distance such as VDI (velocity-distance integration) is that distance is not measured directly but is calculated from the time and velocity inputs. A similar assumption is made in what follows. Next, there is considerable evidence that spatial judgments are influenced by the entire line and the properties of points on the line. McCourt & Jewell (1999) presented lines with ramped and constant contrast profiles to participants and, even though the endpoints were clearly visible, participants bisected the lines towards the lower contrast end. Others have found similar effects (Bradshaw et al., 1987; Valadao, Hurwitz, & Danckert, in press). In other words, each point on the line has a weighting (i.e., a 'representational strength') due to the characteristics of that point and its relationship with other points, and this representational strength influences the overall spatial judgment. A straightforward way of incorporating the representational strength idea is by treating it as a weighting function in the judgment of spatial extent, i.e., the greater the representational strength of a particular point, the greater the influence that point exerts on spatial judgments. Bisection, then, is just the average of the representational strengths for each point sampled on the line.

One way of conceptualizing representational strength is as an on-off indicator. That is, once an object or point on a line has entered spatial memory its representational strength is *immediately* fixed at a certain value determined only by the physical properties of the point such as its luminance. It is also possible to relax this assumption by suggesting that full representational strength is not instantaneously achieved. Rather, representational strength could follow a time course which requires a finite period of time to reach full strength, however short that time may be. In addition, once at full strength, without further processing the strength would decay over time. The model adopted here is one where representational strength varies continuously over time – generally increasing after the initial presentation of a point and then decreasing after a sufficiently long time.

In addition to the concept of representational strength, in Experiments 2 and 3 (and in the fMRI experiment) the line remained visible after scanning had ended. Because of this, it is likely that a static representation of the line developed in conjunction with the dynamic representation, making any biases a mixture of both static and dynamic bisection. Finally, Baek and colleagues (2002) showed that, in a multiple scan paradigm, it is the final direction of scan that is correlated to the bias.

Taken together then, these observations and assumptions form the core of the Cumulative Representational Strength (CRS) model of dynamic judgments of spatial extent are. Specifically:

Assumption 1: Distance is not calculated directly in the absence of a physical line but, rather, it is the indirect result of representational strengths bound to specific locations.

Assumption 2: The representational strength of any point or object in spatial memory varies with time, monotonically increasing for short times and decreasing for sufficiently long times. The maximum value of the representational strength for any point is a function of the characteristics of the point. In the case of an isoluminant line with no positional effects or cueing, this maximum value is uniform across the line length.

Assumption 3: Representational strength computes the bisection point using a weighted average of the contribution of each spatial location.

Assumption 4: The final bisection location is a function of both static and dynamic estimates when the line is available for static as well as dynamic judgments.

4.1.2 Mathematical description of the CRS model

We now construct an analytical model for CRS based on the model assumptions.

Assumption 1: Distance is not calculated directly in the absence of a physical line but, rather, it is the indirect result of representational strengths bound to specific locations.

A constant velocity scan can be parameterized by $x = vt$, where it is assumed that the line extends rightward from a left endpoint of $x = 0$ and the velocity is positive (i.e., a L-R scan). This assumption will be generalized later.

Assumption 2: The representational strength of any point or object in spatial memory varies with time, monotonically increasing for short times and decreasing for sufficiently long times. The maximum value of the representational strength for any point is a function of the characteristics of the point. In the case of an isoluminant line with no positional effects or cueing, this maximum value is uniform across the line length.

The representational strength of a point on the line, *x*, grows at a rate given by:

$$S'_x(t) \equiv \frac{dS_x}{dt} = \begin{cases} 0 & \text{if } t < t_x \\ f(t - t_x) & \text{if } t \geq t_x \end{cases} \tag{4.1}$$

where t_x is the time at which the point *x* is first viewed and S_x (the integral of the rate function) is the representational strength attached to the point *x* at that time *t* (given $t > t_x$). It is possible to build a model using either S_x or S'_x however applying the total representational strength to *x* requires computing the difference between the end of the event and the initial entry time of the memory trace for *x*. This difference cannot be computed until the end of the trial. In other words, every point would have to be bound with its temporal entry time in memory and only once the entire line had been scanned would the total representational strength be computed using these bound values. The

formulation presented in Assumption 3 (i.e., using the rate of change of representational strength rather than total representational strength), does not require maintaining a complex representation in memory and is therefore preferable. For this reason, the final form of the mathematical expression should involve the rate of change of representational strength.

Assumption 3: Representational strength computes the bisection point using a weighted average of the contribution of each spatial location.

The bisection point (BP) is the 'mean' of the position, weighted by representational strength:

$$BP = \frac{\int_0^1 S_x(1)x \cdot dt}{\int_0^1 S_x(1) \cdot dt} \tag{4.2}$$

Inserting assumptions 1 and 2, the BP can be determined from:

$$\begin{aligned} BP &= \frac{\int_0^1 \int_0^1 S_x'(r)\, t \cdot drdt}{\int_0^1 \int_0^1 S_x'(r) \cdot drdt} \\ &= \frac{\int_0^1 \int_t^1 f(r)\, t \cdot drdt}{\int_0^1 \int_t^1 f(r) \cdot drdt} \\ &= \frac{\int_0^1 \int_0^r f(r)\, t \cdot dtdr}{\int_0^1 \int_0^r f(r) \cdot dtdr} \end{aligned} \tag{4.3}$$

The numerator of the first line of Equation 4.3 is interpretable in the following way: starting at the point in time *t* when *x* enters the memory system, integrate the representational strength rate to the end of the scan (i.e., $r \in [t, 1]$) to determine the final representational strength. This variation in time produces a different representational strength by position, as depicted in Figure 16. As a result, a smaller final representational strength becomes associated with points that scanned at later times; for L-R scanning, this means positions near the right endpoint have a representational strength less than 1, while for R-L scanning it is positions near the left endpoint that are less than 1. Next, integrate over

all possible values of *t* to compute the weighted average of different positions. The denominator in this case is just the total value of representational strength for all points on the line (i.e., a normalization factor). The existence of a normalization factor is suggested by data from Foxe and colleagues (2003), for example, who found that the total representational strength of a line does not influence bisection behaviour.

The order of integration was changed in the final step of Equation 4.3 because the initial calculation of BP (the first and second lines in Equation 4.3) incorporates an *a priori* estimate of when the trial ends. In fact the entire first integration occurs over future times (i.e., $r \in [t, 1]$), which is not possible. However, by changing the order of integration in the final line of Equation 4.3 only past information is used (i.e., $t \in [0, r]$). For this reason, the final expression for BP is the appropriate mathematical basis for a computational model. So, while the first line in Equation 4.3 is the standard way for computing means over an arbitrary measure, it cannot be implemented by a temporally constrained system such as the brain. The challenge, then, is in understanding what specific functions neural systems are undertaking because it may not be possible to apply intuitive notions such as VDI. For example, in the above expression there is no integration of time and velocity.

Before incorporating Assumption 4 into the CRS model, it is useful to look at what the current formulation of BP predicts. Consider the class of representational strength functions given by:

$$S_x(t) = \begin{cases} 0, & t < t_x \\ 1 - e^{-a(t-t_x)}, & t \geq t_x \end{cases} \tag{4.4}$$

In this formulation, the variable *a* measures the rate of growth of representational strength over time. For example, if *x* = *t* (i.e., the scanning velocity is 1 unit/s in the L-R direction), the representational strength attached to each point by the end of the scan (i.e., *t = 1*) is given by:

$$S_x(1) = 1 - e^{-a(1-t_x)} \tag{4.5}$$

From Equation 4.5, the later the initial viewing time of each point, the less representational strength becomes attached to it. An example of representational strength functions is given in Figure 16 (the solid lines). The representational strength rate function is given by:

$$S_x'(t) = \begin{cases} 0, & t < t_x \\ e^{-a(t-t_x)}, & t \geq t_x \end{cases} \tag{4.6}$$

where the multiplicative factor of a has been ignored because the denominator in the BP calculation eliminates scaling through normalization. A closed form solution can be derived for the bisection point by substituting this functional form of Equation 4.6 into Equation 4.3. For L-R scanning $(x = t)$, the closed form solution obtained for the bisection point is:

$$BP_{LR} = \frac{a^2 - 2a + 2 - 2e^{-a}}{2a(a - 1 + e^{-a})} \tag{4.7}$$

Equivalently, for R-L scanning (substituting $x = 1 - t$ into Equation 4. 3) the exact solution is:

$$BP_{RL} = \frac{a^2 - 2 + 2e^{-a}(a + 1)}{2a(a - 1 + e^{-a})} \tag{4.8}$$

The bisection points for L-R and R-L scans are symmetric about the midpoint of the line as can be seen from the identity $BP_{LR} + BP_{RL} \equiv 1$. A plot of bisection points as a function of a (Figure 17) suggests that, for larger values of a, the bisection point is closer to centre. As $a \to \infty$, representational strength develops virtually instantaneously and there is no difference between L-R or R-L bisection. Scanning biases only occur because points entering spatial memory early have a slightly greater representational strength to weight the corresponding position than those that enter later.

More generally, a L-R scan with velocity s and line length L is given by $x = st$, and R-L by $x = L - st$, where $t \in [0, L/s]$. Substituting into Equation 4.3, for L-R:

$$BP_{LR} = \frac{\int_0^{L/s}\int_t^{L/s} e^{-a(r-t)}\, st \cdot drdt}{\int_0^{L/s}\int_t^{L/s} e^{-a(r-t)} \cdot drdt} = \frac{\int_0^{L/s}\int_0^{v} se^{-au}\,(v-u) \cdot dudv}{\int_0^{L/s}\int_0^{v} e^{-au} \cdot dudv} \tag{4.9}$$

where a transformation of variables has been used in the last line (u = r-t; v = r). The solution is:

$$BP_{LR} = \frac{a^2L^2 - 2asL + 2s^2 - 2s^2e^{-aL/s}}{2a\left(aL - s + se^{-aL/s}\right)} \tag{4.10}$$

which reduces to Equation 4.7 when $L/s = 1$. A similar expression could be determined for BP_{RL} from:

$$BP_{LR} + BP_{RL} \equiv L \tag{4.11}$$

For any fixed values of *L* and *s* a similar curve to Figure 17 would result.

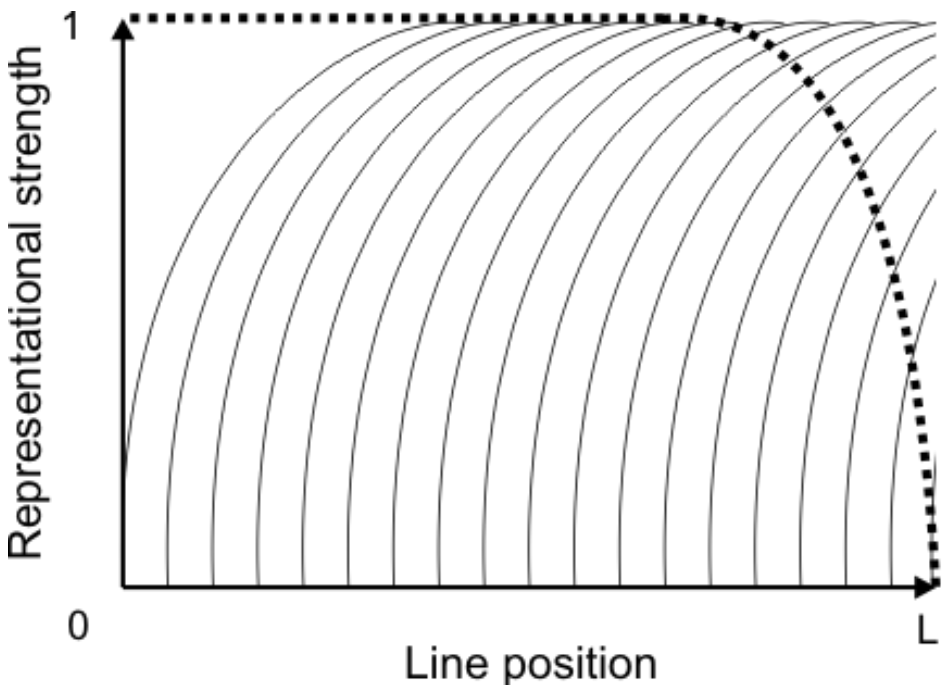

Figure 16. Representational strength applied to a line

In this example, a line of length L is scanned from left to right at a rate given by $x = t$. The ordinate axis thus represents line length as well as time. Representational strength grows at a rate e^{-at} (solid thin lines). The thicker, dotted line is the final representational strength of each point by the end of the scan. Most of the points of the line are at maximum representational strength by the end of the scan. It is only the last scanned section of the line which has less than maximum representational strength.

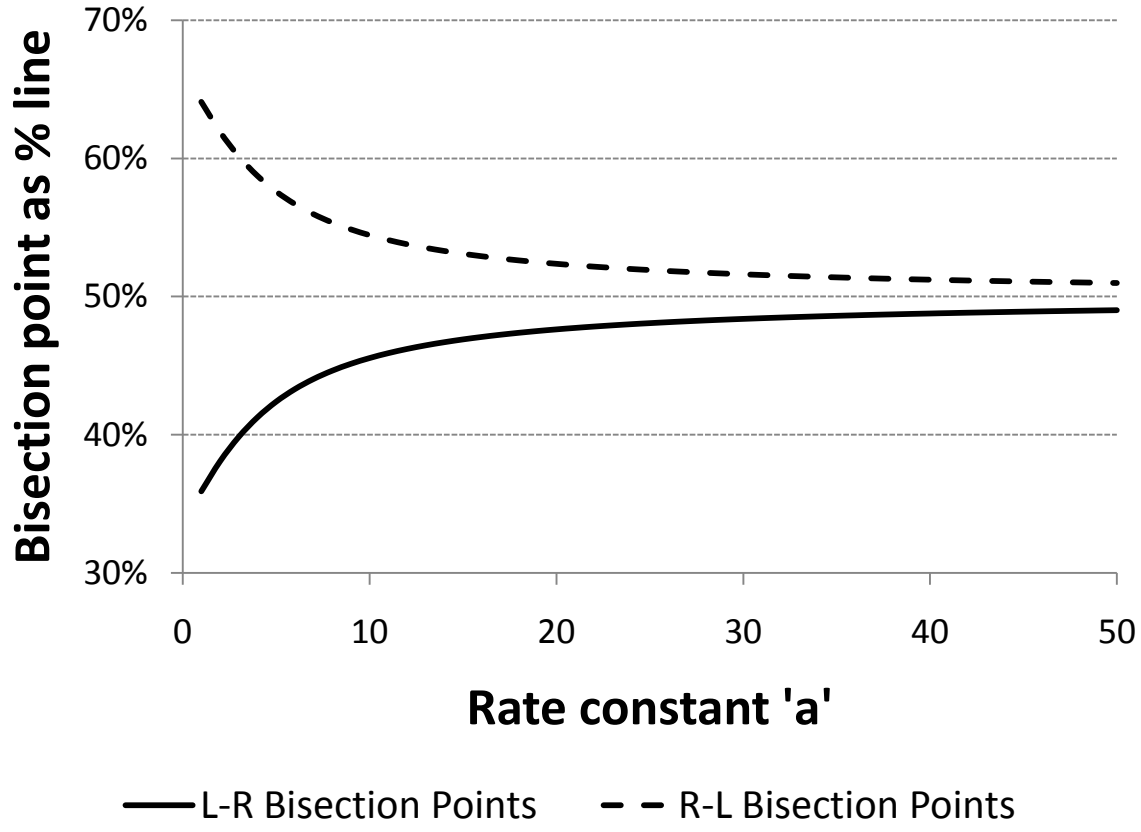

Figure 17. Bisection bias as a function of rate constant for the CRS model

The top curve (dashed) shows the relationship for R-L scanning between the rate constant, *a*, for the representational strength rate function e^{-at} and the bisection point. In this figure, the centre of the line is represented on the vertical axis by 50%; values above 50% indicate bisections biased to the right, and values below 50% to bisections biased to the left. R-L scanning produces a rightward bias but, as the rate constant, *a*, increases the bias asymptotically approaches the midpoint of the line. L-R scanning (solid curve) is mirror symmetric to R-L scanning across the midpoint of the line.

It is useful to look at the functional behaviour of BP for changes in length and speed because, as was evident in the behavioural experiments, there is a dependence on these variables. Assume the length of a line is given by $L \in [0, \infty]$. In the CRS model, the absolute size of bias increases as length increases but it decreases as a percentage of line length (Figure 18). For longer lines, the behaviour approximates a linear increase while for shorter lines it decreases more rapidly as a proportion of line length.

For slow scans, the difference between L-R and R-L scanning biases is small and approximates 0% of the line length. For fast scans the directional differences in scanning bisection biases can be as much as one-third of the line length.

Assumption 4: The final bisection location is a function of both static and dynamic estimates when the line is available for static as well as dynamic judgments.

There are four key experimental results the first three assumptions do not explain. First, the CRS model predicts that L-R and R-L scanning biases are symmetric about the midpoint but experimental results suggest that dynamic bisection produces an overall leftward bias. Second, positional effects are present in the data (Table 9) but are not predicted by the CRS model. Third, slower velocities lead to greater average biases from the true midpoint (Table 6) whereas the model predicts no average bias when the data is collapsed across scan direction. Finally, the difference in bisection biases between L-R and R-L scans is greatest in Experiment 4 (Table 10) when no lines were present, and yet the results are more symmetric about the midpoint in this experiment than in either Experiments 2 or 3.

All of these results can be explained by adding one assumption: since the line is on-screen for Experiment 2 and 3, it is possible that a static representation of the line is created at the same time as a dynamic representation. The two representations are averaged together to produce a mixed representation with a weighting dependent on the time the line appears on-screen. In other words:

$$BP_{LR} = \alpha(t) BP_{LR\ static} + \big(1 - \alpha(t)\big) BP_{LR\ dynamic}(static) \tag{4.12}$$

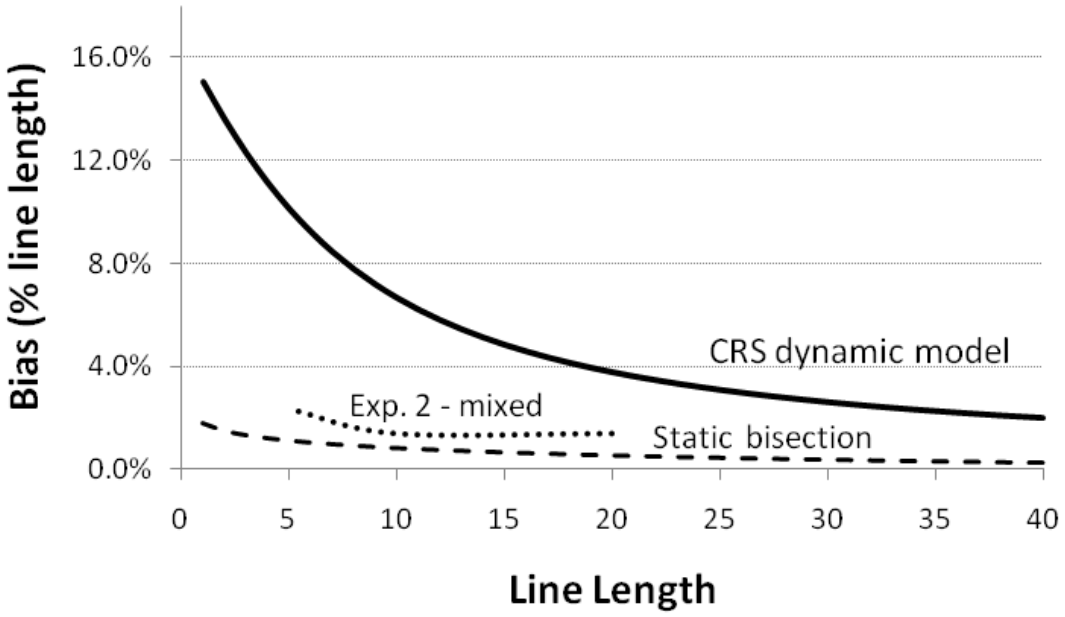

Figure 18. Dependence of bisection bias on line length

Three lines are presented in the graph. The top line, CRS dynamic model, was calculated from Equation 4.10, with s = 16.5 cm/s (the average speed in Experiment 2) and a = 10. The middle line, Exp. 2 – mixed, is taken from L-R scanning in left hemispace for Experiment 2. It represents a mixed model because the line stayed on-screen during and after scanning. The bottom line, Static bisection, was based on data from Chatterjee et al. (1994). As expected, the mixed model lies between the dynamic and static models, and there is a much greater change in bisection bias for dynamic bisection than for static bisection.

In this case, the weighting function (α) increases with the presentation time of the line on-screen: for short times or when there is no line, we expect $\alpha \approx 0$ and, as the line stays on-screen, α approaches 1. In Experiments 2 & 3, dynamic judgments were not isolated from static judgments. Since static bisections are position dependent and biased to the left so, too, are the observed biases. For slower speeds (or longer lines), static judgments have a greater weighting and therefore there is a greater influence of static bisection judgments. As dynamic scanning biases are symmetric between L-R and R-L scans, the overall effect is to produce a greater leftward bias for slower velocities. However, the difference between L-R and R-L scanning increases for faster speeds. This mixed effect (slower scans show overall greater leftward bias while faster scans show greater differences between scan directions) matches the experimental data (Figure 5).

Finally, the mixed model predicts that the no-line experiment (i.e., Experiment 4) leads to the greatest scanning bias differences between scan directions, along with the most symmetry around the midpoint. This corresponds with the behavioural results (Table 10).

The next step was to implement a neural model for dynamic bisection using the theoretical tools developed in this section.

4.1.3 A neural implementation of CRS

The mathematical model of scanning, with a scan speed *s* over a line of length *L,* can be rewritten from Equations 4.9 and 4.12 as:

$$\mathrm{BP_{LR}} = \frac{\mathrm{s}(1-\alpha)\left[\int_0^{\mathrm{T}} \mathrm{v} \int_0^{\mathrm{v}} \mathrm{e}^{-\mathrm{au}}\, dudv - \int_0^{\mathrm{T}} \int_0^{\mathrm{v}} \mathrm{ue}^{-\mathrm{au}}\, dudv\right]}{\int_0^{\mathrm{T}} \int_0^{\mathrm{v}} \mathrm{e}^{-\mathrm{au}} \cdot dudv} + \alpha \mathrm{BP_{static}} \tag{4.13}$$

where the total time of the scan is T. The variables *u* and *v* represent the time elapsed from the beginning of the scan.

Implementing this equation in a neural model requires the following:

1) A population of neurons to represent time (i.e., *u* and *v*).
2) A population of neurons to represent the speed of the scan, s.

3) Populations of neurons to compute the double integrals (this requires a number of steps).

4) Separate pathways for the numerator and denominator, and a population of neurons that computes their quotient.

5) A population of neurons that computes the final, weighted average of static and dynamic judgments.

6) A static bisection input. This value is not implemented in the NEF although it could be modeled and included at a later date.

7) The values of s, L, and T are set by the task characteristics. The best estimate of *a* is calculated from Experiment 4 (no-line) because it is the purest dynamic judgment. The difference between L-R and R-L scans in both positions (left and right hemispace) is about 7 mm. Thus, given L = 20 cm and s = 16.5 cm/s for the constant speed scan condition, a = 22 (the units of a are inverse seconds) from Equation 4.11. For this value of a, it takes about 30 ms of elapsed time for the representational strength to reach half its maximum strength, and about 100 ms to reach 90% of the maximum.

Each of the neural populations can be associated with activation areas identified in Experiment 5, and the appropriate neurons modeled within the NEF using the parameters in Table 12. The model proved to be relatively insensitive to values of the time constants (τ_{PCS} and τ_{RC}) within their normal range for human neurons of that type and so only one value has been shown in the Table.

Details of the code implementing Equation 4.13 are contained in Appendix D. The connections in the graphical model and the function inputs change depending on the specifics of the experimental conditions being investigated (e.g., the length of line and the direction of scan). A graphical representation of the network is presented in Figure 19 and of the bisection point(s) in Figure 20 and Figure 21.

Table 12. Properties of neurons used in implementation of CRS model

Function	Region	Neuron type	Parameters
Time signal	Cerebellar nuclei	Large-bodied neurons with glutamate transmitters	τ_{PSC} = 10 ms τ_{RC} = 20 ms S = 100-200 Hz
Velocity signal	MT or vestibular nucleus	Large-bodied neurons with glutamate transmitters	τ_{PSC} = 10 ms τ_{RC} = 20 ms S = 100-200 Hz
Integration & normalization	Cuneus and precuneus, across parieto-occipital junction	Pyramidal neurons with AMPA synapses for integration connections, and glutamate for inter-population connections	τ_{RC} = 20 ms S = 80-120 Hz τ_{PSC} = 50 ms (other) τ_{PSC} = 7 ms (AMPA)
Weighted average	Right precuneus	Pyramidal neurons, glutamate synapses	τ_{PSC} = 7 ms τ_{RC} = 20 ms S = 80-120 Hz
Mapping to line	Left superior parietal lobule	Pyramidal neurons, glutamate synapses	τ_{PSC} = 7 ms τ_{RC} = 20 ms S = 80-120 Hz

Above are the key parameters used for each population of neurons in the CRS model.

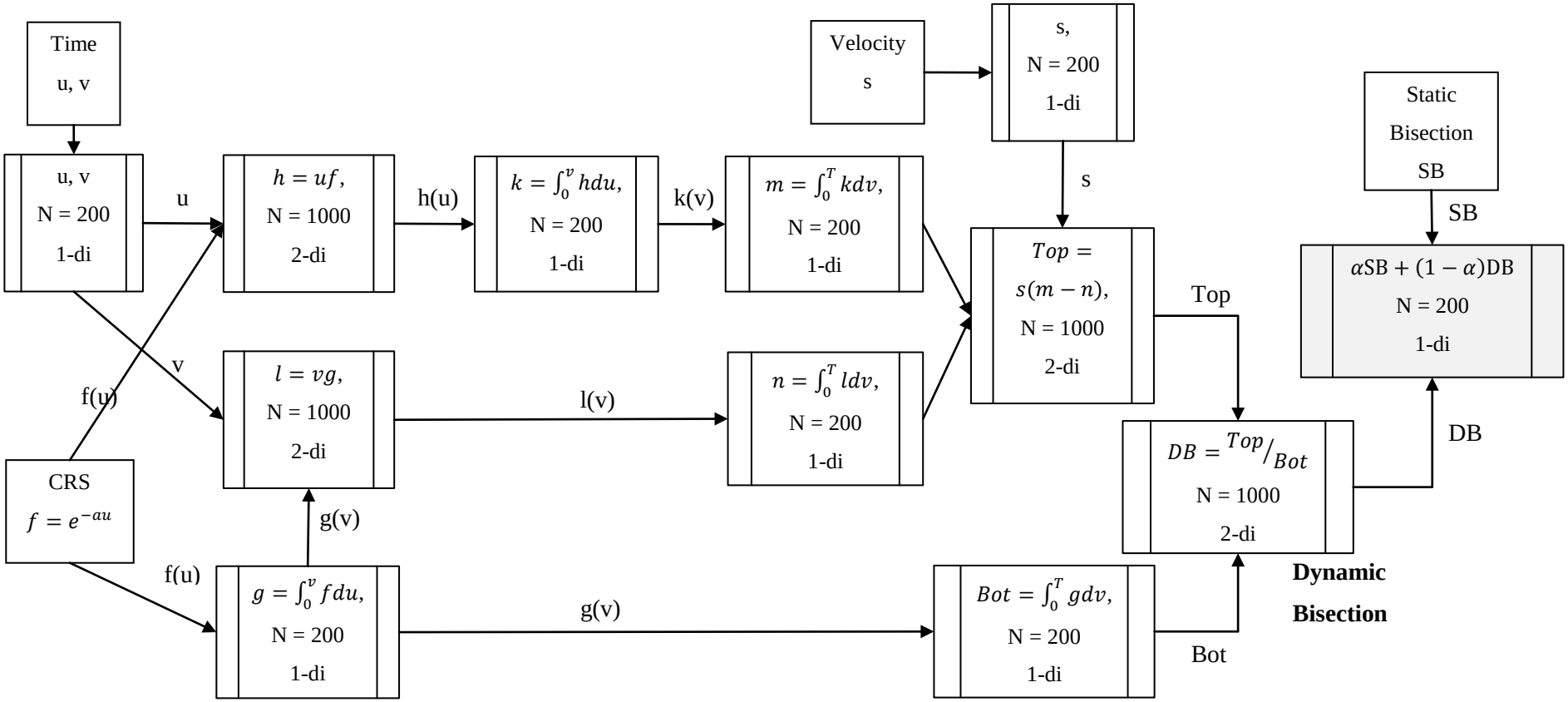

Figure 19. Schematic representation of mixed model bisection neural network

Implementation in the NEF of Equation 4.13. The code in Appendix D creates this network in Nengo. Values of a, T, s, SB, and α are parameters in the code. Where integration is shown in the figure, it is implemented by connecting the population back to itself (not shown). The output population is shown in grey.

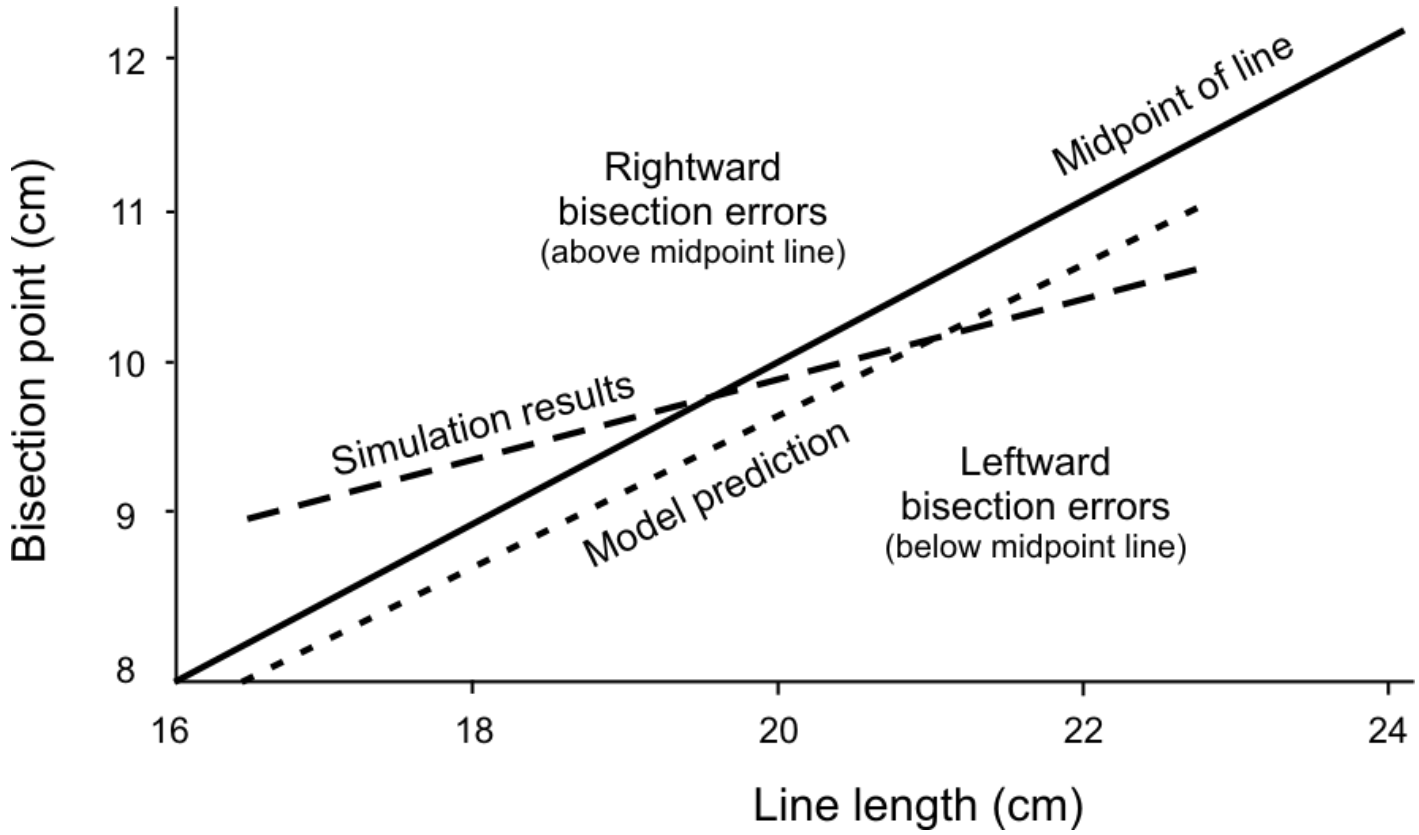

Figure 20. Dynamic bisection of line with no static contribution

Graph of bisection point L-R scan at a speed of 16.5 cm/s with a = 22. The bisection point from the simulation was approximately 9.8 cm for a 20 cm line, i.e., just to the left of centre. The mathematical model predicts a bisection value of 9.6 cm. As we can see from the graph, the simulation bisection point only changed from 9 to 10.5 cm for lines 16.5-23 cm, i.e., about half the change predicted by the mathematical model (8-11 cm) but, as expected, it was a nearly linear increase with line length. The simulation indicates a cross-over point (i.e., where it crosses the midpoint line) at about 19 cm, which is higher than would be expected.

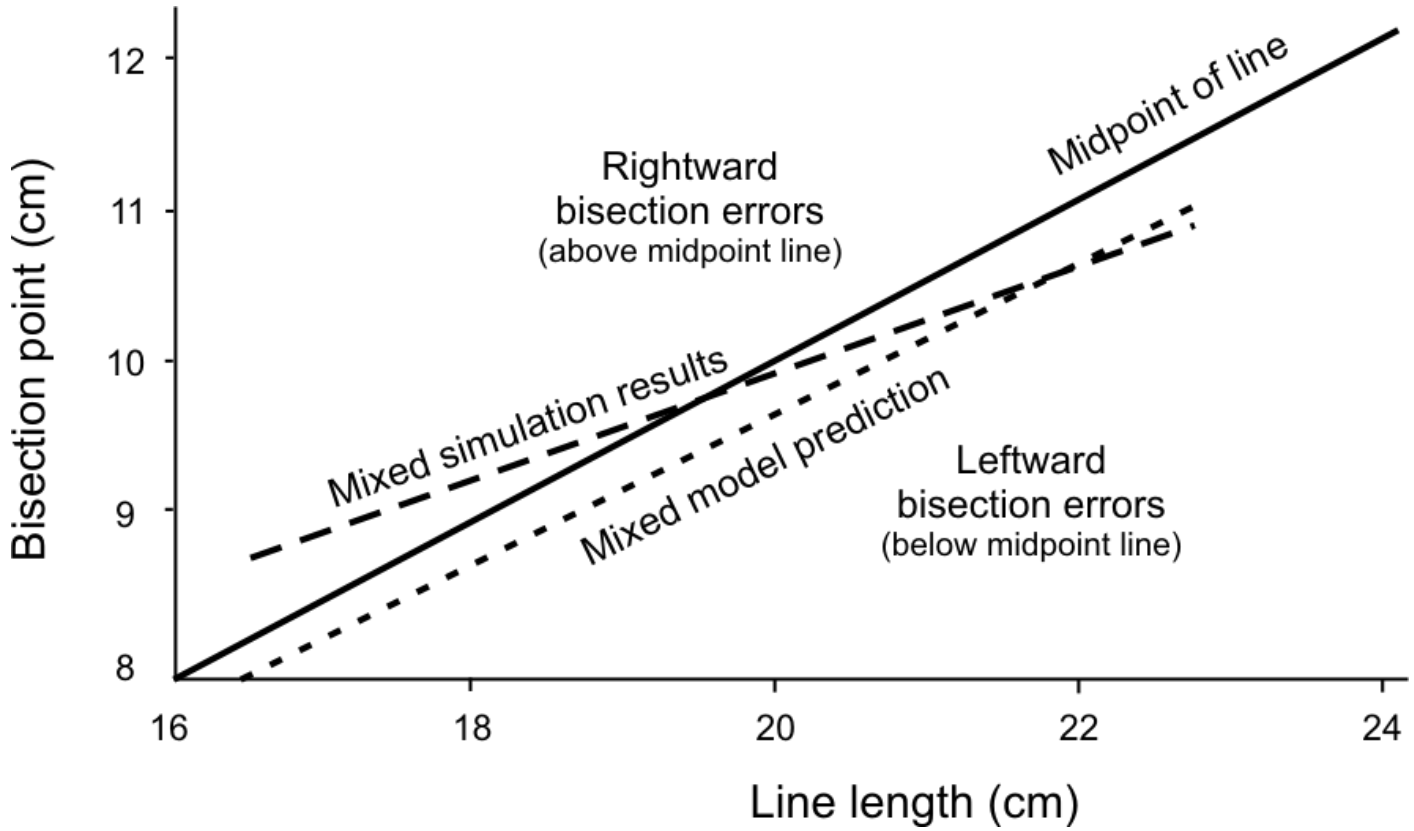

Figure 21. Mixed bisection model

The same simulation as Figure 20 with $\alpha = 0.40$. The slope of the simulation is due to influence of the static bisection component. The mixed model requires an estimate for static bisection over different line lengths: Chatterjee's power law was used for the static bisection estimate with parameters $K = 1.03$ and $\beta = 0.992$ based on an 'average' healthy person (Chatterjee et al., 1994). Although it is not plotted in this figure, the psychophysical power law predicts a curve that lies between the 'Midpoint of line' and the 'Mixed model prediction'.

4.1.4 Results

Longest fixations show significant effects of position in Experiments 1-3 but not Experiment 4 (Table 9), with a leftward bias in left hemispace and a rightward or marginally leftward bias in right space. The CRS model suggests that L-R and R-L scans produce symmetric biases around the midpoint (i.e., when collapsed across the two measures the average bias is 0). However, when static and dynamic judgments are mixed, this symmetric scanning bias is distributed around the value of the static bisection bias, proportionate to the influence of static judgments. As predicted by CRS, Experiment 4 (i.e., the one least affected by static judgments) was also the only experiment not to show an effect of position for LF. Similarly, there was no effect of position for PB in any experiment. Only FF was anomalous, with an effect of position in every case.

Another prediction CRS makes is that the difference in L-R vs. R-L bisection biases change based on the speed of scanning: for slow speeds the difference is a negligible percent of the line length while, for fast scans, the directional differences in scanning bisection biases can be as much as one-third of the line length. In accordance with this prediction, there was a smaller difference between scanning directions for slower speeds than for faster speeds in Experiment 2 (Figure 5b). However, this effect was only seen in FF.

As the time taken during a scan increased (Table 6) so, too, did the bias (collapsed across scan direction) for both ocular measures in accordance with the mixed CRS model. The CRS model also predicts that the proportionate difference between L-R and R-L bisections should decrease as line length increases (Figure 18). This effect would be evident as a length by scan direction interaction. No such interaction was observed for either FF or LF in Experiments 2 or 3 (length was not varied in Experiment 4). On the other hand, static bisection biases increase with line length (Chatterjee et al., 1994) and, in agreement with the predictions of the mixed model, LF had the expected length effect in Experiments 2 & 3 (length was not manipulated in Experiment 4).

4.2 Discussion

Although the agreement between the data and model for the three measures (FF, LF, and PB) was inconsistent, the overall pattern supports the CRS model. Some examples where CRS failed to predict the results were in the lack of a scan direction effect for FF or LF in Experiment 2, and the main effect of scan in Experiment 3 for FF is in the opposite direction to that expected (i.e., L-R scans are

right of centre and R-L scans are left of centre). This lack of full agreement is not surprising given the complex nature of the experimental data. One cause may be because effect sizes were small, while another is that different tasks and instructions may produce different or even conflicting results (Jewell & McCourt, 2000). Furthermore, participants may have adopted different strategies for bisecting the line which highlights the challenge that the CRS model is meant to explain individual data but, instead, is being compared to data at the group level. Validating the model at an individual level would require the inclusion of more values for the various conditions (length, speed, position) than were used in Experiments 2-4, as well as a greater number of trials per cell.

It is unclear to what extent any bisection model, including CRS, can be generalized to other types of dynamic judgments such as two- and three-dimensional shapes. For instance, the results of centre-of-mass judgments have been shown to depend on the geometry and dimensionality of the task (Fink, Marshall, Weiss, Shah, Toni, Halligan, & Zilles, 2000b; Halligan & Marshall, 1991; McCourt & Jewell, 1999; McCourt & Garlinghouse, 2000b). Bisection is a special case, even in one-dimension, because it can be computed as the mean of a statistical distribution and therefore is easily solvable by integration (Equation 4.2) or by geometrical considerations because it is a point of symmetry. Even with these caveats, however, the CRS model is largely in agreement with the data and is only contraindicated by the one FF result in Experiment 3.

While an exponential function is be a biologically plausible choice for the CRS rate, any monotonically increasing function produces the same qualitative predictions (i.e., symmetric L-R (leftward) and R-L (rightward) biases, increasing biases with faster scans, increasing biases for longer lines but decreasing biases proportionate to the line length). The advantage of using an exponential function was that it provided a closed form solution for illustrative purposes. For example, the code in Appendix D implementing the model could be modified with any choice of CRS rate function and the results would be similar[5]. On the other hand, there was no inclusion of the (likely) prospect that the representational strength decays after a sufficiently long time. A proper representational strength function would be shaped like a hillock rather than monotonically increasing. Predicted outcomes for hillock-shaped functions depend on the specific shape of the function (except when the scanning is quick enough that only the increasing part of the hillock is included) making it a less suitable choice

[5] Changing the rate function necessitates refining the scaling constants, f1-5, to accurately multiply and integrate over the appropriate range of values.

for an initial investigation for two reasons. First, the freedom to find a function that fits the data is unconstrained because of the many choices of a rate function. As well, a hillock function adds a layer of complexity more suited to a detailed follow-up study rather than a first exposition.

Most of the predictions of CRS were made using the mathematical model without reference to the computational model. However, building a biologically plausible neural model did produce useful insights into how a neural system might perform dynamic bisection. One way a system could implement CRS is to bind a representational strength to each point, as suggested by Equation 4.2. Doing so, however, is impossible for a neural system to implement because it requires integrating over the past and future simultaneously. Because of this consideration, the final form of integration used (Equation 4.13) depends on the rate of change of representational rate rather than the function itself. However, neither term in the numerator of Equation 4.13 has an intuitive interpretation. Furthermore, while the VDI model of dynamic judgment suggests that velocity and time are integrated together to produce an estimate of the distance, the CRS model uses time as variable in the integrations but it is never multiplied (or integrated) with velocity. Specifically, *there is no explicit computation of distance in bisection.* Indeed, velocity was only applied as a multiplicative factor at the end of the computation of the dynamic bisection point (the *s* in Equation 4.13).

An additional requirement in implementing the CRS model using the NEF was the need for scaling constants to accurately compute multiplications and divisions (the factors f1-5 in the computer code; Appendix D). The purpose of scaling is to optimize the overall efficiency of neural computations by converting inputs with arbitrary magnitudes into values that a downstream neural population is tuned for. For example, in multiplication and division the neural system scales the inputs to values close to unity, performs the multiplication or division, and then rescales the outputs by the same factor. Scaling and rescaling has an interesting consequence when multiple stimuli are included in a single set of trials. In experiments investigating perceptual estimates of brightness, weight, force, or line length it has been found that the psychophysical estimate of a stimulus property is often underestimated for the longest/brightest/heaviest stimulus and overestimated for the shortest/dimmest/lightest, i.e., a context effect (Hollingworth, 1909; Jones & Wearden, 2004; Marshall, Lazar, Krakauer, & Sharma, 1998; Mennemeier, Rapcsak, Dillon, & Vezey, 1998; Mennemeier et al., 2005; Ricci & Chatterjee, 2001). For example, in a study conducted on neglect patients, Marshall and colleagues (1998) found that biases in bisecting different line lengths in isolation were the same percentage rightward shift regardless of the line length. However, when a

second line was added and the stimuli presented within the same set of trials, the bisection bias of the original line shifted to the left if the second line was longer than the original and to the right when it was shorter. Scaling in such situations requires finding optimal scaling factors for the entire set of stimuli; this produces distortions, however, in the computation for each stimulus relative to when scaling is optimized for that single stimulus. Scaling tends to compress the output space for reasons such as saturation in neural firing rates. Consequently, scaling could explain context effects for line bisection (Mennemeier et al., 1998) and therefore predict cross-over as lines get shorter (Figure 20), albeit at values that are considerably higher than expected in this case.

Although the CRS model was only used to account for the data from healthy individuals, it is interesting to speculate on how it might apply to neglect patients. A large region of right supramarginal gyrus was activated in the SB > DB condition and a small portion in the same area for the DB > Control condition. This area often sustains damage in neglect and, if so, the damage could impair both static bisections and how static judgments are combined with dynamic judgments. For example, static judgments could be input into the dynamic system as noise, increasing the variability of the output. Another possibility is that subsecond temporal judgments, known to be impaired in neglect patients (Harrington et al, 1998; Basso et al., 1996), affect the timing signal (the ‘v’ and ‘u’ in the integrands of Equation 4.13, and the neural population in the simulation).

Overall, then, we have seen that the CRS model is able to explain much of the data for dynamic bisection based on a very small set of premises. It also provides a useful framework for future investigation, and makes a number of interesting theoretical statements (e.g., how velocity is incorporated, whether representational strength is instantaneous or not, the context effect, etc.).

Chapter 5: **Conclusions**

The initial motivation for this thesis was to investigate the finding by Jewell & McCourt (2000) that dynamic line bisection, particularly L-R scanning, produces one of the largest leftward bisection biases of the many types of factors that have been studied. Dynamic bisection was investigated here using three techniques: behavioural studies, neuroimaging, and a mathematical/computational model. From the convergence of the three approaches, it is apparent that static judgments differ from dynamic judgments in a number of key respects. Behaviourally (Experiments 1 & 2), ocular fixations have a different pattern of biases for static relative to dynamic conditions, a novel but unsurprising result. The conclusion, i.e., that the two are fundamentally different rather than just separate computations by the same neural network, was supported by neuroimaging evidence showing that dynamic judgments produce large bilateral activations of the cuneus and precuneus relative to static judgments, whereas the reverse contrast shows enhanced activation bilaterally in the inferior parietal lobule – a location often associated with (static) spatial judgments and hemispatial neglect. The cerebellum and left superior parietal lobule may also be involved in dynamic judgments of extent. Overall, then, this thesis adds to the body of literature showing that medial parietal regions are associated with dynamic judgments of spatial extent, our sense of self in motion, mental rotations, the avoidance of objects while walking, and other, higher level motion processing functions.

Although direction specific behavioural effects were found that were similar to the Jewell and McCourt meta-analysis, the fMRI experiment suggests that it is unlikely to be due to hemispheric asymmetry. A simpler and more persuasive explanation is that the processing of dynamic judgments is asymmetric because of *how* it is done, not because of *where* it is done. Cumulative representational strength is a model which predicts scan direction effects based on the *how* rather than the *where*. It is also a model which can be implemented by the (human) brain in accord with the neuroimaging data using a relatively small network of neurons.

Differences in the neural networks used for static and dynamic tasks have important implications for the clinical treatment of neglect patients and research into the disorder, as well as the many other syndromes for which bisection is abnormal (e.g., ADHD and schizophrenia). Some of the standard techniques which are known to supply temporary relief of the symptoms of neglect invoke dynamic judgment mechanisms. A deeper understanding of these mechanisms will aid in the development of clinical treatments. Importantly, there has not been much direct research on dynamic judgments in

neglect patients (the studies on line bisection, for example, were on small samples and may not be generalizable). This is a potentially fruitful area for future research.

A further contribution is the finding that the hand and eyes are not yoked to each other for bisection tasks. For static judgments, the correlations between ocular fixation locations were universally high but the correlations were effectively zero between ocular fixations and pointing. There was also a different pattern of bisections for ocular and pointing behaviour in dynamic bisections, with pointing more resistant to positional effects. This dichotomy between the hand and eyes provides a useful way of explaining seemingly contradictory results in the bisection literature, specifically, that landmark and paper-and-pencil tasks differ and cannot be used interchangeably as probes of spatial extent. Furthermore, tachistoscopic line presentation may result in differences from stimuli with longer presentations (FF versus LF probes, respectively). This also suggests that a single model might not be applicable to ocular and pointing behaviour, or even to different types of ocular behaviour, although CRS was successful in explaining a number of results for both ocular and pointing behaviour. Both the limits and advantages of CRS could be better understood through further experimentation manipulating line length and speed over a wider range of values, especially using the invisible line paradigm of Experiment 4 to reduce or eliminate the confound of static bisection processing. In addition, it would be interesting to see what effect there is of longer scan times, when the representational strength function is proposed to decay.

Another purpose of this thesis was to determine what, if any, are the effects of various stimulus characteristics on dynamic bisection (speed, scan direction, acceleration results, line length, position). Positional effects were consistent with previous research (i.e., leftward positions produced a leftward bias and rightward positions produced a bias to the right of the leftward positional bias). It was shown that scanning speed reduces overall bisection biases, as predicted by CRS but does not consistently increase the directional effect, also predicted by the CRS model. Scan direction generally creates a leftward bias for L-R relative to R-L scans but not always for ocular behaviour. Deceleration also appears to result in a larger bias than a constant speed or accelerating scan. Pointing behaviour was less affected than ocular fixations by these manipulations for short lines, but was affected by scan direction and position for longer lines. Indeed, when the presumed influence of static bisections was removed (Experiment 4) pointing became as subject to the influence of stimulus characteristics as the eyes, with similar effects for everything except position. Perhaps the difference is due to the eyes' role in scanning the environment (for danger, food, etc.) and the hand's role in acting on the

environment, or perhaps separate systems have evolved only for certain aspects of static but not dynamic processing.

Another interesting possibility which arose specifically from the creation of a computational model is the claim that context effects are due to the need to optimize scaling over a range of values on a stimulus dimension. Implementing the mathematical model also demonstrated that a simple model such as VDI may not be the best way to understand the computations being done in the brain. Indeed, while CRS is easily implemented, the calculations involved do not correspond to intuitive notions of how such judgments might be done.

Overall, then, the results of this thesis provide a solid base from which to build and investigate dynamic judgments of spatial extent. It helps interpret and integrate existing data, presents a model that can be explored more fully and tested (or refuted) explicitly, proposes a mapping of particular functions to different brain areas (including an interesting possibility about the role of left superior parietal regions), and suggests future clinical research with the hope of new treatments for patients with spatial disorders.

Appendix A: Line Bisection By Task Type, A Summary

Paper	Line length	Task*			Additional task characteristics	Participant factors	Findings
		LM	PP	Scan			
Brodie & Dunn, 2005	8, 10, 12, 14, 16 cm		✓	✓	Lines were in different places on page, and pages were centered in different hemispatial locations.	Hand used to bisect line was a manipulandum. Both sinistrals and dextrals were tested.	No main effect for hemispace; main effect for scan direction (L-R left of R-L); sinistrals using their left hand from R-L was the only condition to have significant rightward bisections.
Brodie & Pettigrew, 1996	8, 10, 12, 14, 16 cm		✓	✓	Lines were in different places on page, and pages were centered in different hemispatial locations.	Dextrals only, but the task was analyzed with sex and hand used as additional factors.	Main effect of scanning (L-R leftwards of R-L) with both to the left of center.
Chokron et al., 1998	5, 15, and 20 cm	✓			Slowly moving mark across screen (2 cm/s). Scan direction blocked into 24 trials, and line length randomized within blocks.	Half were native Hebrew readers, half were native French readers.	Leftward bias for L-R scan, rightward bias for R-L scan. For French participants, these biases were increased for longer lines.
Chiba et al., 2006	30.6 mm	✓		✓	The slowest of all moving stimuli, at about 1°/sec, as well as the longest line. Any number of retrials was allowed until participant thought at midpoint. Blocked design.	Dextrals only. Only older adults were used (age-matched controls for a patient group).	No difference was seen between L-R scanning and R-L scanning. Both scan directions also produced no significant bias from the midpoint of the line.
Nicholls & Roberts, 2002	11, 13.2, 15.4, 17.6, 19.8 cm	✓		✓	Participants followed a marker moving at 2.2 cm/sec in task 2 of experiment 1 (line bisection). Line length randomized across trials.	Used bimanual button press in both experiments. All dextral.	Bisection task, i.e., based on forced scanning, showed overall leftward bisection for both groups. R-L scanning induced greater leftward bisection. Length-by-scan direction interaction (less effect of scan direction for longer lines).
Reuter-Lorenz & Posner, 1990	5 and 8 cm	✓	✓	✓	Participant says stop at midpoint. Lines could include left, right, or no cues. Track a slowly moving pen being moved across the line by the experimenter.	Healthy older controls (handedness unknown)	No effect of line position or scan direction (‘no cue’ trials only).
Reuter-Lorenz et al., 1990	3.2° visual angle	✓			Tachistoscopic presentation, participants reported verbally whether the transection mark was to the left, right or at the line’s midpoint.	Right-handed healthy undergraduates.	Leftward bias for left position, rightward for right position

Paper	Line length	Task*			Additional task characteristics	Participant factors	Findings
		LM	PP	Scan			
McCourt & Jewell, 1999	22.3°	✓			Lines were formed of two horizontal stripes, one white the other black. At the transection point, the white stripe turned black, and the black stripe turned white. Tachistoscopic presentation followed by forced choice (L, R). Lines were positioned in left, right, superior, and inferior hemispace.	Right-handed healthy undergraduates.	Leftward error at midline, increasing in left hemispace; rightward errors in right hemispace.
Rueckert et al., 2002	1-28 cm (viewed from 30-50 cm)	✓	✓		Lines of various sizes presented on a page, offset either to the left or right of centre. In the PP task, participants put a cross where they believed midpoint was, in the LM task a forced choice of L or R was required. PP and LM were blocked. In last two experiments, one line per page only.	Right-handed healthy undergraduates.	Landmark task biased: leftward bias for right hemispace compared to left hemispace, except longest line where reverse was true. Paper-and-pencil unbiased: showed no difference for position when averaged over length.
Milner et al., 1992	20 cm	✓	✓		For PP, participant transected lines with pencil. Lines were in left, central, or right space. For LM, forced choice made on pre-transected lines (transection marks to left, right, or on midpoint). Final experiment was LM but pointing response rather than verbal response.	Healthy right-handed adults.	Landmark task biased: small leftward bias in left space. However, no effect was seen when pointing. Paper-and-pencil biased: leftward bias in left and central space, not in right space.
Luh, 1995	2-12 cm	✓	✓		Two PP manual line bisection tasks, one with lines in L, C, R space, the other with lines only in L and R space. The LM task was a forced choice of whether transection mark was to the left or right of centre when, in actuality, it was in the centre. The computerized task required line bisection by using a mouse to place a hatch mark over the apparent line centre.	Healthy undergraduates including both dextral and sinistrals, but no differences were found by handedness.	Paper-and-pencil biased: overall leftward bias, more so in left space. Computerized task: no overall bias, but differences in position (lines in left space produced greater leftward biases). Landmark task unbiased: greater variability was seen, but no bias overall, or due to the position of the line.
Ishiai et al., 1989	Variable between 30° to 50° visual angle	✓	✓		Lines placed in right, central, and left hemispace. The page was moved (line always centred on page). A head-mounted camera tracked eye movements.	Right-handed older adults with no neurological deficits.	Paper-and-pencil unbiased: no significant results reported for position. Eye-fixation unbiased: no significant difference between the total 'area' searched left compared to right.

Paper	Line length	Task* LM	PP	Scan	Additional task characteristics	Participant factors	Findings
Nichelli et al., 1989	8-24 cm		✓		Lines placed in right, central, and left hemispace. Bisections were done with a pencil.	Right-handed older adults with no neurological deficits.	Overall rightward bias. rightward bias for lines in left hemispace, leftward bias for lines in right hemispace.
Butter et al., 1988	10-30 cm		✓		Lines placed in right, central, and left hemispace. Bisections were done with a pencil	Right-handed older medical patients with no neurological deficits.	No significant results reported (but no ANOVA conducted so could be left-right differences).
Fukatsu et al., 1990	8-20 cm		✓		Lines placed in right, central, and left hemispace. Bisections were done with a pencil. The page was moved (line always centred on page).	Right-handed older medical patients with no neurological deficits	No significant results reported for position.
Mennemeier et al., 1997	25-34 cm		✓		Lines placed in right, central, and left hemispace. Bisections were done with a pencil	Right-handed older adults with no neurological deficits.	No significant bias in all (non-cued) conditions.
Mennemeier et al., 2001	0.5-80 cm		✓		Lines placed in right, central, and left hemispace. Bisections were done with a pencil	Right-handed older adults with no neurological deficits.	Paper-and-pencil biased: overall leftward bias with no effect of spatial location and some effect of size for small lines.

*LM = landmark task or perceptual (i.e., not pointing or paper-and-pencil); PP = paper-and-pencil task; Scan = task involved scanning

Appendix B: Neural Data from Previous Bisection Experiments

Previous neural probes of bisection

BA	Description	Talairach Coords			Timing	
		x	y	z		
Cerebellum						
—	Left posterior lobe	-28	-64	-20		F1
—	Left cerebellar vermis	-4	-72	-20		F1
—	Left posterior lobe	-34	-54	-32		F2
—	Left culmen	-8	-58	-6		F3
—	Right posterior lobe	10	-76	-8		F4a
—	Right insula					M
—	Left posterior lobe	-6	-78	-30		F5
—	Left posterior lobe	-28	-66	-36		F5
Cuneus						
17	Right cuneus	4	-84	8		F1
18	Right cuneus	16	-72	18		F2
19	Right cuneus	16	-78	32		F3
19	Right cuneus	12	-90	32		F6a
18	Left cuneus	-8	-76	20		F1
—	Right TPJ and right occipital cortices				170-190 ms	Fo
Middle occipital gyrus						
18	Right middle occipital gyrus	36	-90	-2		F2
18	Right middle occipital gyrus	8	-92	14		F6a
18	Right middle occipital gyrus	28	-80	-10		F6b
18	Right middle occipital gyrus	32	-94	-2		F3
18	Right middle occipital gyrus				90-110 ms, 160-170 ms, 210-220 ms decreased relative to controls from 300 ms	W
19	Right middle occipital gyrus	32	-88	8		F1
18	Left middle occipital gyrus	-34	-88	-8		F2
18	Left middle occipital gyrus	-30	-92	0		F3
18/19	Right lateral occipital cortex				240-400 ms	Fo
Lingual gyrus						
17	Right lingual gyrus	22	-90	2		F6b
18	Right lingual gyrus	2	-74	0		F6a
18	Right lingual gyrus	16	-80	-10		F6b
18	Left lingual gyrus	-6	-80	-8		F4a
19	Right inferior occipital gyrus				150-160 ms, decreased from 280 ms	W

BA	Description	Talairach Coords			Timing	
		x	y	z		
19	Left inferior occipital gyrus				135-155 ms, 200-245 ms, decreased from 260 ms	W
Transverse occipital gyri						
7/18	Right lateral and medial occipital cortex				Sources increased up to 400 ms	B
7/18	Left lateral and medial occipital cortex				More active than other left hemisphere regions during first 300 ms only	B
19	Right superior occipital gyrus	34	-78	32		F5
Precuneus						
19	Right precuneus	12	-86	42		F6a
Temporal regions						
—	Bilateral superior temporal cortex				Significant activity sources (some leftward bias)	B
19	Right middle temporal gyrus	44	-80	18		F3
22	Right superior temporal cortex					M
Inferior parietal cortex						
—	Right inferior and superior parietal cortices				240-400 ms	Fo
—	Right inferior parietal cortex				200-300 ms after stimulus onset	B
40	Right lateral inferior parietal cortex	44	-32	52		F1
40	Right inferior posterior parietal cortex				190-210 ms	W
40	Right inferior parietal lobe	40	-50	56		F2
40	Right inferior parietal lobe	40	-40	42		F5
40	Left inferior parietal lobe	-38	-42	40		F5
Superior parietal cortex						
—	Right superior parietal cortex				190-240 ms	Fo
7	Right superior posterior parietal cortex				115-140 ms, 170-190 ms	W
7	Right lateral superior parietal cortex	24	-52	64		F1
7	Left superior posterior parietal cortex	-12	-64	56		F4b
7	Right superior posterior parietal cortex	22	-64	58		F5
7	Left superior posterior parietal cortex	-26	-58	54		F5

BA	Description	Talairach Coords			Timing
		x	y	z	
7	Right superior parietal lobule	24	-64	58	F6a
7	Left superior parietal lobule	-6	-68	56	F6a
Frontal Regions					
9	Right medial frontal gyrus	2	38	28	F5
9	Left medial frontal gyrus	-6	32	28	F5
10	Superior frontal gyrus	18	54	-6	F3
46	Right middle frontal gyrus	50	20	20	F5
46	Right middle frontal gyrus	46	53	6	F5
47	Right inferior frontal gyrus	34	28	-10	F5
47	Left inferior frontal gyrus	-32	26	-8	F5
45, 46	Right dorsolateral prefrontal cortex				M

In this table, the description of each region has been changed from the original paper to correspond with conventions being used in the rest of thesis. As well, the Talairach coordinates did not always correspond with the descriptions given in the original paper; in all cases, the description and BA area has been changed to match the coordinates.

B - Billingsley et al. (2004) – magnetic source imaging (MSI); a landmark task for which participants were to decide whether the line was transected veridically, or to the left or right of centre (responses were made via button press after the stimulus disappeared from a back-projection screen). Only specific regions of interest (areas seen in previous studies mentioned in this table, for the most part) were actually investigated.

F1 - Fink et al. (2000) – fMRI experiment; a landmark task (i.e., participants were to indicate by means of button press whether a line was properly bisected and, if not, in what direction it was misbisected, left or right) was contrasted with a control condition (indicate whether a line did or did not contain a transection mark)

F2 - Fink et al. (2000b) – fMRI experiment; a landmark task, i.e., participants were to indicate by means of button press whether a line was properly bisected, and a control condition for which the only response was whether the line did or did not contain a transection mark

F3 - Fink et al. (2000b) – fMRI experiment; a "Squaremark" task, i.e., participants were to indicate whether a mark inside a rectangle was at the center contrasted with a control condition for which the response was whether the line did or did not contain a mark

F4 - Fink et al. (2002) – fMRI experiment; a landmark task was given to all participants with one of two sets of instructions. The first instruction was to judge whether the transection mark was at the centre of the line, the second instruction was to determine whether the length of the line to the left of the transection mark was the same as to the right. In (a) length judgment was subtracted from centre judgment; and in (b) centre judgment was subtracted from length judgment

F5 - Fink et al. (2001) – fMRI experiment; landmark tasks (participants were to indicate by means of button press whether a line was properly bisected or not) with lines in horizontal aspect was contrasted with a control condition (indicate whether a line did or did not contain a transection mark)

F6 - Fink et al. (2001) – fMRI experiment; landmark tasks (participants were to indicate by means of button press whether a line was properly bisected or not) with (a) lines in vertical aspect was contrasted with lines in horizontal aspect; (b) lines in horizontal aspect contrasted with lines in vertical aspect

Fo - Foxe et al. (2003) – ERP experiment; participants were to state the transection location (left or right) of pre-transected lines of various contrasts (3, 25, 100%); the control condition was stating whether lines possess a transection mark or not (25% of lines were not transected)

M - Marshall et al. (1997) – PET experiment; a landmark task was given with the instruction to press a key corresponding to the longer side (left or right of the transection mark), or a third button if both sides were equal. The control condition was to press a button when a (transected) line that appeared on-screen stopped flickering

W - Waberski et al. (2008) – ERP experiment; a landmark task (i.e., participants were to indicate by means of button press whether a line was properly bisected) was contrasted with a control condition (indicate whether a line did or did not contain a transection mark)

Appendix C: Basics of the NEF

Introduction to the Neural Engineering Framework

The main *level* of analysis in the NEF is a 'population', composed of a collection of neurons differing only by the specific parameter values of their tuning curves (i.e., maximum firing rate and intercept). Separate populations, however, can differ in the basic physiological properties of their neurons (e.g., time constants) and macro properties of the tuning curves (e.g., dimensionality). The brain is divided into many such populations, connected to other populations by synaptic junctions between individual neurons. Each neuron (indexed by *i*) in the transmitting population is connected to a neuron in the receiving population (indexed by *j*) by a connection weight, ω_{ji}. The connection weight specifies the gain between pre-synaptic input spikes and output somatic currents and, as such, the structure of the weights connecting two populations of neurons can convey or modify information during transmission between populations (how this happens will be discussed shortly). Properties of the neuron such as the maximum firing rate, post-synaptic time constant, and membrane time constant are important to the overall ability of a specific population to encode or transmit information and, as such, are included in NEF models.

As an example of how the NEF works, consider the case of a brain consisting of a single neuron. When a touch-screen is pressed, the location of the press is converted to an electrical signal which is passed to a machine-neuron synapse. From there, the electrical signal travels along the dendritic tree of the neuron to the soma. The neuron's tuning curve is illustrated in Figure 22; we see that it fires more rapidly as the location touched on the screen increases between 0 and 1. To further simplify this example, assume that the screen is continuously pressed for exactly one second. With this system, it is possible to say that the brain 'encodes' the position of the press and then outputs this information unaltered as follows: if, for example, 300 spikes were produced by the neuron during one second of stimulation then, from the tuning curve, we see that the point touched was 1.0 (i.e., an x-axis value of 1.0 results in a y-axis output of 300). If 150 spikes were produced over the stimulation interval, the input x-value was 0.5. In other words, we could infer (decode) the press position using the relationship:

press position = (1/300) x (# spikes emitted by brain over one second) (C.1)

While this is a very efficient brain, there are problems with using only a single neuron. First, any damage to the neuron disrupts the ability of the brain to compute the press position. Next, any 'noise' in the system (e.g., spikes generated from extraneous inputs or other minor disruptions) leads to an equivalent error in the position estimate. Real brains are noisy places and noise reduction is imperative to effective information transmission. One way of reducing information loss would be to have multiple neurons receiving the input signal, all with the same tuning curve and all hooked up in the same way. If noise was normally distributed around a mean of zero[6], then the average response of this population of neurons would be close to the actual value (within error bounds given by the Central Limit Theorem). It would take no more than 10-20 neurons to remediate the first two problems, but there are other challenges which a homogeneous population of neurons with identical tuning curves could not solve as readily. First, for values of screen press close to 0, neurons only fire occasionally and thus the accuracy of the system degrades due to noise. As well, our original formulation required counting the number of spikes over one second. If the press lasts for an unknown length of time then a timing unit must be added and additional calculations required to divide the number of presses by the time. Finally, and perhaps most importantly, this is not an optimal way of representing the information for any given number of neurons.

[6]For neurons with a low background firing rate, noise is likely to be positively skewed. However, the assumption of Gaussian normal error is often reasonable for the purposes of modeling.

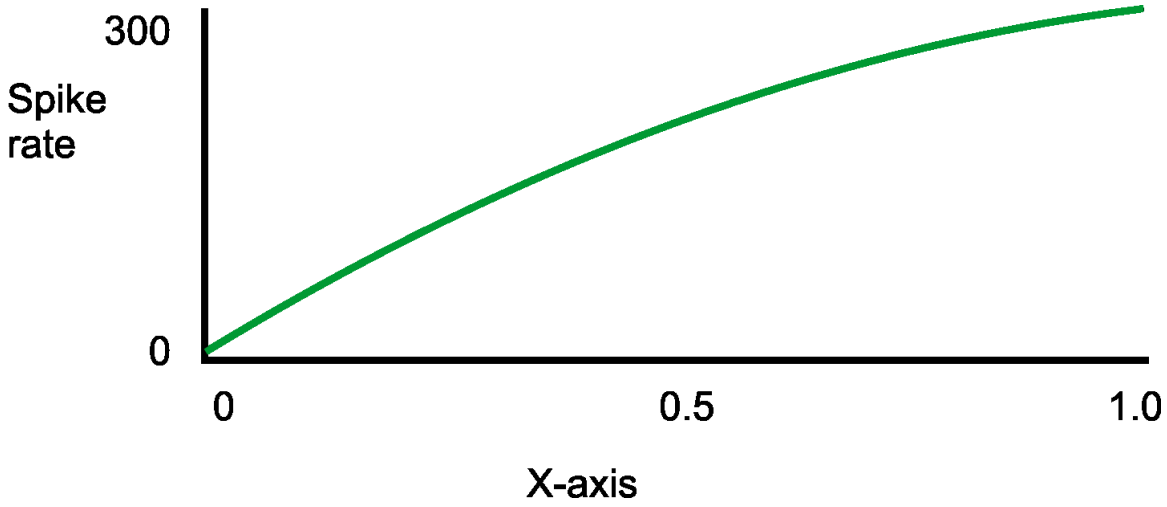

Figure 22. Tuning curve for a single neuron

A single neuron's tuning curve. As the input goes from 0.0-1.0, the neuron fires at a rate given by the curve, from 0 for an x-value of 0.0, to 300 times per second for an x-value of 1.0.

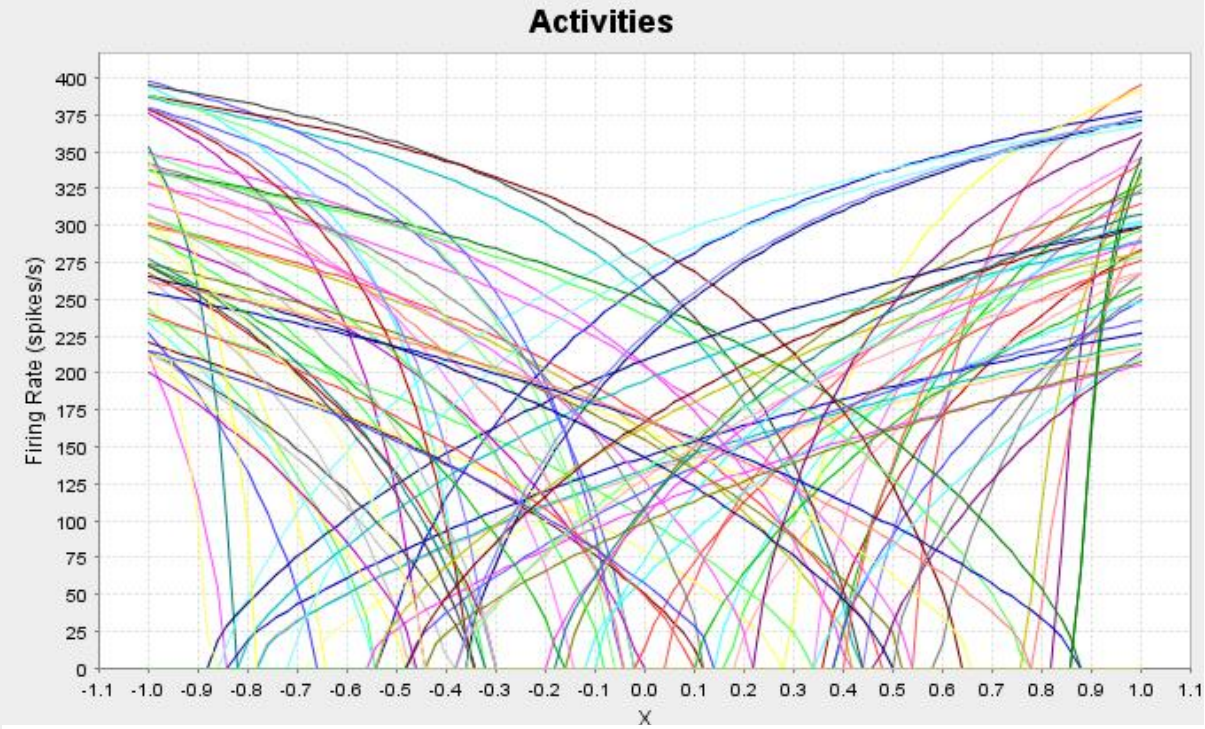

Figure 23. Tuning curves for 100 neurons

Pictured here are the tuning curves for a random sample of 100 neurons, each with maximum firing rates between 200-400 Hz. This population of neurons is able to very accurately represent any value of *x* between -1 and 1, even given a signal on the order of milliseconds.

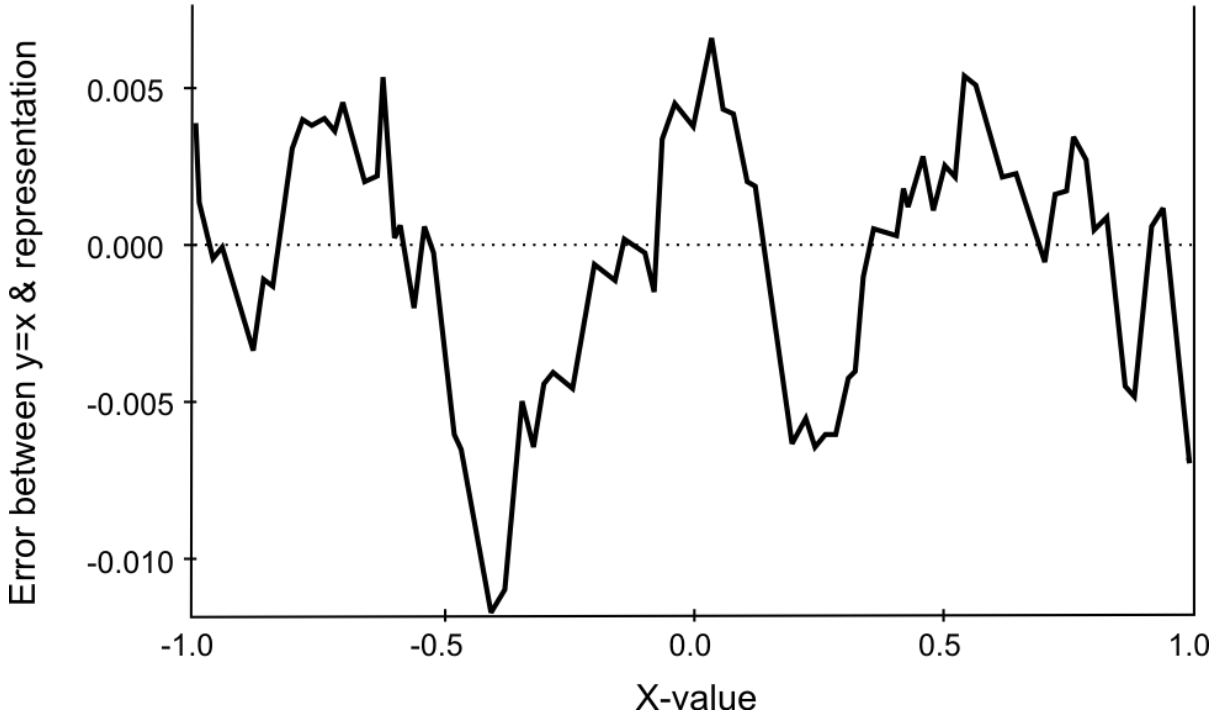

Figure 24. Error in estimating a line using 100 neurons

A graph of the distortion (error) between the line $y = x$, and a representation of the line using the 100 neurons in Figure 23. To create the model, connection weights were chosen between the input (i.e., any point within the range of x-values [-1,1]) and the 100 neurons to minimize the error (i.e., least squares). Using only 100 neurons, the distortion between the input and the representation is extremely small, between about -0.012 and .006.

An alternate solution involves varying the tuning curves within the population of neurons (Figure 23). In this case, 100 neurons were used, each of which has a tuning curve sensitive to a different range of x-values, and a maximum firing rate somewhere between 200 and 400 Hz. Now, instead of using firing rate or the number of spikes[7] as the determinant of position, both firing rate and the identity of the neuron combine to supply the necessary information. Even though the tuning curves in this example were generated randomly, choosing an optimal decoding for the output produces a very accurate representation across the entire range of *x*-values (Figure 24).

The decoder used to interpret the spiking output (i.e., to give the x-value) was just a probe of the state of the brain. Whether a probe was physically present or not, the brain still represents the value of *x* within the neural population. Of course, a real brain has to do more than just encode inputs, it also has to transform, combine, and transmit the information for different downstream uses. For example, a more complex task could require the brain to determine the average *x*-value of two simultaneous screen presses. A sample neural architecture for this computation is graphically presented in Figure 25. It can be seen that the entire system consists of three components and two steps. In the first step, both presses are encoded by two neural populations, X and Y. In the second step, a third population (Z) sums half the currents from each population in Step 1 to form an average of the two. The reduction of the current by a factor of 2 can be implemented using the connection weights at the synaptic junctions and, since electric currents are additive so, too, are the inputs from separate sources.

This method of transforming data with a neural network is effective for linear transformations but it does not generalize to non-linear transformations acting over more interesting domains. As well, the approach taken here rapidly degrades information because the neurons in Step 2 were not optimized to take full advantage of the information available from populations of neurons in Step 1. The NEF solves both issues by optimizing connection weights between neural populations to transmit and transform the information available in the upstream system for the inputs to the downstream system.

[7] One of the strengths of the NEF is that it is fundamentally equivalent between firing rate models and spiking models. In other words, there is no need for a separate timer to implement a rate coding system. A fuller discussion can be found in Eliasmith & Anderson (2003).

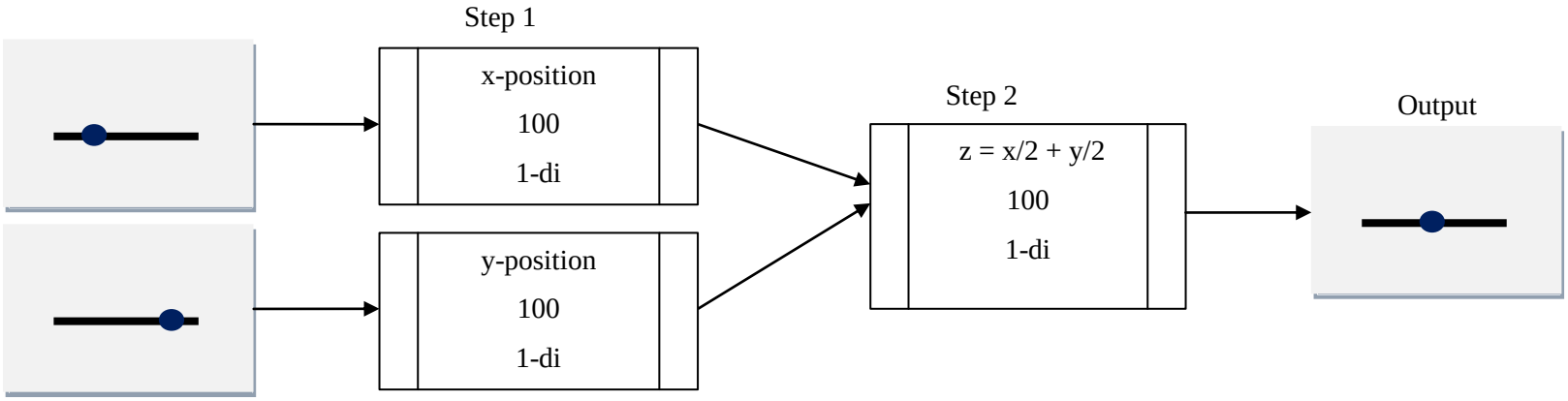

Figure 25. Double touch: a network to compute the average position

In Step 1 and Step 2, the tuning curves of each population of neurons are the same as in Figure 23 and produce an accurate representation of the position touched. Each neuron in Step 1 connects to every neuron in Step 2 with connection weights that only transmit half the current (although many of the connection weights can have a value of 0). The net result is to produce a sum of half the inputs, i.e., the average. The first line in each population (the boxes with double lines) is the representation or transformation carried out by the population. The second line is the number of neurons and the third line is the dimension of the neurons' tuning curves.

Details of the NEF

In this section, some key ideas of the NEF are developed within its mathematical/computational framework. More thorough expositions are available in the context of discussions on working memory, rat navigation, or vestibular function (Conklin & Eliasmith, 2005; Eliasmith, Westover, & Anderson, 2002; Singh & Eliasmith, 2006).

The total current in the soma of a neuron, J_i, is the sum of all the input currents from external sources, J_i^d, plus a background current, J_i^{bias}, which is intrinsic to the neuron or arises from background, non-specific environmental inputs. In other words,

$$J_i(x) = J_i{}^d(x) + J_i{}^{bias} \tag{C.2}$$

For the single neuron press experiment above, J^d and $\boldsymbol{x}$ are related by:

$$J^d(x) = \frac{1}{300}x \tag{C.3}$$

A more general formulation for arbitrary $\boldsymbol{x}$ (i.e., scalar, vector, or Hilbert space) is given by:

$$J^d(\boldsymbol{x}) = \alpha\langle\tilde{\boldsymbol{\varphi}} \cdot \boldsymbol{x}\rangle \tag{C.4}$$

where α is a conversion factor that translates neural units into physical dimensions (it can also be considered a gain factor), and $\tilde{\varphi}$ is the preferred direction of the neuron (i.e., the direction of maximum firing).

We have seen how the somatic current, *J*, can be modeled by a neuron discharging an electrical spike down its axon in response to input currents. An approximation for the *rate* of spiking as a function of J is the leaky-integrate-and-fire model (LIF). The mathematical representation of a LIF neuron's tuning curve is denoted by G, and the firing rate as a function of the input parameter *x* is determined from:

$$a(x) = G[J(x)] = \begin{cases} \dfrac{1}{\tau^{ref} - \tau^{RC}\ln\left(1 - \dfrac{J^{threshold}}{J(x)}\right)}, & \text{if } J(x) > J^{threshold} \\ 0, & \text{if } J(x) \le J^{threshold} \end{cases} \tag{C.5}$$

Estimates for the values of the parameters τ^{ref}, τ^{RC}, and $J^{threshold}$ can be determined experimentally for each type of neuron. The LIF model provides a reasonable approximation for the response characteristics of many types of neurons, including the pyramidal neurons of parietal and occipital cortex which are the focus of the models to be developed here.

One important question yet to be addressed is how a population of neurons represents information. For example, in Step 1 of our two-screen problem (Figure 25), each of the two neural populations encoded the position of press for one screen. How this was done, and how this information is transmitted to Step 2 is now explained. Assume that a decoding weight can be applied to each neuron, x_i (i.e., multiplying the input currents by a constant weighting factor, φ_i). If we include Gaussian noise in the system, η_i, then the information represented by a population of neurons is given by:

$$\hat{x} = \sum_{i=1}^{N} (a_i(x) + \eta_i)\varphi_i \tag{C.6}$$

where $\hat{x}$ is an estimate of the true value, x. The weights are then chosen to minimize the least squared error between x and $\hat{x}$.

Even though the encoding was non-linear and the decoding was linear, this estimate preserves most of the information in the system (Rieke, Warland, de Ruyter van Steveninick, & Bialek, 1997) and is has been shown to produce estimates that only lose about 5% of the information available from optimal non-linear decoders. For example, Figure 24 illustrates the error when a population of 100 neurons represents any point on a line, $\in [-1,1]$. In this case, the absolute error at every point was less than 0.0125 even though the noise in the output of each decoded neuron, η_i, had a standard deviation of 10% of the total spike rate.

To complete the story, it is important to understand how information can be transmitted and transformed in neural systems. Each neuron connects to other neurons through synapses. At the synapse, neurotransmitters are released into the synaptic cleft by a spike arriving at the terminal button of the axon of the presynaptic neuron. Neurotransmitters induce a post-synaptic current (PSC) in the post-synaptic neuron. The functional form of the PSC can be approximated by:

$$h_{psc}(t) = e^{-t/\tau_s} \tag{C.7}$$

where τ_s is the synaptic time constant. Assume spikes arrive at the terminal button at times t_n, then the current arriving at the soma of the post-synaptic neuron is the convolution of the spike with the PSC, and the representation of that information contained in the spiking input is given by the decoding:

$$\hat{x}(t) = \sum_{i,n} h_i(t - t_n)\, \varphi_i^x \tag{C.8}$$

for a population of neurons, i, receiving a series of spikes, n. If two populations of neurons are connected as in Figure 26, with connection weights from population a_i to population b_j, the output of b_j is given by:

$$b_j(x) = G_j\left[\sum_{i,n} \omega_{ji} h_{ij}(t - t_{in}) + J_j^{bias}\right] \tag{C.9}$$

where the connection weights are given by $\omega_{ji} = \alpha_j \tilde{\varphi}_j \varphi_i^x$, and the φ_i^x are determined from a least-squares error optimization on the information contained in population j. A linear supposition of populations such as we had in the two-press example (Figure 25) can be written as:

$$c_k(z) = G_k\left[\sum_{i,n} \omega_{ki} h_{ik}(t - t_{in}) + \sum_{j,m} \omega_{kj} h_{jk}\left(t - t_{jm}\right) + J_k^{bias}\right] \tag{C.10}$$

where $\omega_{ki} = \frac{1}{2}\alpha_k \tilde{\varphi}_k \varphi_i^x$, $\omega_{kj} = \frac{1}{2}\alpha_k \tilde{\varphi}_k \varphi_j^y$, and z = ½(x+y).

A schematic indicates how the two-press example can be implemented in the NEF using three populations of neurons (Figure 27). Networks of this sort can perform linear transformations of two or more populations or arbitrary transformations of a single population including integration (implemented through recurrence, i.e., by having neurons in a population connected amongst themselves). It remains to discuss how non-linear transformations of multiple inputs can be modeled. One important non-linear transformation is multiplication. For example, how would a system compute the geometric average of inputs in the two-press example?

$$z = \frac{1}{2}\sqrt{xy} \tag{C.11}$$

One possibility is to assume multiplication is performed by non-linearities in the dendritic tree (Koch & Poggio, 1992; Mel, 1994). It is possible, however, to perform multiplication directly using a two-dimensional hidden layer of neurons. Within this hidden layer, each neuron has a two dimensional tuning curve: the input populations are each assigned to a separate dimension and then the inner product of the hidden layer is calculated at output. The hidden layer can be interpreted as a new set of neurons or even as the dendritic tree by recasting the meaning of inputs, outputs, and soma as the NEF need not be interpreted purely in terms of neurons. A network implementing the two-press example for a geometric mean is shown in Figure 28. Multiplication is performed by the two-dimensional neural population denoted by 'Multiply'. The first dimension represents the value of *x* and the second dimension the value of *y*. The population computes the inner product by finding optimum decoders that minimize the error of the inner product of the two-dimensional representation. Similarly, the square root is decoded by the final population, 'Square root'.

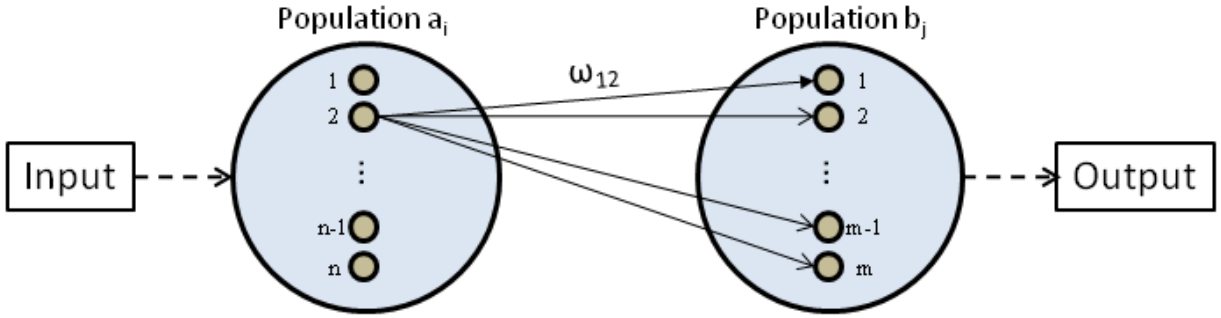

Figure 26. Transmittal and transformation of information between neural populations

In this case, only the connections between one neuron in population a_i with all the neurons in b_j is shown but in a real brain all the neurons in population a_i would have synaptic connections (and weights) with neurons in population b_j although that is not to say every neuron in population a_i is connected to every neuron in population b_j (some weights = 0).

A. Schematic of NEF model for average press position calculation

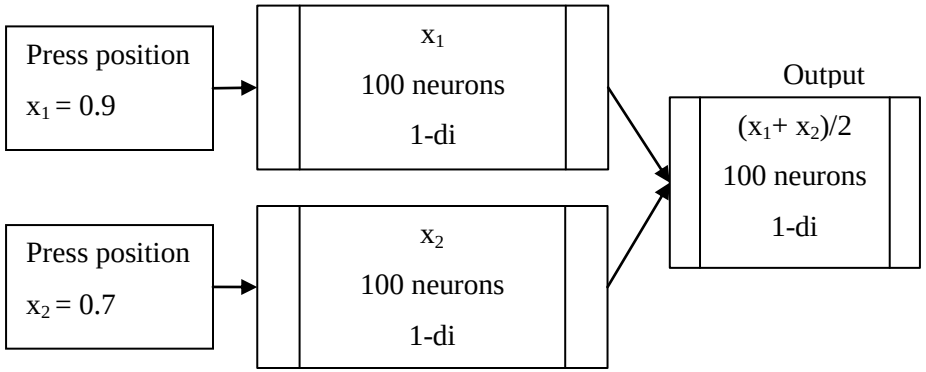

B. Output from NEF model

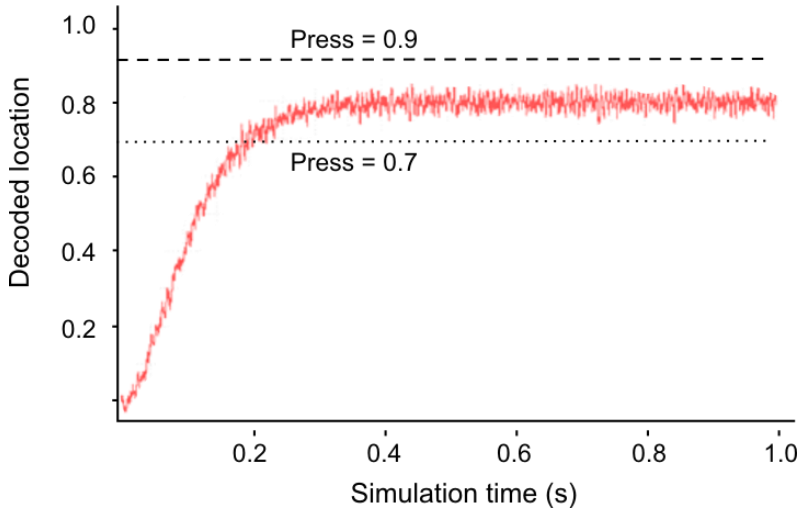

Figure 27. Two- press experiment – NEF simulation

This is an NEF network for calculating the average position on the line of two simultaneous screen presses. The inputs are 0.90 for x_1 and 0.7 for x_2, so the expected value is 0.8. (A) The schematic on the left is the network diagram for the NEF model. Plain boxes represent inputs into the system and therefore do not have neurons. Double boxes represent neural populations: inside double boxes the first line indicates the transformation or representation performed by the population, the second line is the number of neurons in the population, and the third line is the dimensionality of the tuning curves; (B) On the right is a graph of the Output population (in this case, the final step in calculating the average of two presses). It accurately represents the decoded value of the average press position, 0.8, given inputs of 0.7 and 0.9. This output is based on the underlying spiking activity of the neurons. There is a 'start-up' period in the first 200 ms which produces an artifact that is not present in the biological system.

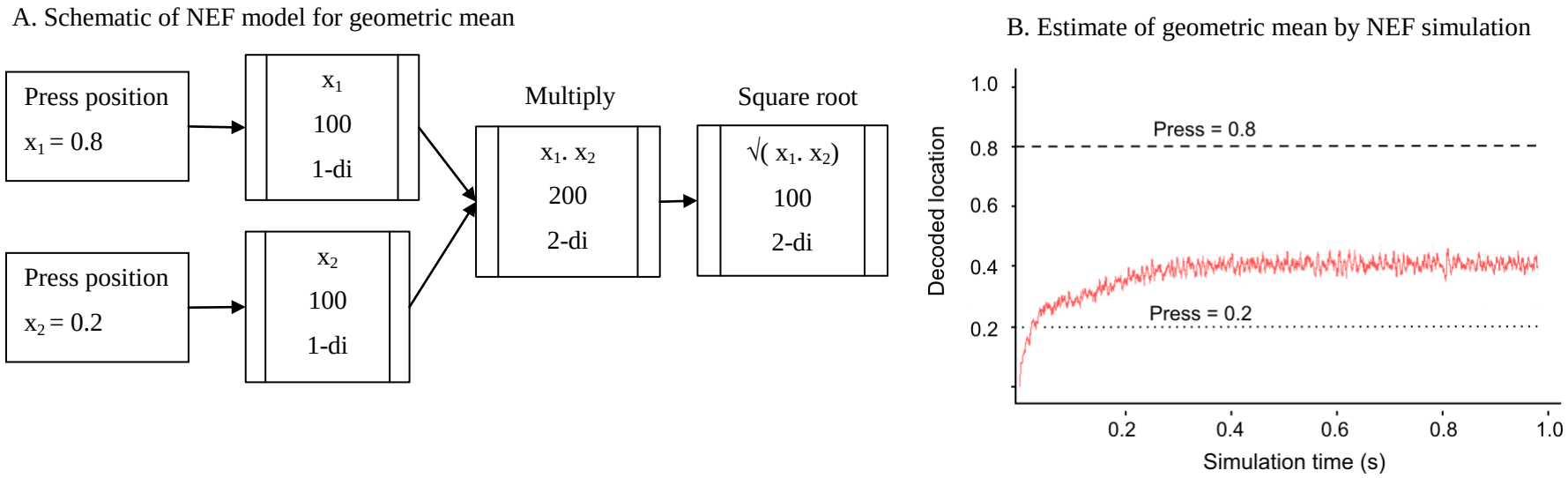

Figure 28. Multiplication by a neural network

The model shown on the left calculates the geometric mean of two input numbers. This includes all the steps for illustration only because the same computations could be handled by one population of neurons with the functions as inputs and the geometric mean as output (i.e. the final step occurs in the connection weights at the decoding stage). The number of neurons in the population multiplying the inputs is 200 neurons; because each neuron has a two-dimensional tuning curve and multiplication is involved, it requires a greater number of neurons to maintain accuracy.

Appendix D: Code Used in Computational Model

Python script for creating dynamic bisection network in Nengo (graphical software for quickly developing NEF systems). Before using this program, you need to install the Nengo software. Details about how to do this, including documentation and code, can be found at www.nengo.ca.

```
import nef
net=nef.Network('DynamicBisection')

################################################
#### Scaling parameters:
#### Reduce errors in multiplication and
#### thresholding by scaling x (or  y) axis
################################################
f1=5.0
f2=0.05
f3=20
f4=50
f5=10


################################################
#### Neural parameters:
################################################
alpha=.4
alphap=f5*(1-alpha)
N=200
Nm=1000
LowRate=80
HighRate=120

################################################
#### Create the neural populations
################################################
vi=net.make('velocityInput',N,1,quick=True,radius=20)
ti=net.make('timeInput', N, 1, quick=True, radius=2)
m1=net.make('InnerMultiplier', Nm, 2, quick=True, radius=.1)
ii1=net.make('InnerIntegrator1', N, 1,
max_rate=(LowRate,HighRate),quick=True, radius=.06)
ii2=net.make('InnerIntegrator2', N, 1,
max_rate=(LowRate,HighRate),quick=True, radius=.005)
oi1=net.make('OuterIntegrator1', N, 1,
max_rate=(LowRate,HighRate),quick=True, radius=.01)
m2=net.make('OuterMultiplier', Nm, 2, quick=True, radius=2)
oi2=net.make('OuterIntegrator2', N, 1,
max_rate=(LowRate,HighRate),quick=True, radius=.08)
m3=net.make('Numerator', Nm, 2, quick=True, radius=2)
```

```
ts=net.make('TotalCRS', N, 1, max_rate=(LowRate,HighRate),quick=True,
radius=.08)
bp=net.make('BisectionPoint', N, 1,
max_rate=(LowRate,HighRate),quick=True, radius=12)

################################################
#### Create the quotient neural population
################################################
import random
random.seed(10)
def generate_point():
    while True:
        a=random.random()
        b=random.random()
        if a>0.1 and b<0.9*a<1.1*b:
            return (b,a)

eval_points=[generate_point() for i in range(5000)]
qt=net.make('DynamicBisection', Nm, 2, quick=False, radius=1,
eval_points=eval_points)

################################################
#### Create a threshold function:
#### eliminates extraneous inputs to integrals
################################################
thresh=net.make('Threshold', N, 1, quick=True, intercept=(.2,1.0))


################################################
#### Create the input functions
################################################
def timeInput(x):
    if x<0.08: return 0
    return x-0.08
inputt=net.make_input('TimeInput', timeInput)

def velocityInput(x):
    return 16.5
inputv=net.make_input('Velocity', velocityInput)

def CRSRate(x):
    if x<0.1: return 0
    return exp(-22*(x-0.1))
inputs=net.make_input('CRSRate', CRSRate)

def staticBis(x):
    return 9.5
sb=net.make_input('StaticBisection',staticBis)


################################################
#### Computed functions at origins
```

```
################################################
def product(x):
    return x[0]*x[1]

def product1(x):
    return x[0]*x[1]*f1

def product2(x):
    return x[0]*x[1]

def ii1in(x):
    return x[0]*f3

def omout(x):
    return x[0]*x[1]/f3

def quotient(x):
    return x[0]/x[1]

def inner1(x):
    return .7*x[0]

def threshout(x):
    return x[0]/f4


################################################
#### Connect the neural populations
################################################
net.connect(inputt,ti,pstc=.007,weight=1)
net.connect(inputv,vi,pstc=.007,weight=1)
net.connect(ti, m1, pstc=.007, transform=[1,0])
net.connect(inputs, m1, pstc=.007, transform=[0,1])
net.connect(m1,thresh,pstc=.007,func=product1,weight=f4)
net.connect(thresh,ii2,pstc=.007,func=threshout, weight=.05)
net.connect(inputs, ii1, pstc=.007, weight=.05)
net.connect(ii1,ii1,pstc=.05, weight=1)
net.connect(ii2, ii2, pstc=.05, weight=1)
net.connect(ti, m2, pstc=.007, transform=[1,0])
net.connect(ii1, m2, pstc=.007, func=ii1in, transform=[0,1])
net.connect(ii1,ts, pstc=.007, func=inner1, weight=.05)
net.connect(ii2, oi1, pstc=.007, weight=.05)
net.connect(oi1,oi1,pstc=.05, weight=1)
net.connect(ts,ts,pstc=.05, weight=1)
net.connect(m2, oi2, pstc=.05, func=omout, weight=.05)
net.connect(oi2,oi2, pstc=.05, weight=1)
net.connect(oi1,m3, pstc=.007,transform=[0,-1/f2])
net.connect(oi2,m3,pstc=.007, transform=[0,1/f2])
net.connect(vi,m3, pstc=.007, transform=[f2,0])
net.connect(m3,qt,pstc=.007, func=product2, transform=[1,0])
net.connect(ts,qt,pstc=.007, transform=[0,f5])
net.connect(qt,bp,pstc=.007,func=quotient, weight=alphap)
```

```
net.connect(sb,bp,pstc=.007,weight=alpha)


##############################################
#### Add probes for viewing output
##############################################
net.network.simulator.addProbe('velocityInput','X',True)
net.network.simulator.addProbe('timeInput','X',True)
net.network.simulator.addProbe('InnerIntegrator1','X',True)
net.network.simulator.addProbe('InnerIntegrator1','inner1',True)
net.network.simulator.addProbe('InnerMultiplier','X',True)
net.network.simulator.addProbe('InnerIntegrator2','X',True)
net.network.simulator.addProbe('OuterIntegrator1','X',True)
net.network.simulator.addProbe('OuterMultiplier','X',True)
net.network.simulator.addProbe('OuterIntegrator2','X',True)
net.network.simulator.addProbe('Numerator','X',True)
net.network.simulator.addProbe('Threshold','X',True)
net.network.simulator.addProbe('Threshold','threshout',True)
net.network.simulator.addProbe('TotalCRS','X',True)
net.network.simulator.addProbe('BisectionPoint','X',True)
net.network.simulator.addProbe('DynamicBisection','X',True)
net.network.simulator.addProbe('Numerator','product2',True)
net.network.simulator.addProbe('OuterMultiplier','omout',True)
net.network.simulator.addProbe('InnerMultiplier','product1',True)
net.network.simulator.addProbe('DynamicBisection','quotient',True)


#################################
#### Add the model to Nengo
#################################
net.add_to(world)
```

Bibliography

Adair, J. C., Na, D. L., Schwartz, R. L., & Heilman, K. M. (2003). Caloric stimulation in neglect: Evaluation of response as a function of neglect type. *Journal of the International Neuropsychological Society, 9*(7), 983-988.

Anderson, B. (1996). A mathematical model of line bisection behaviour in neglect. *Brain, 119 (Pt 3)*, 841-850.

Baek, M. J., Lee, B. H., Kwon, J. C., Park, J. M., Kang, S. J., Chin, J., et al. (2002). Influence of final search direction on tactile line bisection in normal subjects. *Neurology, 58*(12), 1833-1838.

Barton, J. S., Behrmann, M., & Black, S. (1998). Ocular search during line bisection: The effects of hemi-neglect and hemianopia. *Brain: A Journal of Neurology, 121*(6), 1117-1131.

Basso, G., Nichelli, P., Frassinetti, F., & Di Pellegrino, G. (1996). Time perception in a neglected space. *Neuroreport, 7*(13), 2111-2114.

Battelli, L., Pascual-Leone, A., & Cavanagh, P. (2007). The 'when' pathway of the right parietal lobe. *Trends in Cognitive Sciences, 11*(5), 204-210.

Becchio, C., & Bertone, C. (2006). Time and neglect: Abnormal temporal dynamics in unilateral spatial neglect. *Neuropsychologia, 44*(14), 2775-2782.

Billingsley, R. L., Simos, P. G., Sarkari, S., Fletcher, J. M., & Papanicolaou, A. C. (2004). Spatio-temporal brain activation profiles associated with line bisection judgments and double simultaneous visual stimulation. *Behavioural Brain Research, 152*(1), 97-107.

Bisiach, E., Pizzamiglio, L., Nico, D., & Antonucci, G. (1996). Beyond unilateral neglect. *Brain, 119* (Pt 3), 851-857.

Bisiach, E., Ricci, R., & Mòdona, M. N. (1998). Visual awareness and anisometry of space representation in unilateral neglect: A panoramic investigation by means of a line extension task. *Consciousness and Cognition: An International Journal, 7*(3), 327-355.

Bisiach, E., Rusconi, M. L., Peretti, V. A., & Vallar, G. (1994). Challenging current accounts of unilateral neglect. *Neuropsychologia, 32*(11), 1431-1434.

Bowers, D., & Heilman, K. M. (1980). Pseudoneglect: Effects of hemispace on a tactile line bisection task. *Neuropsychologia, 18*(4-5), 491-498.

Bradshaw, J. L., Bradshaw, J. A., & Nathan, G. (1986). Leftwards error in bisecting the gap between two points: Stimulus quality and hand effects. *Neuropsychologia, 24*(6), 849-855.

Bradshaw, J. L., Bradshaw, J. A., & Nettleton, N. C. (1989). Direction and location of movement in kinesthetic judgements of extent. *Neuropsychologia, 27*(9), 1139-1151.

Bradshaw, J. L., Nathan, G., Nettleton, N. C., Wilson, L., & Pierson, J. (1987). Why is there a left side underestimation in rod bisection? *Neuropsychologia, 25*(4), 735-738.

Bradshaw, J. L., Nettleton, N. C., Nathan, G., & Wilson, L. (1983). Head and body space to left and right, front and rear. II. visuotactual and kinesthetic studies and left-side underestimation. *Neuropsychologia, 21*(5), 475-486.

Bradshaw, J. L., Nettleton, N. C., Nathan, G., & Wilson, L. (1985). Bisecting rods and lines: Effects of horizontal and vertical posture on left-side underestimation by normal subjects. *Neuropsychologia, 23*(3), 421-425.

Bradshaw, J. L., Nettleton, N. C., Wilson, L. E., & Bradshaw, C. S. (1987). Line bisection by left-handed preschoolers: A phenomenon of symmetrical neglect. *Brain and Cognition, 6*(4), 377-385.

Brodie, E. E., & Dunn, E. M. (2005). Visual line bisection in sinistrals and dextrals as a function of hemispace, hand, and scan direction. *Brain Cognition, 58*(2), 149-156.

Brodie, E. E., & Pettigrew, L. E. (1996). Is left always right? Directional deviations in visual line bisection as a function of hand and initial scanning direction. *Neuropsychologia, 34*(5), 467-470.

Buneo, C. A., Jarvis, M. R., Batista, A. P., & Andersen, R. A. (2002). Direct visuomotor transformations for reaching. *Nature, 416*(6881), 632-636.

Butter, C. M., Mark, V. W., & Heilman, K. M. (1988). An experimental analysis of factors underlying neglect in line bisection. *Journal of Neurology, Neurosurgery & Psychiatry, 51*(12), 1581-1583.

Cavanna, A. E., & Trimble, M. R. (2006). The precuneus: A review of its functional anatomy and behavioural correlates. *Brain, 129*(3), 564-583.

Cavézian, C., Danckert, J., Lerond, J., Daléry, J., d'Amato, T., & Saoud, M. (2007). Visual-perceptual abilities in healthy controls, depressed patients, and schizophrenia patients. *Brain and Cognition*, 64(3), 257-264.

Chatterjee, A. (2002). Spatial anisometry and representational release in neglect. In H. O. Karnath, A. D. Milner & G. Vallar (Eds.), *The cognitive and neural bases of spatial neglect*. New York, NY: Oxford University Press.

Chatterjee, A., Mennemeier, M., & Heilman, K. M. (1994). The psychophysical power law and unilateral spatial neglect. *Brain and Cognition, 25*(1), 92-107.

Chiba, Y., Yamaguchi, A., & Eto, F. (2006). Assessment of sensory neglect: A study using moving images. *Neuropsychological Rehabilitation, 16*(6), 641-652.

Choi, K. M., Ku, B. D., Jeong, Y., Lee, B. H., Ahn, H. J., Kang, S. J., et al. (2005). The influence of illusory motion on line bisection performance in normal subjects. *Journal of the International Neuropscyhological Society, 11*(7), 881-888.

Choi, K. M., Lee, B. H., Lee, S. C., Ku, B. D., Kim, E. J., Suh, M. K., et al. (2007). Influence of moving background on line bisection performance in the normal elderly versus patients with hemispatial neglect. *American Journal of Physical Medicine and Rehabilitation, 86*(7), 515-526.

Chokron, S., & Agostini, M. D. (1995). Reading habits and line bisection: A developmental approach. *Cognitive Brain Research, 3*(1), 51-58.

Chokron, S., Bartolomeo, P., Perenin, M. T., Helft, G., & Imbert, M. (1998). Scanning direction and line bisection: A study of normal subjects and unilateral neglect patients with opposite reading habits. *Cognitive Brain Research, 7*(2), 173-178.

Chokron, S., & Imbert, M. (1993a). Egocentric reference and asymmetric perception of space. *Neuropsychologia, 31*(3), 267-275.

Chokron, S., & Imbert, M. (1993b). Influence of reading habits on line bisection. *Cognitive Brain Research, 1*(4), 219-222.

Conklin, J., & Eliasmith, C. (2005). A controlled attractor network model of path integration in the rat. *Journal of Computational Neuroscience, 18*(2), 183-203.

Culham, J. C., Brandt, S. A., Cavanagh, P., Kanwisher, N. G., Dale, A. M., & Tootell, R. B. H. (1998). Cortical fMRI activation produced by attentive tracking of moving targets. *Journal of Neurophysiology, 80*(5), 2657-2670.

Culham, J. C., Danckert, S. L., DeSouza, J. F. X., Gati, J. S., Menon, R. S., & Goodale, M. A. (2003). Visually guided grasping produces fMRI activation in dorsal but not ventral stream brain areas. *Experimental Brain Research, 153*(2), 180-189.

Danckert, J., & Ferber, S. (2006). Revisiting unilateral neglect. *Neuropsychologia, 44*(6), 987-1006.

Danckert, J., Ferber, S., Pun, C., Broderick, C., Striemer, C., Rock, S., et al. (2007). Neglected time: Impaired temporal perception of multisecond intervals in unilateral neglect. *Journal of Cognitive Neuroscience, 19*(10), 1706-1720.

Dellatolas, G., Vanluchene, J., & Coutin, T. (1996). Visual and motor components in simple line bisection: An investigation in normal adults. *Cognitive Brain Research, 4*(1), 49-56.

Desmurget, M., Turner, R. S., Prablanc, C., Russo, G. S., Alexander, G. E., & Grafton, S. T. (2005). Updating target location at the end of an orienting saccade affects the characteristics of simple point-to-point movements. *Journal of Experimental Psychology: Human Perception and Performance, 31*(6), 1510-1536.

Diekmann, V., Jürgens, R., & Becker, W. (2009). Deriving angular displacement from optic flow: A fMRI study. *Experimental Brain Research, 195*(1), 101-116.

Dieterich, M., Müller-Schunk, S., Stephan, T., Bense, S., Seelos, K., & Yousry, T. A. (2009). Functional magnetic resonance imaging activations of cortical eye fields during saccades, smooth pursuit, and optokinetic nystagmus. *Basic and Clinical Aspects of Vertigo and Dizziness: Ann. N.Y. Acad. Sci., 1164*, 282-292.

Doricchi, F., Guariglia, P., Figliozzi, F., Silvetti, M., Gasparini, M., Merola, S., et al. (2008). No reversal of the oppel-kundt illusion with short stimuli: Confutation of the space anisometry interpretation of neglect and 'cross-over' in line bisection. *Brain, 131*(5)

Dunai, J., Bennett, K., Fotiades, A., Kritikos, A., & Castiello, U. (1999). Modulation of unilateral neglect as a function of direction of object motion. *Neuroreport, 10*(5), 1041-1047.

Eliasmith, C., & Anderson, C. H. (2003). *Neural engineering: Computation, representation, and dynamics in neurobiological systems*. Cambridge, MA: MIT Press/Bradford Books.

Eliasmith, C., Westover, M. B., & Anderson, C. H. (2002). A general framework for neurobiological modeling: An application to the vestibular system. *Neurocomputing, 44-46*, 1071-1076.

Failla, C. V., Sheppard, D. M., & Bradshaw, J. L. (2003). Age and responding-hand related changes in performance of neurologically normal subjects on the line-bisection and chimeric-faces tasks. *Brain and Cognition, 52*(3), 353-363.

Ferber, S., & Karnath, H. O. (2001). Size perception in hemianopia and neglect. *Brain, 124*(3), 527-536.

Ferber, S., Mraz, R., Baker, N., & Graham, S. J. (2007). Shared and differential neural substrates of copying versus drawing: A functional magnetic resonance imaging study. *Neuroreport, 18*(11), 1089-1093.

Fink, G. R., Marshall, J. C., Shah, N. J., Weiss, P. H., Halligan, P. W., Grosse-Ruyken, M., et al. (2000). Line bisection judgments implicate right parietal cortex and cerebellum as assessed by fMRI. *Neurology, 54*(6), 1324-1331.

Fink, G. R., Marshall, J. C., Weiss, P. H., Shah, N. J., Toni, I., Halligan, P. W., et al. (2000a). Position discrimination in one - versus two - dimensions: An fMRI-study. *NeuroImage, 11*(5 PART II)

Fink, G. R., Marshall, J. C., Weiss, P. H., Shah, N. J., Toni, I., Halligan, P. W., et al. (2000b). 'Where' depends on 'what': A differential functional anatomy for position discrimination in one- versus two-dimensions. *Neuropsychologia, 38*(13), 1741-1748.

Fink, G. R., Marshall, J. C., Weiss, P. H., Toni, I., & Zilles, K. (2002). Task instructions influence the cognitive strategies involved in line bisection judgements: Evidence from modulated neural mechanisms revealed by fMRI. *Neuropsychologia, 40*(2), 119-130.

Fink, G. R., Marshall, J. C., Weiss, P. H., & Zilles, K. (2001). The neural basis of vertical and horizontal line bisection judgments: An fMRI study of normal volunteers. *NeuroImage, 14*(1 II), S46-S51.

Foxe, J. J., McCourt, M. E., & Javitt, D. C. (2003). Right hemisphere control of visuospatial attention: Line-bisection judgments evaluated with high-density electrical mapping and source analysis. *NeuroImage, 19*(3), 710-726.

Frassinetti, F., Magnani, B., & Oliveri, M. (2009). Prismatic lenses shift time perception. *Psychological Science, 20*(8), 949-954.

Fujii, T., Fukatsu, R., Yamadori, A., & Kimura, I. (1995). Effect of age on the line bisection test. *Journal of Clinical and Experimental Neuropsychology, 17*(6), 941-944.

Fukatsu, R., Fujii, T., Kimura, I., Saso, S., & Kogure, K. (1990). Effects of hand and spatial conditions on visual line bisection. *Tohoku Journal of Experimental Medicine, 161*(4), 329-333.

Gallace, A., Auvray, M., & Spence, C. (2007). The modulation of haptic line bisection by a visual illusion and optokinetic stimulation. *Perception, 36*(7), 1003-1018.

Geminiani, G., Corazzini, L. L., Stucchi, N., & Gindri, P. (2004). Acceleration perception and spatial distortion in a left unilateral neglect patient. *Cortex, 40*(2), 315-322.

Ghaem, O., Mellet, E., Crivello, F., Tzourio, N., Mazoyer, B., Berthoz, A., et al. (1997). Mental navigation along memorized routes activates the hippocampus, precuneus, and insula. *Neuroreport, 8*(3), 739-744.

Hahn, B., Ross, T. J., & Stein, E. A. (2006). Neuroanatomical dissociation between bottom-up and top-down processes of visuospatial selective attention. *NeuroImage, 32*(2), 842-853.

Halligan, P. W., & Marshall, J. C. (1988). How long is a piece of string? A study of line bisection in a case of visual neglect. *Cortex, 24*(2), 321-328.

Halligan, P. W., & Marshall, J. C. (1991). Figural modulation of visuo-spatial neglect: A case study. *Neuropsychologia, 29*(7), 619-628.

Halligan, P. W., & Marshall, J. C. (1993). The bisection of horizontal and radial lines: A case study of normal controls and ten patients with left visuospatial neglect. *International Journal of Neuroscience, 70*(3-4), 149-167.

Halligan, P. W., & Marshall, J. C. (1991). Spatial compression in visual neglect: A case study. *Cortex, 27*(4), 623-629.

Harrington, D. L., Haaland, K. Y., & Knight, R. T. (1998). Cortical networks underlying mechanisms of time perception. *Journal of Neuroscience, 18*(3), 1085-1095.

Harrington, D. L., Lee, R. R., Boyd, L. A., Rapcsak, S. Z., & Knight, R. T. (2004). Does the representation of time depend on the cerebellum? Effect of cerebellar stroke. *Brain, 127*(3), 561-574.

Harvey, M., Milner, A. D., & Roberts, R. C. (1995a). Differential effects of line length on bisection judgements in hemispatial neglect. *Cortex, 31,* 711-722.

Harvey, M., Milner, A. D., & Roberts, R. C. (1995b). An investigation of hemispatial neglect using the landmark task. *Brain and Cognition, 27*(1), 59-78.

Harvey, M., Pool, T. D., Roberson, M. J., & Olk, B. (2000). Effects of visible and invisible cueing procedures on perceptual judgments in young and elderly subjects. *Neuropsychologia, 38*(1), 22-31.

Hatta, T., & Yamamoyto, M. (1986). Hemispheric asymmetries in a tactile bisection task: Effects of hemispace of presentation. *Neuropsychologia, 24*(2), 265-269.

Henriques, D. Y., Klier, E. M., Smith, M. A., Lowy, D., & Crawford, J. D. (1998). Gaze-centered remapping of remembered visual space in an open-loop pointing task. *Journal of Neuroscience, 18*(4), 1583-1594.

Hollingworth, H. L. (1909). The indifference point. In H. L. Hollingworth (Ed.), *The inaccuracy of movement.* New York, NY: The Science Press.

Ishiai, S., Furukawa, T., & Tsukagoshi, H. (1987). Eye-fixation patterns in homonymous hemianopia and unilateral spatial neglect. *Neuropsychologia, 25*(4), 675-679.

Ishiai, S., Furukawa, T., & Tsukagoshi, H. (1989). Visuospatial processes of line bisection and the mechanisms underlying unilateral spatial neglect. *Brain, 112* (6), 1485-1502.

Ishiai S., Koyama Y., Seki K., Hayashi K., Izumi Y. (2006). Approaches to subjective midpoint of horizontal lines in unilateral spatial neglect. *Cortex, 42*(5), 685-691.

Ishiai S., Sugishita M., Mitani K., Ishizawa M. (1992) Leftward search in left unilateral spatial neglect. *Journal of Neurology, Neurosurgery, and Psychiatry, 55*, 40-44.

Ishiai, S., Koyama, Y., Seki, K., & Nakayama, T. (1998). What is line bisection in unilateral spatial neglect? analysis of perceptual and motor aspects in line bisection tasks. *Brain and Cognition, 36*(3), 239-252.

Ivry, R. B., Keele, S. W., & Diener, H. C. (1988). Dissociation of the lateral and medial cerebellum in movement timing and movement execution. *Experimental Brain Research, 73*(1), 167-180.

Ivry, R. B., & Spencer, R. M. C. (2004). The neural representation of time. *Current Opinion in Neurobiology, 14*(2), 225-232.

Jewell, G., & McCourt, M. E. (2000). Pseudoneglect: A review and meta-analysis of performance factors in line bisection tasks. *Neuropsychologia, 38*(1), 93-110.

Jones, L. A., & Wearden, J. H. (2004). Double standards: Memory loading in temporal reference memory. *Quarterly Journal of Experimental Psychology Section B: Comparative and Physiological Psychology, 57*(1), 55-77.

Jueptner, M., Rijntjes, M., Weiller, C., & Faiss, J. H. (1995). Localization of a cerebellar timing process using PET. *Neurology, 45*(8), 1540-1545.

Karnath, H. O. (2001). New insights into the functions of the superior temporal cortex. *Nature Reviews Neuroscience, 2*(8), 568-576.

Karnath, H. O., Ferber, S., & Himmelbach, M. (2001). Spatial awareness is a function of the temporal not the posterior parietal lobe. *Nature, 411*(6840), 950-953.

Karnath, H. O., Fetter, M., & Dichgans, J. (1996). Ocular exploration of space as a function of neck proprioceptive and vestibular input - observations in normal subjects and patients with spatial neglect after parietal lesions. *Experimental Brain Research, 109*(2), 333-342.

Kerkhoff, G., Keller, I., Ritter, V., & Marquardt, C. (2006). Repetitive optokinetic stimulation induces lasting recovery from visual neglect. *Restorative Neurology and Neuroscience, 24*(4-6), 357-369.

Kerkhoff, G., Schindler, I., Keller, I., & Marquardt, C. (1999). Visual background motion reduces size distortion in spatial neglect. *Neuroreport, 10*(2), 319-323.

Kinsbourne, M. (1970). The cerebral basis of lateral asymmetries in attention. *Acta Psychologica, 33*(C), 193-201.

Koch, C., & Poggio, T. (1992). Multiplying with synapses and neurons. In T. McKenna, J. Davis & S. F. Zornetzer (Eds.), *Single neuron computation*. Boston, MA: Academic Press.

Lancaster, J. L., Rainey, L. H., Summerlin, J. L., Freitas, C. S., Fox, P. T., Evans, A. C., et al. (1997). Automated labeling of the human brain: A preliminary report on the development and evaluation of a forward-transform method. *Human Brain Mapping, 5*(4), 238-242.

Lancaster, J. L., Woldorff, M. G., Parsons, L. M., Liotti, M., Freitas, C. S., Rainey, L., et al. (2000). Automated talairach atlas labels for functional brain mapping. *Human Brain Mapping, 10*(3), 120-131.

Lavanchy, L., Mayer, E., & Hauert, C. A. (2004). Lost in the middle. attentional modulation of the pseudoneglect phenomenon in a no hands line bisection paradigm. *Cortex, 40*(1), 181-182.

Levander, M., Tegnér, R., & Caneman, G. (1993). Tactile line-bisection in normal subjects. *Perceptual and Motor Skills, 76*(3 Pt 1), 831-836.

Lewis, P. A., & Miall, R. C. (2003a). Brain activation patterns during measurement of sub- and supra-second intervals. *Neuropsychologia, 41*(12), 1583-1592.

Lewis, P. A., & Miall, R. C. (2003b). Distinct systems for automatic and cognitively controlled time measurement: Evidence from neuroimaging. *Current Opinion in Neurobiology, 13*(2), 250-255.

Luh, K. E. (1995). Line bisection and perceptual asymmetries in normal individuals - what you see is not what you get. *Neuropsychology, 9*(4), 435-448.

Malouin, F., Richards, C. L., Jackson, P. L., Dumas, F., & Doyon, J. (2003). Brain activations during motor imagery of locomotor-related tasks: A PET study. *Human Brain Mapping, 19*(1), 47-62.

Manning, L., Halligan, P. W., & Marshall, J. C. (1990). Individual variation in line bisection: A study of normal subjects with application to the interpretation of visual neglect. *Neuropsychologia, 28*(7), 647-655.

Marshall, J. C., & Halligan, P. W. (1989). When right goes left: An investigation of line bisection in a case of visual neglect. *Cortex, 25*(3), 503-515.

Marshall, J. C., & Halligan, P. W. (1990). Line bisection in a case of visual neglect: Psychophysical studies with implications for theory. *Cognitive Neuropsychology, 7*(2), 107-130.

Marshall, R. S., Lazar, R. M., Krakauer, J. W., & Sharma, R. (1998). Stimulus context in hemineglect. *Brain, 121* (Pt 10*)*, 2003-2010.

Marshall, R. S., Lazar, R. M., Van Heertum, R. L., Esser, P. D., Perera, G. M., & Mohr, J. P. (1997). Changes in regional cerebral blood flow related to line bisection discrimination and visual attention using HMPAO-SPECT. *NeuroImage, 6*(2), 139-144.

Mattingley, J. B., Berberovic, N., Corben, L., Slavin, M. J., Nicholls, M. E. R., & Bradshaw, J. L. (2004). The greyscales task: A perceptual measure of attentional bias following unilateral hemispheric damage. *Neuropsychologia, 42*(3), 387-394.

Mattingley, J. B., Bradshaw, J. L., & Bradshaw, J. A. (1994). Horizontal visual motion modulates focal attention in left unilateral spatial neglect. *Journal of Neurology, Neurosurgery and Psychiatry, 57*(10), 1228-1235.

Mattingley, J. B., Pierson, J. M., Bradshaw, J. L., Phillips, J. G., & Bradshaw, J. A. (1993). To see or not to see: The effects of visible and invisible cues on line bisection judgements in unilateral neglect. *Neuropsychologia, 31*(11), 1201-1215.

McCourt, M. E., & Jewell, G. (1999). Visuospatial attention in line bisection: Stimulus modulation of pseudoneglect. *Neuropsychologia, 37*(7), 843-855.

McCourt, M. E., & Garlinghouse, M. (2000a). Asymmetries of visuospatial attention are modulated by viewing distance and visual field elevation: Pseudoneglect in peripersonal and extrapersonal space. *Cortex, 36*(5), 715-731.

McCourt, M. E., & Garlinghouse, M. (2000b). Stimulus modulation of pseudoneglect: Influence of line geometry. *Neuropsychologia, 38*(4), 520-524.

McCourt, M. E., Garlinghouse, M., & Reuter-Lorenz, P. A. (2005). Unilateral visual cueing and asymmetric line geometry share a common attentional origin in the modulation of pseudoneglect. *Cortex, 41*(4), 499-511.

McCourt, M. E., Shpaner, M., Javitt, D. C., & Foxe, J. J. (2008). Hemispheric asymmetry and callosal integration of visuospatial attention in schizophrenia: A tachistoscopic line bisection study. *Schizophrenia Research, 102*(1-3), 189-196.

McIntosh, R. D. (2006). The eyes have it: Oculomotor exploration and line bisection in neglect. *Cortex, 42*(5), 692-698.

McIntosh, R. D., Schindler, I., Birchall, D., & Milner, A. D. (2005). Weights and measures: A new look at bisection behaviour in neglect. *Cognitive Brain Research, 25*(3), 833-850.

Meck, W. H. (2005). Neuropsychology of timing and time perception. *Brain and Cognition, 58*(1), 1-8.

Medendorp, W. P., Goltz, H. C., Vilis, T., & Crawford, J. D. (2003). Gaze-centered updating of visual space in human parietal cortex. *Journal of Neuroscience, 23*(15), 6209-6214.

Mefferd Jr., R. B., Wieland, B. A., & Dufilho, L. P. (1969). Systematic alterations of the apparent centers of lines. *Perceptual and Motor Skills, 28*(3), 803-825.

Mel, B. W. (1994). Information processing in dendritic trees. *Neural Computation, 6*(6), 1031-1085.

Mennemeier, M., Pierce, C. A., Chatterjee, A., Anderson, B., Jewell, G., Dowler, R., et al. (2005). Biases in attentional orientation and magnitude estimation explain crossover: Neglect is a disorder of both. *Journal of Cognitive Neuroscience, 17*(8), 1194-1211.

Mennemeier, M., Rapcsak, S. Z., Pierce, C., Dillon, M., & Vezey, E. (1998). A search for the optimal stimulus. *Brain and Cognition, 37*, 439-459.

Mennemeier, M., Rapcsak, S. Z., Pierce, C., & Vezey, E. (2001). Crossover by line length and spatial location. *Brain and Cognition, 47*(3), 412-422.

Mennemeier, M., Vezey, E., Chatterjee, A., Rapcsak, S. Z., & Heilman, K. M. (1997). Contributions of the left and right cerebral hemispheres to line bisection. *Neuropsychologia, 35*(5), 703-715.

Mesulam, M. (1981). A cortical network for directed attention and unilateral neglect. *Annals of Neurology*, 10, 309-325.

Milner, A. D. (1987). Animal models for the syndrome of spatial neglect. In M. Jeannerod (Ed.), *Neurophysiological and neuropsychological aspects of spatial neglect* (pp. 259-288). Amsterdam: Elsevier Science.

Milner, A. D., Brechmann, M., & Pagliarini, L. (1992). To halve and to halve not: An analysis of line bisection judgements in normal subjects. *Neuropsychologia, 30*(6), 515-526.

Milner, A. D., Harvey, M., Roberts, R. C., & Forster, S. V. (1993). Line bisection errors in visual neglect: Misguided action or size distortion? *Neuropsychologia, 31*(1), 39-49.

Monaghan, P., & Shillcock, R. (1998). The cross-over effect in unilateral neglect: Modelling detailed data in the line-bisection task. *Brain, 121*(5), 907-921.

Mort, D. J., Malhotra, P., Mannan, S. K., Rorden, C., Pambakian, A., Kennard, C., et al. (2003). The anatomy of visual neglect. *Brain, 126*(9), 1986-1997.

Mozer, M. C. (1991). *The perception of multiple objects: A connectionist approach*. Cambridge, MA: The MIT Press.

Mozer, M. C., Halligan, P. W., & Marshall, J. C. (1997). The end of the line for a brain-damaged model of unilateral neglect. *Journal of Cognitive Neuroscience, 9*(2), 171-190.

Nichelli, P., Rinaldi, M., & Cubelli, R. (1989). Selective spatial attention and length representation in normal subjects and in patients with unilateral spatial neglect. *Brain and Cognition, 9*(1), 57-70.

Nicholls, M. E. R., Mattingley, J. B., Berberovic, N., Smith, A., & Bradshaw, J. L. (2004). An investigation of the relationship between free-viewing perceptual asymmetries for vertical and horizontal stimuli. *Cognitive Brain Research, 19*(3), 289-301.

Nicholls, M. E. R., Mattingley, J. B., & Bradshaw, J. L. (2005). The effect of strategy on pseudoneglect for luminance judgements. *Cognitive Brain Research, 25*(1), 71-77.

Nicholls, M. E. R., & Roberts, G. R. (2002). Can free-viewing perceptual asymmetries be explained by scanning, pre-motor or attentional biases? *Cortex, 38*(2), 113-136.

Nielsen, K. E., Intriligator, J., & Barton, J. J. (1999). Spatial representation in the normal visual field: A study of hemifield line bisection. *Neuropsychologia, 37*(3), 267-277.

Olk, B., Wee, J., & Kingstone, A. (2004). The effect of hemispatial neglect on the perception of centre. *Brain and Cognition, 55*(2), 365-367.

Penhune, V. B., Zatorre, R. J., & Evans, A. C. (1998). Cerebellar contributions to motor timing: A PET study of auditory and visual rhythm reproduction. *Journal of Cognitive Neuroscience, 10*(6), 752-766.

Petit, L., & Haxby, J. V. (1999). Functional anatomy of pursuit eye movements in humans as revealed by fMRI. *Journal of Neurophysiology, 82*(1), 463-471.

Pierce, C. A., Jewell, G., & Mennemeier, M. (2003). Are psychophysical functions derived from line bisection reliable? *Journal of the International Neuropsychological Society, 9*(1), 72-78.

Plummer, P., Dunai, J., & Morris, M. E. (2006). Understanding the effects of moving visual stimuli on unilateral neglect following stroke. *Brain and Cognition, 60*(2), 156-165.

Pouget, A., Deneve, S., & Sejnowski, T. J. (1999). Frames of reference in hemineglect: a computational approach. In J. A. Reggia, E. Ruppin & D. Glanzman (Eds.), *Progress in Brain Research, Vol. 121* (pp. 81-97). Amseterdam: Elsevier Science.

Pouget, A., & Sejnowski, T. J. (1995). Spatial representations in the parietal cortex may use basis functions. In G. Tesauro, D. S. Touretzky & T. K. Leen (Eds.), *Advances in neural information processing systems* (pp. 157-164). Cambridge, MA: MIT Press.

Pouget, A., & Sejnowski, T. J. (1997). Spatial transformations in the parietal cortex using basis functions. *Journal of Cognitive Neuroscience,* 9, 222-237.

Pouget, A., & Sejnowski, T. J. (2001). Simulating a lesion in a basis function model of spatial representations: Comparison with hemineglect. *Psychological Review, 108*(3), 653-673.

Pouget, A., & Snyder, L. H. (2000). Computational approaches to sensorimotor transformations. *Nature Neuroscience, 3*(SUPPL.), 1192-1198.

Reuter-Lorenz, P. A., Kinsbourne, M., & Moscovitch, M. (1990). Hemispheric control of spatial attention. *Brain and Cognition, 12*(2), 240-266.

Reuter-Lorenz, P. A., & Posner, M. I. (1990). Components of neglect from right-hemisphere damage: An analysis of line bisection. *Neuropsychologia, 28*(4), 327-333.

Ricci, R., & Chatterjee, A. (2001). Context and crossover in unilateral neglect. *Neuropsychologia, 39*(11), 1138-1143.

Rieke, F. D., Warland, R. R., de Ruyter van Steveninick, R., & Bialek, W. (1997). *Spikes: Exploring the neural code*. Cambridge, MA: MIT Press.

Riestra, A. R., Womack, K. B., Crucian, G. P., & Heilman, K. M. (2002). Is the middle between both halves? Midpoint location and segment size estimation in neglect. *Neurology, 59*(10), 1580-1584.

Rolfe, M. H. S., Hamm, J. P., & Waldie, K. E. (2008). Differences in paper-and-pencil versus computerized line bisection according to ADHD subtype and hand-use. *Brain and Cognition, 66*(2), 188-195.

Rubens, A. B. (1985). Caloric stimulation and unilateral visual neglect. *Neurology, 35*(7), 1019-1024.

Rueckert, L., Deravanesian, A., Baboorian, D., Lacalamita, A., & Repplinger, M. (2002). Pseudoneglect and the cross-over effect. *Neuropsychologia, 40*(2), 162-173.

Sampaio, E., & Chokron, S. (1992). Pseudoneglect and reversed pseudoneglect among left-handers and right-handers. *Neuropsychologia, 30*(9), 797-805.

Schuett, S., Kentridge, R. W., Zihl, J., & Heywood, C. A. S. (2009). Is the origin of the hemianopic line bisection error purely visual? Evidence from eye movements in simulated hemianopia. *Vision Research, 49*(13), 1668-1680.

Sheppard, D. M., Bradshaw, J. L., & Mattingley, J. B. (2002). Abnormal line bisection judgements in children with tourette's syndrome. *Neuropsychologia, 40*(3), 253-259.

Sheppard, D. M., Bradshaw, J. L., Mattingly, J. B., & Lee, P. (1999). Effects of stimulant medication on the lateralisation of line bisection judgements of children with attention deficit hyperactivity disorder. *Journal of Neurology, Neurosurgery & Psychiatry, 66*(1), 57-63.

Singh, R., & Eliasmith, C. (2006). Higher-dimensional neurons explain the tuning and dynamics of working memory cells. *Journal of Neuroscience, 26*(14), 3667-3678.

Speedie, L. J., Wertman, E., Verfaellie, M., Butter, C., Silberman, N., Liechtenstein, M., et al. (2002). Reading direction and spatial neglect. *Cortex, 38*(1), 59-67.

Talairach, J. (1988). In Tournoux P. (Ed.), *Co-planar stereotaxic atlas of the human brain : 3-dimensional proportional system: An approach to medical cerebral imaging*. Stuttgart: Stuttgart : Georg Thieme.

Tikhonov, A., Haarmeier, T., Thier, P., Braun, C., & Lutzenberger, W. (2004). Neuromagnetic activity in medial parietooccipital cortex reflects the perception of visual motion during eye movements. *NeuroImage, 21*(2), 593-600.

Tracy, J. I., Faro, S. H., Mohamed, F. B., Pinsk, M., & Pinus, A. (2000). Functional localization of a 'time keeper' function separate from attentional resources and task strategy. *NeuroImage, 11*(3), 228-242.

Valadao, D., Hurwitz, M., & Danckert, J. Examining the influence of ‘noise’ on judgments of spatial extent. *Experimental Brain Research* (in press).

Varnava, A., & Halligan, P. W. (2007). Influence of age and sex on line bisection: A study of normal performance with implications for visuospatial neglect. *Neuropsychology, Development, and Cognition Section B: Aging, Neuropsychology and Cognition, 14*(6), 571-585.

Waberski, T. D., Gobbelé, R., Lamberty, K., Buchner, H., Marshall, J. C., & Fink, G. R. (2008). Timing of visuo-spatial information processing: Electrical source imaging related to line bisection judgements. *Neuropsychologia, 46*(5), 1201-1210.

Walsh, V. (2003). A theory of magnitude: Common cortical metrics of time, space and quantity. *Trends in Cognitive Sciences, 7*(11), 483-488.

Weiss, P. H., Marshall, J. C., Wunderlich, G., Halligan, P. W., Tellmann, L., Zilles, K., et al. (2000). Differential neural mechanisms for action in peri- versus extra-personal space. *NeuroImage, 11*(5 PART II), S851.

Weiss, P. H., Marshall, J. C., Wunderlich, G., Tellmann, L., Halligan, P. W., Freund, H., et al. (2000). Neural consequences of acting in near versus far space: A physiological basis for clinical dissociations. *Brain, 123*(12), 2531-2541.

Wolfe, H. K. (1923). On the estimation of the middle of lines. *American Journal of Psychology, 34*, 313-358.